Development of a Machine Learning-based Marker-less Gait Analysis System for Clinical Applications

Svonko Galasso

svonko.galasso@unicas.it

In Partial Fulfillment of the Requirements for the Degree of

PHILOSOPHIAE DOCTOR in

Electrical and Information Engineering

18/12/2024

TUTOR   **COORDINATOR**

Prof. Mario Molinara   Prof. Fabrizio Marignetti

Prof. Alessandro Marco De Nunzio

Università degli Studi di Cassino e del Lazio Meridionale

Corso di Dottorato in Metodi, Modelli e Tecnologie per l'Ingegneria

Date: **18/12/2024**

Author: **Svonko Galasso**

Title: **Development of a Machine Learning-based Marker-less Gait Analysis System for Clinical Applications**

Department: **Dipartimento di Ingegneria Elettrica e dell'Informazione**

Degree: **Philosophiae Doctor**

Permission is herewith granted to university to circulate and to have copied for non-commercial purposes, at its discretion, the above title upon the request of individuals or institutions.

_____
Signature of Author

To all those who have been part of my journey,

"Life goes by so fast,
You only want to do what you think is right.
Close your eyes, and then it's past—
Story of my life."

Thank you for the memories,
the lessons,
and the moments
that made these years unforgettable.

Acknowledgements

First and foremost, I would like to express my deepest gratitude to my supervisors, Alessandro and Mario, for believing in me and offering me this incredible opportunity during the challenging times of COVID.

Mario, I will always cherish our discussion about embarking on this Ph.D. journey—a conversation late in the evening, just two days before the application deadline. Your confidence in my abilities after only one meeting during my master's thesis was genuinely inspiring and instrumental in shaping my path.

Alessandro, thank you for your unwavering support and for collaborating with Mario and me to refine and prepare the project at such a critical time. I am especially grateful for recognizing my potential early on and encouraging me to apply for the Industrial Fellowship two months after arriving in Luxembourg. Your guidance and vision have been invaluable, and I sincerely appreciate the faith you have shown in me throughout this journey.

Over the years, both of you have provided unwavering support, guidance, and appreciation for my work, and I will be deeply grateful for everything I have learned under your mentorship.

A huge thank you goes to my parents for their endless support from the beginning of my career. Living and working abroad has made me miss them even more, but I hope they know I have found my path and always carry their love with me.

To my father, thank you for your practical help and thoughtful advice, always offering me a perspective I deeply value when facing challenges. Your stories about your time living in Germany and the countless trips we took together as a child undoubtedly inspired my curiosity and motivated me to pursue opportunities beyond Italy. Your support has been a constant source of strength throughout this journey.

To my mother, thank you for your warmth, love, and incredible adaptability whenever I return to Italy. Whether adjusting to my routines, accommodating my timetable when I come back late from the gym, or preparing meals that make me feel at home, you always make everything seem effortless. Thank you for never saying no when I need something, even when it means setting aside your plans. Your unwavering support means the world to me.

I deeply treasure the time we share and will always make it a priority to return home whenever I have the opportunity.

To my brother Davide, thank you for being my rock and always stepping in to help me navigate life's challenges. I can always count on you, and your readiness to support me is something I never take for granted. When I hear stories about siblings growing distant, I feel incredibly lucky to have our bond. I hope we can finally plan our motorcycle trip together next year.

To Fabi, my "right arm," thank you for your invaluable advice and the incredible strength you display in handling life's obstacles. Your resilience and determination are truly inspiring, and I deeply admire how you handle challenges with such naturalness. You are the strongest person I have ever met, and I often wonder how I would manage in your place—I still don't have an answer.

To Greta, my lovely niece and dearest friend. Being away from you is one of the hardest parts of my journey, and I often feel guilty for not being present as much as I wish I could be. You are probably the one I miss the most. Thank you for showing me, in your special way, that

I still hold a special place in your heart.

I can't forget to mention a few words about Bing, who is undeniably part of the family. Even though you're annoying most of the time, your antics always bring a smile to my face—you're pretty cool in your own way.

To Renato, I could not place you under "work" because you are more than a colleague—you are like a brother to me. Thank you for guiding me when I first arrived and continuing to help me after all these years. Your friendship has been a cornerstone of my experience here, and I am endlessly grateful for it.

Finally, to Sere. Thank you for being the best companion, friend, and work colleague I could ever ask for. I'm always amazed by your ability to fully immerse yourself in a problem whenever I ask for your advice, always offering me the best suggestions possible, even when the matter is completely outside your interests.

I am especially grateful for the incredible support you've given me during the final stages of my Ph.D.. Thanks to your help and presence, my stress levels were much more manageable, and I could focus on completing this important chapter of my life. Your strength and encouragement made all the difference.

You are, without a doubt, the most patient person on earth—something I deeply admire, especially considering how much patience it takes to deal with me. Your support is unparalleled, and knowing I can always look beside myself to find you there gives me a profound sense of comfort—it feels like home. Sharing this life abroad with you is an incredible gift, and I couldn't imagine a better partner to navigate this journey with.

Ringraziamenti

Prima di tutto, desidero esprimere la mia più profonda gratitudine ai miei supervisori, Alessandro e Mario, per aver creduto in me e per avermi offerto questa incredibile opportunità durante i difficili tempi del COVID.

Mario, ricorderò sempre con affetto la nostra conversazione sulla possibilità di intraprendere questo percorso di dottorato—un dialogo avvenuto in tarda serata, solo due giorni prima della scadenza per la domanda. La tua fiducia nelle mie capacità, dopo un solo incontro durante la mia tesi di laurea magistrale, è stata davvero fonte di ispirazione e fondamentale per definire il mio percorso.

Alessandro, grazie per il tuo costante supporto e per aver collaborato con Mario e me nella definizione e preparazione del progetto in un momento così cruciale. Sono particolarmente grato per aver riconosciuto il mio potenziale fin dall'inizio e per avermi incoraggiato a candidarmi per l'Industrial Fellowship solo due mesi dopo il mio arrivo in Lussemburgo. La tua guida e visione sono state preziose, e apprezzo sinceramente la fiducia che hai dimostrato in me durante questo percorso.

Nel corso degli anni, entrambi mi avete offerto un supporto costante, preziosi consigli e un riconoscimento per il mio lavoro, e vi sarò profondamente grato per tutto ciò che ho imparato sotto la vostra guida.

Un enorme grazie va ai miei genitori per il loro infinito sostegno sin dall'inizio della mia carriera. Vivere e lavorare all'estero mi ha fatto sentire la loro mancanza ancora di più, ma spero sappiano che ho trovato la mia strada e che porto sempre con me il loro amore.

A mio padre, grazie per il tuo aiuto pratico e i tuoi preziosi consigli, offrendo sempre una prospettiva che considero fondamentale quando affronto delle difficoltà. Le tue storie sul tuo periodo in Germania, insieme ai tanti viaggi che abbiamo fatto insieme quando ero bambino, hanno sicuramente alimentato la mia curiosità e mi hanno motivato a cercare opportunità oltre i confini dell'Italia. Il tuo sostegno è stato una costante fonte di forza durante tutto questo percorso.

A mia madre, grazie per il tuo calore, amore e incredibile capacità di adattamento ogni volta che torno in Italia. Che si tratti di adattarti alle mie routine, accogliere i miei orari quando rientro tardi dalla palestra, o preparare pasti che mi fanno sentire a casa, riesci sempre a far sembrare tutto semplice. Grazie per non aver mai detto di no quando ho bisogno di qualcosa, anche se significa mettere da parte i tuoi piani. Il tuo supporto incondizionato significa il mondo per me.

Apprezzo profondamente il tempo che passiamo insieme e farò sempre del mio meglio per tornare a casa ogni volta che ne avrò l'opportunità.

A mio fratello Davide, grazie per essere il mio punto fermo e per aiutarmi sempre a superare le difficoltà della vita. Posso sempre contare su di te, e il tuo essere sempre pronto ad aiutarmi è qualcosa che non do mai per scontato. Quando sento storie di fratelli che si allontanano, mi sento incredibilmente fortunato per il legame che abbiamo. Spero che finalmente riusciremo a pianificare il nostro viaggio in moto insieme l'anno prossimo.

A Fabi, il mio "braccio destro," grazie per i tuoi preziosi consigli e per la straordinaria forza che dimostri nell'affrontare gli ostacoli della vita. La tua resilienza e determinazione sono davvero fonte di ispirazione, e ammiro profondamente come affronti le sfide con tanta naturalezza. Sei

la persona più forte che abbia mai conosciuto, e spesso mi chiedo come farei al tuo posto—e ancora non ho una risposta.

A Greta, la mia adorata nipote e mia più cara amica. Essere lontano da te è una delle parti più difficili del mio percorso, e spesso mi sento in colpa per non essere presente quanto vorrei. Sei probabilmente la persona di cui sento più la mancanza. Grazie per mostrarmi, a modo tuo, che occupo ancora un posto speciale nel tuo cuore.

Non posso non spendere qualche parola per Bing, che è indiscutibilmente parte della famiglia. Anche se la maggior parte delle volte sei piuttosto fastidioso, le tue buffe abitudini riescono sempre a farmi sorridere—sei davvero unico nel tuo genere.

A Renato, non potevo collocarti sotto "lavoro" perché sei molto più di un collega—sei come un fratello per me. Grazie per avermi guidato quando sono arrivato per la prima volta e per continuare ad aiutarmi dopo tutti questi anni. La tua amicizia è stata una pietra miliare della mia esperienza qui, e te ne sono infinitamente grato.

Infine, a Sere. Grazie per essere la migliore compagna, amica e collega di lavoro che avrei mai potuto desiderare. Rimango sempre colpito dalla tua capacità di immergerti completamente in un problema ogni volta che ti chiedo consiglio, riuscendo a offrirmi sempre i migliori suggerimenti possibili, anche quando quella questione esula completamente da te.

Ti sono particolarmente grato per il supporto incredibile che mi hai dato durante le fasi finali del mio Dottorato. Grazie al tuo aiuto e alla tua presenza, il mio livello di stress è stato molto più gestibile, e ho potuto concentrarmi sul completamento di questo importante capitolo della mia vita. La tua forza e il tuo incoraggiamento hanno fatto tutta la differenza.

Sei, senza alcun dubbio, la persona più paziente sulla terra—qualcosa che ammiro profondamente, soprattutto considerando quanta pazienza serve per avere a che fare con me. Il tuo supporto è impareggiabile, e sapere che posso sempre guardare accanto a me e trovarti lì mi dà un profondo senso di conforto—è come sentirsi a casa. Condividere questa vita all'estero con te è un dono incredibile, e non potrei immaginare un partner migliore con cui affrontare questo viaggio.

Contents

List of Figures

List of Tables

Acronyms

AI	Artificial Intelligence.
ALS	Amyotrophic Lateral Sclerosis.
Caffe	Convolutional Architecture for Fast Feature Embedding.
CNN	Convolutional Neural Network.
COCO	Common Objects in Context.
CV	Computer Vision.
DL	Deep Learning.
GAn	Gait Analysis.
GC	Gait Cycle.
HPE	Human Pose Estimation.
IMUs	Inertial Measurement Unit sensors.
IoT	Internet of Things.
IPAQ	International Physical Activity Questionnaire.
IR	Infrared.
MB	Marker-Based.
ML	Machine Learning.
MLB	Marker-Less-Based.
MoCap	Motion Capture.
NCA	Neighborhood Component Analysis.
OP	OpenPose.
OpenCV	Open Source Computer Vision Library.
PAL	Physical Activity Level.
PD	Parkinson's Disease.
RNN	Recurrent Neural Network.
STPs	Spatiotemporal Parameters.
UPDRS	Parkinson's Disease Rating Scale.
XAI	Explainable Artificial Intelligence.

Chapter 1

Introduction

1.1 Motivation

Deep Learning (DL) is a highly promising area of research in various biomedical fields, particularly in Computer Vision (CV). It has gained widespread popularity in recent years due to its remarkable potential in designing, implementing, and deploying a wide range of complex applications in modern fields, such as biomedical engineering [1, 2, 3]. With recent technological advancements, including high computational power and modern graphic processing units, DL has proven effective in analyzing and recognizing medical images and events. Gait is an important biomarker and can provide valuable information for predicting various conditions, including neurological disorders such as stroke, dementia, and Parkinson's Disease (PD), as well as diseases like arthritis [4, 5, 6]. While DL models are sensitive to subtle gait changes that can serve as early predictors for the onset of these disorders, they are equally valuable in continuously monitoring disease progression. Predictive models require high specificity and sensitivity, similar to clinical diagnostic tests, to detect early disease indicators accurately. For example, recent studies have shown that DL-based Gait Analysis (GAn) can identify early motor impairments in patients at risk for PD's by detecting distinct gait changes that precede more severe symptoms [7, 8]. These predictive applications allow timely intervention and play a critical role in preventative healthcare. DL models are equally valuable in continuously monitoring disease progression, where the focus shifts to sensitivity to changes over time, as they track longitudinal gait pattern variations that reflect treatment effects or gradual health declines. For example, recent studies have demonstrated that DL-based GAn can monitor neurological health over time, providing insights into the progression of conditions such as PD's [9]. Similarly, wearable sensor systems combined with Machine Learning (ML) have effectively tracked gait changes in patients with chronic conditions such as knee osteoarthritis. This allows for regular assessment of treatment efficacy and functional mobility [10].

Therefore, using DL methods for video-based GAn is highly beneficial for monitoring the progression of these disorders. As people age, they become more susceptible to certain disorders affecting their ability to walk properly. This increased susceptibility, due to conditions such as stroke, PD's disease, and Amyotrophic Lateral Sclerosis (ALS), contributes to a higher risk of falls, even on flat surfaces. Stroke survivors, for example, often experience motor impairments and balance issues that make them prone to falls, particularly during rehabilitation and in community settings [11, 12]. Similarly, PD's lead to gait disturbances like shuffling and freezing, which increase fall risk and injury potential in affected individuals [13]. Treating these gait-related diseases is expensive and can take significant resources [14, 11]. Studies have shown that about one-third of elderly adults over the age of 75 who live in the community will fall at least once in a calendar year due to a gait disorder, and nearly one-fourth of these falls will result in serious injuries. These findings highlight the need for preventative measures and improved treatments for gait-related disorders in the elderly [15, 16]. The United Kingdom incurs significant medical expenses due to falls, particularly in adults aged 60 and above. The annual cost associated with fall-related injuries in this demographic is over 981 million pounds. This highlights the need for effective fall prevention interventions to reduce the economic burden on the healthcare system and improve the health outcomes of older adults [17]. The medical expenses for elderly individuals who suffer from falls vary significantly across different states in

the United States. According to a study conducted on fall-related injuries, lifetime healthcare costs ranged from \$68 million in Vermont to \$2.8 billion in Florida. This indicates that the economic burden of fall-related injuries on the healthcare system is substantial and varies widely across different regions of the country [17]. With the growing number of elderly people, falling has become a significant issue [15, 16, 18]. Amyotrophic Lateral Sclerosis is a progressive disease that affects the nervous system, leading to the loss of motor neurons in the upper and lower limbs. As ALS progresses, patients experience increasing mobility challenges, heightening their fall risk. These fall-related events can lead to severe injuries, further complicating care and driving up medical costs for these individuals. In Germany, for example, the healthcare costs associated with treating ALS are substantial, with fall prevention and injury management representing significant components of the total expenses. The need for ongoing support and interventions to manage these fall risks contributes to the high lifetime cost of treating this condition [19]. Recently, there has been a growing awareness of gait-related issues and the risk of falls. As a result, measures have been implemented in high-risk workplaces, hospitals, and nursing homes to detect and address these concerns. These efforts have led to an improvement in safety standards in these settings [20].

Gait Analysis is a method for studying how a person walks. Originally, GAn was conducted through visual observation, allowing healthcare professionals to assess walking patterns and detect deviations without the assistance of technology. Early methods relied on skilled observation to identify physical changes that might signify gait-related disorders or an increased risk of falling. Despite its limitations, this approach established a foundational understanding of gait as a critical health marker [21, 22]. Over time, the field evolved with the integration of technology, which allowed for more precise and objective measurements of gait parameters. The introduction of Motion Capture (MoCap) systems, force platforms, and, more recently, wearable sensors have significantly enhanced healthcare professionals' ability to quantify gait characteristics, offering valuable insights into disease progression and treatment efficacy [23, 24, 25]. Today, technology-aided GAn provides researchers and healthcare professionals with advanced tools to assess and monitor patients' health in detail, far beyond what is possible through visual observation alone. Using kinematic and kinetic data, these systems allow for precise identification of gait deviations, contributing to accurate diagnosis, monitoring of disease progression, and assessment of treatment outcomes [26, 27]. As a result, GAn has become an essential component of clinical assessments for neurological, musculoskeletal, and systemic conditions, guiding therapeutic interventions to improve patient outcomes. Analyzing a person's gait makes it possible to identify patterns and detect any physical changes indicative of gait-related diseases or an increased risk of falling. It is a valuable tool for healthcare professionals and researchers to assess and monitor patients' health and study the effects of different treatments [28].

The term "gait" refers to how a person walks, specifically the movements of their legs while walking upright. A normal gait is characterized by naturalness, leg coordination, efficiency, and regularity. Any deviation from a normal gait may signify an underlying gait disorder. While minor gait deviations are common and may not signify any underlying issues, certain patterns or deviations have been associated with developing specific conditions and are recognized as potential biomarkers for disease. There are various reasons why a person may exhibit an abnormal gait, including neurological conditions like stroke, PD's disease, or multiple sclerosis, as well as musculoskeletal issues such as arthritis or limb deformities. Neurological disorders can affect motor coordination, muscle tone, and balance, leading to gait patterns such as the shuffling gait often seen in PD's disease or the hemiplegic gait that may occur after a stroke [29]. Musculoskeletal issues, on the other hand, typically involve joint function and movement mechanics. Conditions like osteoarthritis can cause joint pain or stiffness, resulting in an antalgic gait where the stance phase is shortened to avoid discomfort [30]. Systemic conditions, such as diabetes, may also contribute to gait abnormalities by impairing peripheral sensation or circulation. These gait abnormalities can be systematically identified and evaluated through GAn, which provides healthcare professionals with the tools to assess deviations from a normal gait pattern and diagnose underlying causes. Using kinematic and kinetic data, GAn enables the quantification of gait deviations, allowing for precise diagnosis and tracking of disease progression or treatment outcomes [21]. This process is critical for assessing patients with neurological, musculoskeletal, and systemic conditions and optimizing therapeutic interventions [31].

Analyzing gait patterns is crucial for guiding lower limb training and fall prevention strategies

in medical rehabilitation. By monitoring gait patterns in elderly patients, healthcare professionals can recommend preventive measures to reduce the risk of gait disorders. Studies have shown that early screening and monitoring of gait parameters allow for personalized interventions, such as balance training, strength exercises, and improved walking techniques. For instance, research published in BMC Public Health highlights how GAn can be used to develop models for predicting fall risks in elderly patients, enabling tailored exercise and mobility programs that can significantly reduce the likelihood of falls [32]. The study also emphasizes that wearable devices for gait feature collection, such as stride length and speed, can provide valuable insights into the mobility challenges older adults face, which is crucial to designing effective rehabilitation plans [32]. Similarly, a review in Applied Sciences underscores the importance of gait biomechanics in fall prevention among older adults. The authors discuss how improving dynamic balance through interventions targeting minimum foot clearance (MFC) and optimizing gait patterns can prevent tripping and slipping, two primary causes of falls. They further note that exercise interventions focusing on the ankle dorsiflexors and core stabilizers can enhance stability and reduce fall risk [33]. This study highlights practical strategies, such as footwear modification and exercise programs, that prevent falls in the elderly population. In addition, research featured in Lower Extremity Review Magazine discusses the importance of early gait assessment in identifying balance dysfunctions, which are strong predictors of future falls. The article points out that targeted interventions, such as physical therapy and specific exercise regimens, can reduce fall risks by up to 40%, making GAn a critical component of fall prevention programs [34]. Technologies such as the Timed Up and Go (TUG) test, which assesses mobility and balance, are recommended for the early detection of gait disorders in older adults. Gait disorders can also be diagnosed by analyzing various parameters associated with gait patterns [35].

Traditional GAn has limitations despite being widely applied and providing rich data. One of the most significant challenges in the field of GAn is its subjective nature. Traditionally, healthcare professionals have relied on observational techniques, which involve making qualitative judgments based on visual analysis of patient walk trials. While this method is non-invasive and readily available, it can introduce subjectivity influenced by the observer's experience and potential biases. This subjectivity can result in inconsistencies in assessments, which may ultimately impact the accuracy of diagnoses and the effectiveness of treatment plans. Reliance on visual assessment can be problematic in complex cases where subtle gait deviations might go unnoticed or in conditions where comprehensive quantitative analysis is essential. Therefore, the medical community strives for objective and quantifiable gait measures that provide a more detailed and consistent evaluation. The need for objectivity highlights the search for innovative approaches to complement and enhance traditional GAn methods. One of the first technological advancements toward objectivity in GAn was the use of video MoCap systems that relied on markers attached to the body, often referred to as Marker-Based (MB) systems. Video data from MB GAn systems transformed the landscape, as MB methods offered precise movement tracking, primarily within controlled environments. These systems use markers placed on specific body parts, allowing for high precision in measuring spatial-temporal parameters in GAn. MB systems, such as those offered by Qualisys, are widely regarded for their precision. They are frequently employed in clinical settings for diagnosing and tracking movement disorders like cerebral palsy [36]. However, these methods can be invasive and may inadvertently influence the natural movement of patients due to the markers, resulting in potentially biased data.

With advancements in sensor technology, inertial measurement units (Inertial Measurement Unit sensors (IMUs)) have become a prominent tool in GAn, offering a versatile, portable, and less restrictive alternative. Unlike traditional methods that require a laboratory setup and rely on markers attached to the body, IMUs allow for capturing movement patterns in more natural environments, minimizing the risk of artificial stimulus that could mask the natural gait characteristics. This is particularly important in clinical approaches for assessing and treating conditions where subtle gait deviations are critical. The ability to accurately measure locomotion without intrusive fixtures provides more authentic insights into both normal and pathological human movement [37]. IMUs, equipped with accelerometers and gyroscopes, offer a detailed account of an individual's movements in three-dimensional space, enabling the detection of subtle deviations that may indicate underlying health issues such as PD's disease, stroke recovery challenges, and musculoskeletal disorders. For instance, wearable IMUs are widely used in diagnosing and monitoring motor symptoms in patients with PD's disease. These sensors can detect gait

deviations like tremors, bradykinesia, and postural instability, which are characteristic of PD's disease, thus aiding in both diagnosis and treatment tracking [38]. Similarly, in stroke recovery, gait abnormalities are common, and IMUs are increasingly being used to monitor rehabilitation progress by identifying asymmetries in walking patterns, providing critical insights into recovery trajectories [39, 40]. Additionally, musculoskeletal disorders like osteoarthritis can be assessed using IMUs, as they allow healthcare professionals to monitor deviations in gait patterns over time and evaluate the effectiveness of therapeutic interventions [41]. Despite their advantages, IMUs have some limitations. For example, they may struggle to capture certain aspects of abnormal gait, especially in individuals with significant motor impairments. Prolonged use of wearable sensors can also become uncomfortable for patients, which may affect data accuracy over time.

Computer Vision applications have become a popular subject in biomechanics and healthcare research in recent years due to the limitations of human vision in identifying and measuring gait patterns [28, 42, 43]. In recent years, DL techniques have shown promise in addressing the limitations of 2D MLB systems, particularly in estimating joint angles accurately. While 2D MLB systems offer a non-invasive and accessible way to capture gait parameters, they can be prone to errors in joint angle estimation due to the constraints of working in two dimensions. DL models have the potential to detect and correct these errors by learning patterns from 3D data, enabling more accurate gait assessments without requiring additional equipment. This capability could significantly improve the reliability of GAn in clinical settings, making DL a valuable tool for enhancing the precision of 2D MLB-based systems. Several studies have used CV to analyze human gait patterns, with applications ranging from identifying individuals based on their walking style to understanding movement patterns in different conditions [44, 45]. However, most of these articles focus on using this technology to identify individuals based on their walking patterns. Only a few articles have specifically used CV to detect abnormal walking patterns [28, 42, 43]. Gait parameters are often measured in controlled environments using a combination of wearable and non-wearable systems, such as floor sensors or multiple cameras, which can result in unnatural movements from patients. In [42], the authors highlighted the potential biases in GAn conducted in controlled laboratory environments, observing that patients often move with unnatural caution when observed. As a result, there is a risk of bias in the collected data. Furthermore, in [46], the authors discussed the reliability of wearable technology in capturing gait data, pointing out that although wearable sensors such as accelerometers provide valuable insights, they may struggle to accurately measure abnormal gait events, particularly in individuals with significant impairments.

Building upon advancements in CV, recent developments in Marker-Less-Based (MLB) MoCap systems have provided solutions to the limitations posed by traditional, sensor-based systems. These MLB systems allow for natural, unrestricted movement without physical markers, significantly reducing the risk of data bias due to conscious or unnatural movements in controlled lab settings. Utilizing depth cameras and CV algorithms, MLB systems offer reliable data capture even in flexible, real-world environments. For example, in [47], the authors conducted a systematic review and meta-analysis comparing MB and MLB MoCap systems, demonstrating that MLB systems are comparable in terms of accuracy and reliability for measuring spatiotemporal parameters while also reducing errors related to skin motion artifacts commonly seen in MB systems. Similarly, in [48], the authors demonstrated how MLB systems, using depth cameras and CV, provide reliable data even in more flexible, real-world environments. In clinical settings, [49] highlights the applicability of MLB MoCap systems for GAn in children with cerebral palsy, showing that these systems can provide reliable kinematic data without the need for physical markers, thereby improving the accuracy of assessments.

1.2   Aim of the Thesis

Combining IMUs and video data has revolutionized the study of gait characteristics, leading to a deeper understanding of gait dynamics. These advanced technologies utilize complex algorithms to analyze gait patterns in real-time, detecting deviations that may signify a range of conditions. With these noninvasive GAn tools, medical professionals can develop new diagnostic and rehabilitative strategies to enhance patient outcomes.

The overarching goal of this thesis is to develop and validate a novel GAn system that utilizes a DL-based MLB approach. IMUs will be used to validate the proposed GAn system. This system aims to facilitate objective GAn in clinical settings, thus supporting specialists by enhancing the precision of gait assessments conducted outside the conventional laboratory environment. By providing a portable, DL-based solution, the proposed system enables high-precision gait assessments that are not confined to costly, stationary lab equipment. This flexibility allows for gait evaluations in diverse settings, making it feasible to conduct assessments more frequently and in environments that better reflect the patient's natural movement patterns, ultimately improving both accessibility and the clinical relevance of GAn.

The progress in this field has enabled a more comprehensive evaluation of gait and has opened up new avenues for research and treatment in the healthcare industry. This thesis sets out to devise a cost-effective and clinically viable solution for GAn by leveraging the potential of DL algorithms to process gait images obtained through widely available commercial camera systems, which are significantly more affordable and accessible than specialized laboratory equipment. By using commercially available cameras, the approach minimizes costs associated with traditional GAn technologies. It makes it feasible for a broader range of healthcare providers and clinics with limited budgets to adopt. This shift toward accessible technology can potentially extend advanced GAn capabilities beyond specialized facilities and everyday clinical settings, significantly expanding its reach and impact. The intention is to create a software tool that does not rely on sensors or markers attached to the skin which can quickly and accurately deliver clinically relevant gait parameters.

The research conducted herein will address several critical questions:

- Using a 45-degree acquisition angle to reduce occlusion limitations compared to a single plane (e.g., sagittal), is it possible to obtain the same gait features provided by state-of-the-art IMU-based technologies using the 2D MLB system?

- What is the precision of a 2D MLB system compared to the IMU-based methods?

- Can an ML or DL model be trained to detect and correct errors in joint angle estimation from a 2D MLB system?

The thesis aims to provide a foundational framework for developing innovative software to revolutionize GAn by making it more accessible, affordable, and efficient—characteristics essential for broad clinical adoption. This will be achieved through a 2D MLB system that requires minimal equipment and can be implemented in non-laboratory settings, thus reducing costs and allowing healthcare professionals to perform assessments directly in clinical environments. The system combines ML algorithms and CV techniques to streamline data analysis and automate gait feature extraction, making GAn cost-effective and feasible in various healthcare settings. The ultimate objective is to bridge the gap between the current clinical needs and the available GAn technologies, thereby creating a solution that aligns with the healthcare system's pressing demands. These demands include the need for scalable, non-invasive diagnostic tools that can be easily deployed in diverse settings and solutions that provide objective, reliable GAn without the prohibitive expenses of traditional lab-based systems. Such advancements are essential to support widespread monitoring, early diagnosis, and effective rehabilitation for various movement disorders.

1.3 Structure of the Thesis

The remainder of this Thesis is organized as follows: Chapter 2 serves as the foundational background, introducing the principal concepts while discussing gait and GAn. Moreover, an overview of neurodegenerative diseases and the main applications of Artificial Intelligence (AI) in healthcare are provided. In Chapter 3, the focus shifts to the GAn technologies that underpin this study, particularly detailing the development and functionalities of the MLB GAn software. This includes an in-depth look at how knee flexion and ankle dorsiflexion angles were derived from two-dimensional position data acquired via the OpenPose (OP) framework. Chapter 4 describes the data acquisition campaigns. The methodology and findings that guide the research are thoroughly outlined in Chapter 5. Finally, conclusions and suggested avenues for future research to build upon the work presented in this thesis are described in Chapter 6.

Chapter 2

Background

2.1 Gait

Gait refers to the unique way in which an individual walks. The muscular coordination and equilibrium required for ambulatory propulsion enable the body to advance in a periodic sequence termed the stride [50, 51]. Bipedal progression involves a cyclical process known as the Gait Cycle (GC), characterized by repetitive motions executed by the left and right extremities. Within the scope of the GC, there are two primary phases: the stance phase, wherein the foot maintains contact with the substrate, and the swing phase, which spans the interval from the initial elevation of the foot to the subsequent contact of the heel with the substrate. The stride interval, or GC duration, is the interval between two consecutive gait events of the same foot [52, 29]. This duration is defined from when the heel of one foot makes initial ground contact to when the same heel contacts the ground again. **Figure 2.1** shows an entire GC starting with the right heel's ground contact and concludes upon its subsequent contact.

Gait Phases

During walking, the stride can be divided into two main phases: stance and swing.

The stance phase begins with the heel striking the ground (heel strike) and ends with the foot lifting off (toe-off). At a natural walking speed, this phase accounts for approximately 60% of the total duration of the gait cycle (**Figure 2.2**).

The swing phase begins with the toe-off and ends with the subsequent heel contact of the same foot on the ground. At a natural walking speed, this phase accounts for approximately 40% of the total duration of the gait cycle (**Figure 2.3**).

Each of these phases can be further broken down into specific sub-phases related to the normal function of walking. These sub-phases include initial contact, loading response, mid stance, terminal stance, pre-swing, initial swing, mid swing, and terminal swing. By understanding these sub-phases, we can better understand the biomechanics of walking and the normal function of the human body during locomotion [29, 51]. During the stance phase, the foot is in contact with the ground, and weight is accepted onto it. During the swing phase, on the other hand, the foot is lifted and advances forward. These terms are commonly used to describe different aspects of gait in cases of abnormal movement patterns. **Figure 2.4** shows the different gait phases.

- **Initial Contact**: The heel is the first part of the foot that makes contact with the ground during walking. When the right foot touches the ground, it is referred to as the initial contact of the right leg. Currently, the knee is straight, the hip is bent, and the ankle is not pointing downwards or upwards. During this time, the left leg is just finishing its terminal stance phase [53, 51].

- **Loading Response**: During walking, one foot remains in contact with the ground while the other is lifted for forward movement. The foot in contact with the ground supports the entire body weight and helps absorb shocks while the other foot is in a pre-swing phase. This is followed by a phase where only one limb supports the body weight while the other
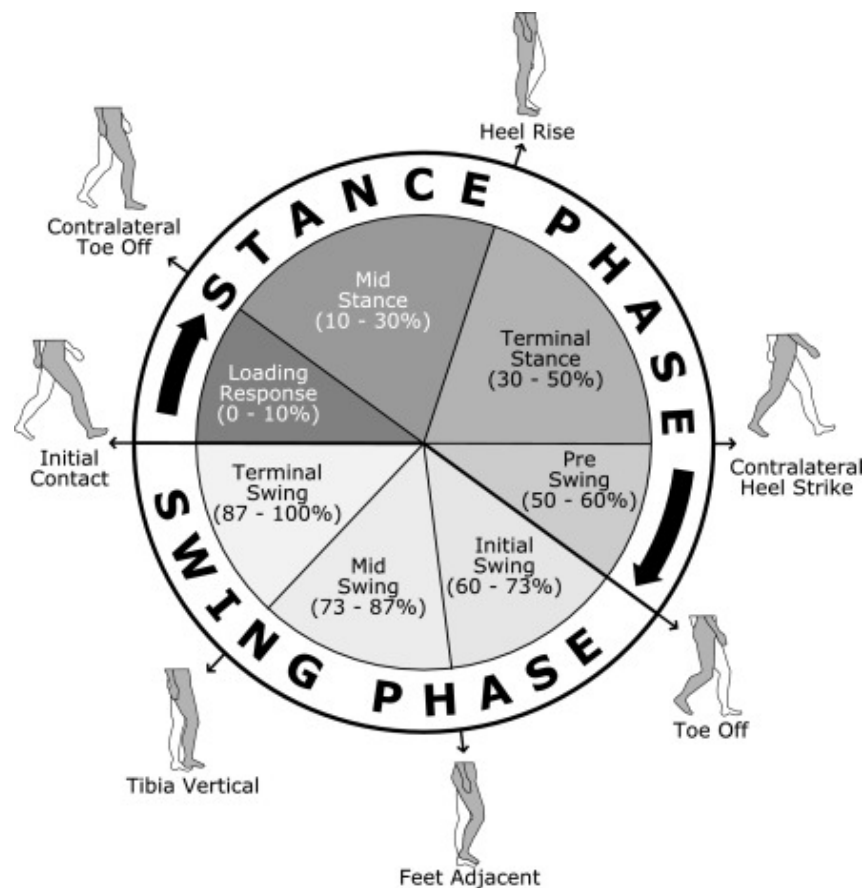
Figure 2.1: The Gait Cycle Phases. *A representation of the gait cycle, divided into two primary phases: the stance and swing phases. Each phase is further segmented into specific events such as initial contact, loading response, mid-stance, and terminal stance for the stance phase, as well as pre-swing, initial swing, mid-swing, and terminal swing for the swing phase. Key events, like heel rise, toe-off, and tibia vertical, are also indicated, illustrating the cyclical nature of walking biomechanics*

limb swings forward. This phase ensures stability and balance while allowing for continued forward movement [53, 51].

- **Mid-Stance**: The initial phase of single-leg support involves raising the left leg until the body's weight is balanced on the other foot. During this phase, the right leg moves forward over the right foot with the ankle raised while the knee and hip are fully extended. At the same time, the left leg is bearing the body's weight in the loading response stage [53, 51].

- **Terminal Stance**: Starts when the right heel is upswing and remains until the left foot heel touches the ground. The body's weight progresses away from the right foot because the increased extension in the hip places the leg in a more trailing situation [53, 51].

- **Pre-Swing**: The second interval of a double stance during one GC. It begins with the left foot's initial contact and ends with the right foot's toe-off. During this phase, the left leg contracts while the right foot moves towards ankle plantar flexion, reduced hip extension, and increased knee flexion. The body weight is then transferred to the opposite limb from the same side [53, 51].

- **Initial Swing**: Begins when one foot is lifted off the ground and ends when the other leg swings past the standing leg. During this cycle, the right leg moves forward with increased knee and hip flexion while the ankle is slightly raised to avoid touching the ground. A
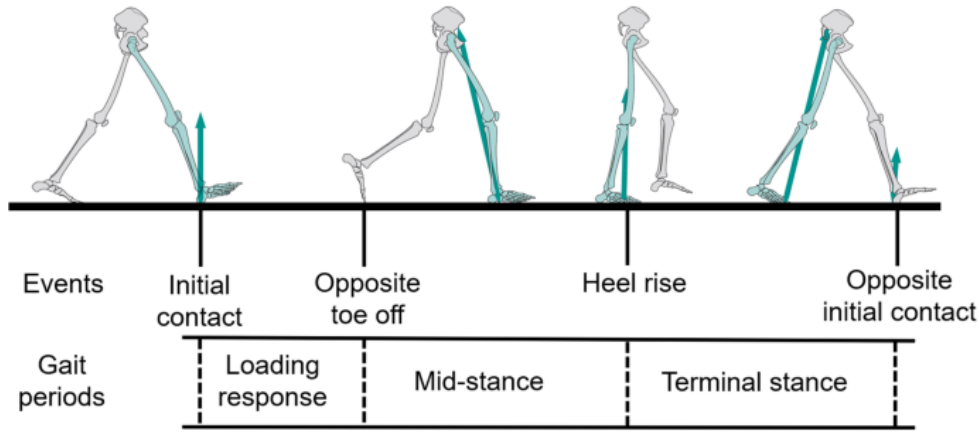
Figure 2.2: Stance Phase of the Gait Cycle. *A visual depiction of the stance phase of the gait cycle, highlighting key events such as initial contact, opposite toe-off, heel rise, and opposite initial contact. The diagram also outlines the corresponding gait periods: loading response, mid-stance, and terminal stance. Skeleton illustrations demonstrate the body's alignment and movement during each event, emphasizing the biomechanical transitions within the stance phase*
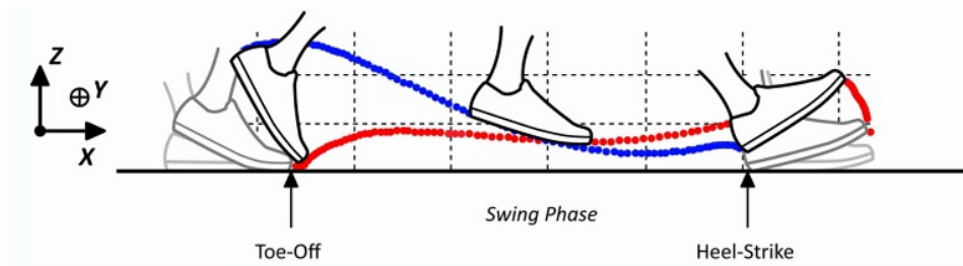
Figure 2.3: Swing Phase with Toe and Heel Trajectory. *A diagram illustrating the swing phase of the gait cycle, showing the movement trajectory of the toe (red path) and heel (blue path) during toe-off and heel-strike. The coordinate axes (X, Y, Z) indicate spatial dimensions, while the dotted lines track the biomechanical motion. This image highlights the dynamics of foot motion as the leg transitions through the air before making contact with the ground again*

footdrop gait is visible in this phase. Meanwhile, the left leg is in the mid-stance phase [53, 51].

- **Mid-Swing**: Commences at the end of the first swing and lasts until the leg is straightened, with the swinging limb positioned in front of the body. To make progress with the right leg, the hip is flexed further. As a result of gravity, the knee is allowed to straighten. This phase is known as the late mid-stance phase of the left leg [53, 51].

- **Terminal Swing**: Starts when the lower leg bone is upright and ends with the foot striking the ground. During this phase, the knee joint extends, which helps in the forward movement of the limb. The ankle joint remains in a neutral position, while the hip joint maintains its normal motion. The terminal swing phase is an essential part of the GC and is crucial in the smooth transition from one gait event to another [53, 51].

2.2 Gait Analysis

Gait Analysis is a standard diagnostic laboratory and research procedure providing an intricate locomotion overview by observing, capturing, analyzing, and interpreting human gait patterns [23]. It encompasses a range of specialized equipment to capture complex motion, muscle activity, and force distribution data [22]. A comprehensive clinical GAn allows for a detailed evaluation of gait patterns, quantifies physical impairments, and provides a foundation for targeted interventions. Despite its clinical benefits, there is currently no standardized approach
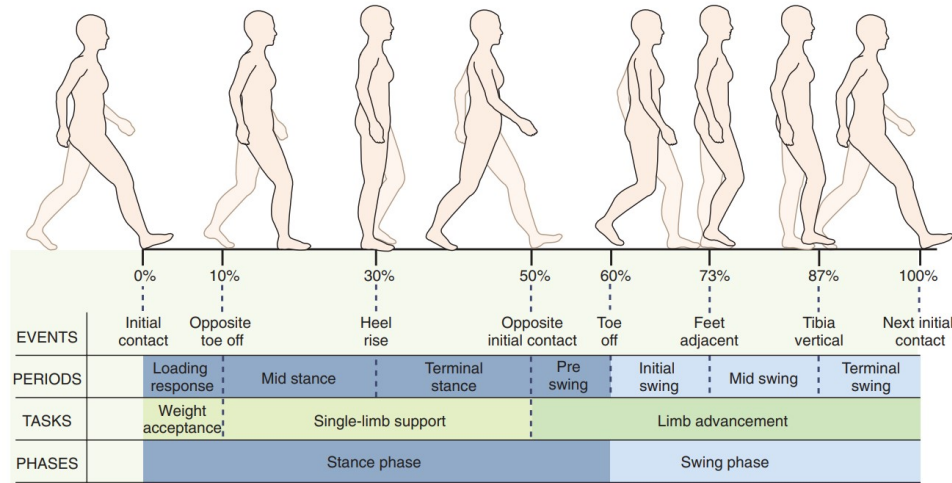
Figure 2.4: Gait Cycle Phases and Key Events. *Gait cycle phases with key events and tasks. The stance phase (0-60%) includes initial contact, heel rise, and toe-off, focusing on weight acceptance and single-limb support. The swing phase (60-100%) encompasses limb advancement tasks, transitioning from pre-swing to terminal swing, marked by events such as feet adjacent and tibia vertical. This diagram highlights the cyclical and biomechanical progression of walking.*

across different countries, which has led to variability in laboratory practices and equipment usage. Establishing consistent standards for clinical GAn could facilitate better interoperability and clinical decision-making and improve reimbursement practices across national healthcare systems [22].

2.2.1 Traditional and Modern Approaches

Studying the way people walk can provide valuable insights into diagnosing and treating various medical conditions related to walking. This includes monitoring athletes and their performance, observing exercises during rehabilitation and training, and designing equipment like prosthetic limbs and exoskeletons to improve mobility [25]. Recent advancements in sensor technology and ML have greatly enhanced the capability of GAn to support the diagnosis and monitoring of neurodegenerative diseases. By quantifying specific gait abnormalities characteristic of these diseases, technological tools now play a vital role in clinical assessment and tracking the progression of neurodegenerative conditions, thereby providing critical insights for early diagnosis and intervention [25].

The primary reason for numerous physical issues like lower back pain, muscle strain, and joint pain in the lower limbs is an unusual way of walking or moving, known as abnormal gait [54, 51]. The development of reliable techniques for studying human walking patterns is crucial. However, irregularities in gait can arise due to various factors like physical limitations, injuries, neurological conditions, and more. Developing accurate and effective methods for analyzing gait is crucial, as it requires tools capable of supporting healthcare professionals in the diagnosis and treatment process [55, 21]. A systematic approach to GAn relies on a foundational understanding of normal gait patterns and their variations, essential for identifying abnormal gait and creating targeted interventions. By focusing on the core components of human movement, GAn offers a structured framework that enables healthcare professionals to effectively evaluate and address gait-related issues [21]. While GAn has shown substantial utility in clinical settings by providing precise assessments that aid in clinical decision-making, further research is needed to establish its impact on broader healthcare outcomes, including cost-effectiveness [26].

Despite its widespread application and the richness of data it provides, traditional GAn has limitations. The most pervasive challenge lies in the subjective nature of the assessment. Healthcare professionals have traditionally relied on observational techniques, making qualitative judgments based on visual analysis during patient walk trials. While this method benefits from being non-invasive and readily available, it introduces subjectivity influenced by the observer's experience and potential biases. Such subjectivity can lead to inconsistencies in assessments, potentially affecting the accuracy of diagnoses and the subsequent effectiveness of treatment plans.

Reliance on visual assessment can be particularly problematic in complex cases where subtle gait deviations might go unnoticed or in conditions where comprehensive quantitative analysis is crucial. Consequently, there has been a push within the medical community for objective and quantifiable gait measures that could provide a more detailed and consistent evaluation. This need for objectivity underscores the search for innovative approaches to complement and enhance the traditional GAn methods.

Traditional gait analysis methods include observational techniques and marker-based systems. Observational techniques rely on healthcare professionals visually analyzing patient gait and making qualitative judgments during walk trials. While these techniques are non-invasive and accessible, they often introduce subjectivity and variability based on the observer's experience. Marker-based systems, such as optoelectronic setups, have long been considered the gold standard for precise kinematic measurements. These systems involve placing reflective markers on anatomical landmarks, which are tracked by specialized cameras to capture detailed motion data [56]. **Figure 2.5** demonstrates the placement of reflective markers on a subject, essential for accurate kinematic analysis in marker-based motion capture systems.
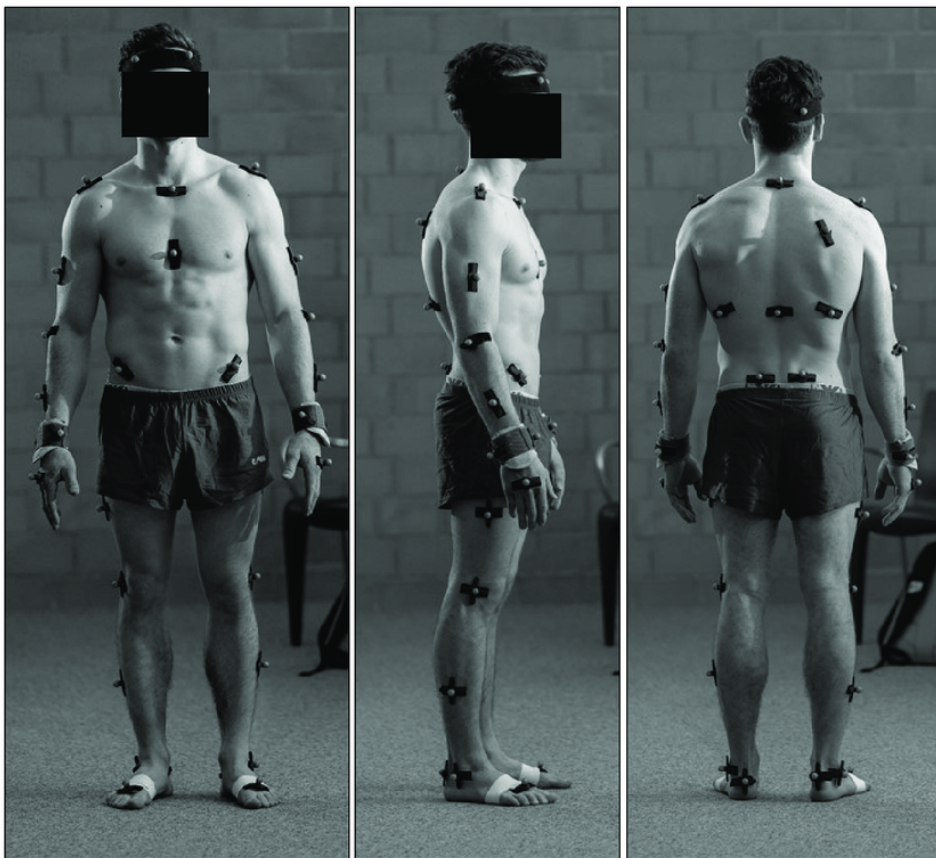
Figure 2.5: Reflective Marker Placement for Motion Capture. Front, side, and rear views of a subject equipped with reflective markers placed at key anatomical landmarks for motion capture analysis. The markers are strategically positioned to facilitate accurate tracking of joint movements and body segments during biomechanical assessments. This setup is commonly used in gait and posture studies to capture precise kinematic data. Adapted from [57]

Marker-Based systems, while highly accurate, are typically confined to controlled laboratory environments due to their reliance on expensive equipment and invasive setups. **Figure 2.6** depicts a typical motion capture laboratory setup, highlighting the controlled environment required for precise biomechanical analyses.

Building on the strengths and addressing the limitations of traditional methods, wearable systems offer an innovative approach to gait analysis, providing objective, real-time data collection in diverse settings beyond the laboratory. Such systems have revolutionized gait analysis by enabling real-time motion monitoring outside traditional laboratory settings. These systems utilize sensors such as IMUs, pressure insoles, and accelerometers to capture spatiotemporal
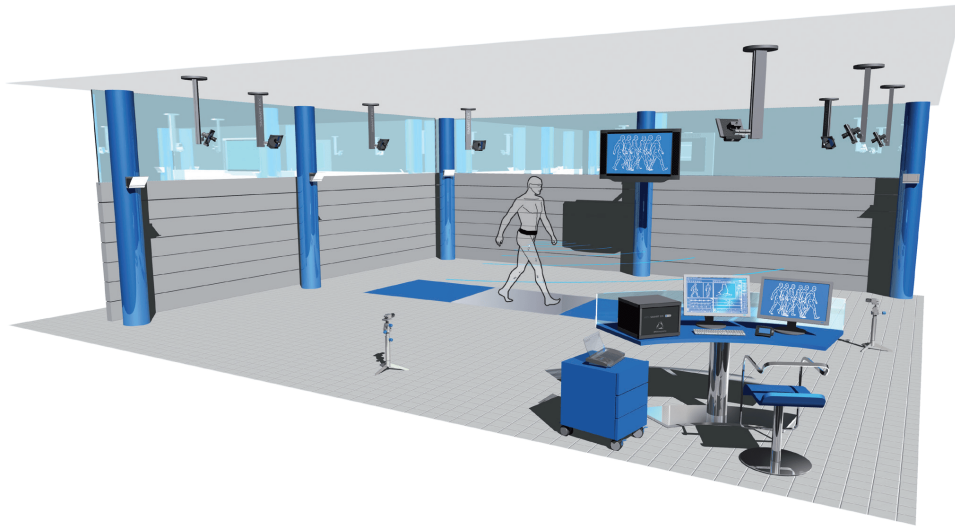
Figure 2.6: Motion Capture Laboratory Setup. A 3D visualization of a motion capture laboratory equipped with multiple cameras positioned around the perimeter for comprehensive biomechanical analysis. The system includes a walking platform for subject movement, force plates embedded in the floor, and a central control station with computers for data processing and real-time gait and posture metrics visualization. The setup is designed for detailed kinematic and kinetic evaluations in research and clinical applications

parameters and biomechanical data [58, 59]. Their portability and affordability make them particularly valuable for clinical and community applications. Wearable systems have proven effective in assessing gait impairments caused by conditions such as PD and post-stroke rehabilitation. For instance, studies have shown that IMUs placed on the lower back or shins can reliably track parameters such as stride length and cadence, offering critical insights into disease progression and treatment efficacy [60, 61]. Additionally, wearable devices have been employed to monitor bradykinesia and tremors in PD patients, enabling objective quantification of motor symptoms often subjectively assessed in clinical settings [62]. **Figure 2.7** illustrates the placement of wearable sensors on a subject, showcasing their distribution across the body for real-time biomechanical and gait analysis.

Despite their potential, wearable systems face challenges related to user compliance and technical constraints. Issues such as sensor misplacement, battery limitations, and data gaps from non-adherence can compromise the reliability of long-term monitoring [64]. Furthermore, the complexity of managing multiple sensors can deter widespread adoption, particularly in non-specialist settings. For detailed technical insights and advancements in wearable systems, see Chapter 3, **Section 3.1**.

Although marker-based systems offer unparalleled accuracy in controlled laboratory environments, their reliance on expensive equipment and invasive setups limits their accessibility and utility in real-world settings [65]. These limitations have driven the development of more accessible, markerless solutions that will be broadly discussed in the following subsection. Marker-Less-Based systems represent a significant advancement in GAn, addressing the limitations of traditional MB systems. By leveraging advancements in CV, AI, and ML, MLB systems eliminate the need for physical markers, offering a non-invasive and cost-effective alternative [66, 67]. **Figure 2.8** presents a markerless motion analysis framework, demonstrating the progression from the original scene to skeletal modeling using detected body landmarks.

These systems utilize video recordings to estimate joint positions, track movement trajectories, and calculate spatiotemporal parameters, enabling a more natural and accessible approach to study human motion. Marker-Less-Based systems allow for natural movement analysis in diverse environments, including homes, clinics, and community settings [24, 67]. This accessibility broadens their applicability, especially for populations with limited access to advanced laboratories. The applications of MLB systems span various domains. They have been employed in clinical settings to assess gait in patients with neurological conditions such as Parkinson's disease and post-stroke impairments [27]. In sports science, these systems aid in optimizing

Figure 2.7: Wearable Sensor Placement for Biomechanical Analysis. *Front and rear views of a subject equipped with wearable sensors positioned on the head, chest, arms, wrists, thighs, and legs. These sensors capture precise motion data for biomechanical and gait analysis. The setup allows for real-time monitoring of body movements, making it ideal for research on human motion and activity tracking. Adapted from [63]*

athletic performance by analyzing motion mechanics in real-time [24]. Furthermore, emerging applications include integrating MLB systems with wearable technologies for hybrid solutions that deliver more robust gait data [67].

Despite their promise, MLB systems are not without limitations. Occlusions, variability in lighting conditions, and algorithmic biases continue to challenge accuracy and reliability. Addressing these issues requires refining AI algorithms and improving data acquisition techniques. For further details on specific implementations and recent advancements in MLB systems, see **Chapter 3**, **Section 3.2.2**.

The development of new technologies has led to the creation of devices and methods that accurately assess various aspects of an individual's gait, providing healthcare professionals with valuable insights into treating various disorders [24]. These advancements have improved the precision of GAn and expanded its application beyond traditional lab settings, thanks to wearable and non-wearable systems that enable continuous and objective monitoring of gait patterns. Such innovations have enabled specialists to access reliable, real-time gait data in clinical and non-clinical environments [27].

2.2.2 Applications, Challenges and Future Directions

Gait analysis has broad applications across clinical, sports, and research domains. It is critical in diagnosing neurological disorders, guiding rehabilitation strategies, and monitoring disease progression. For example, GAn provides insights into motor impairments in conditions such as PD and stroke, enabling tailored interventions [61, 60]. In clinical contexts, gait analysis supports the early detection of neurodegenerative conditions and assesses the efficacy of therapeutic interventions. For instance, wearable sensors combined with motion analysis techniques have effectively quantified motor symptoms like bradykinesia and tremors in PD patients [62, 38]. Despite its potential, gait analysis faces several challenges. The variability in environmental settings, differences in methodologies, and technical limitations such as occlusion and sensor drift can affect data accuracy. Additionally, the cost and complexity of traditional systems often

Figure 2.8: Markerless-based Motion Analysis framework. A sequence of images illustrating the application of markerless motion analysis. The first image represents the original scene; the second shows detected key body landmarks, and the third connects these landmarks to create a skeletal model. This approach leverages computer vision techniques to analyze human motion without physical markers, enabling efficient and non-invasive movement assessment in various settings. Adapted from [68]

restrict their accessibility, particularly in resource-limited settings [27].

The field of gait analysis is evolving rapidly, with advancements in AI, ML, and wearable technology paving the way for more accessible, accurate, and personalized solutions. These developments aim to overcome the limitations of traditional systems and expand the reach of gait analysis to diverse environments. Emerging technologies enable real-time analysis of gait parameters by integrating AI models and IoT frameworks. For instance, IoT-enabled wearable devices can continuously monitor gait in home settings, transmitting data for remote analysis and personalized feedback [69, 70]. Advances in AI also facilitate the development of personalized rehabilitation programs. By analyzing individual gait patterns, these systems can recommend tailored exercises and monitor progress over time, enhancing therapeutic outcomes [38].

For detailed technical implementations of these advancements, refer to Chapter 3, **Section 3.1** and **Section 3.2.4**.

2.2.3 Spatiotemporal Gait Parameters

Gait Analysis involves measuring various parameters that quantify walking patterns, broadly classified into spatial and temporal parameters, collectively known as Spatiotemporal Parameters (STPs). These parameters assess symmetry, variability, and gait quality, providing critical insights into normal and abnormal gait [51]. Alterations in key parameters such as gait speed and stride length often signal potential declines in physical abilities or serve as prognostic markers for falls and cognitive impairments [51, 71, 21].

Key Parameters

Some key STPS commonly used in GAn [72, 71, 21, 73, 74, 75, 51] are described below and showed in **Figure 2.9**.

- **Step Length**: Step length refers to the distance between two successive occurrences of the same foot making contact with the ground. When both feet are in contact with the ground, the right step length can be measured by calculating the distance from the left heel to the right heel, expressed in meters (m) (**Figure 2.9**).

- **Stride Length**: Stride length refers to the distance between the first contact of one foot and the next first contact of the same foot. It is often described as "cycle length" measured in meters (m) (**Figure 2.9**).
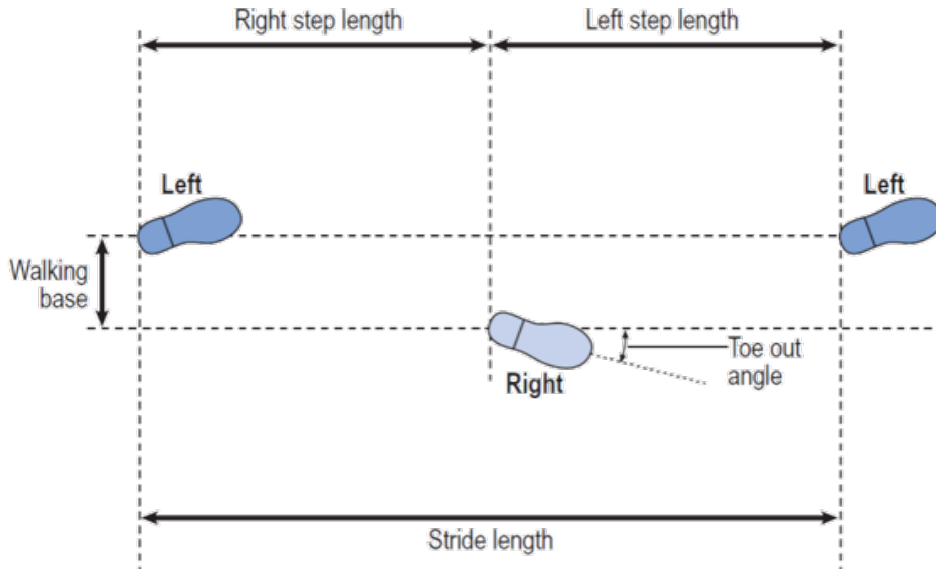
Figure 2.9: Spatial Gait Parameters. *A diagram illustrating key spatial gait parameters, including stride length, step length (left and right), walking base, and toe-out angle. These measurements are fundamental for analyzing walking patterns, assessing symmetry, and identifying gait abnormalities in biomechanical studies*

- **Stride Width or Walking base**: Stride width, or walking base, refers to the lateral distance between the two feet during walking. Variations in stride width are associated with balance and specific gait-related conditions (**Figure 2.9**).

- **Foot Progression Angle (FPA) or Toe Out Angle**: The Foot Progression Angle (FPA), or Toe Out Angle, quantifies the angle of foot orientation relative to the walking direction. Positive angles indicate toe-in patterns, while negative angles reflect toe-out movements [76] (**Figure 2.9**).

- **Cadence**: Cadence, or step frequency, denotes the number of steps taken per minute. Changes in cadence can indicate improvements or deteriorations in walking ability and are linked to walking intensity and functional mobility [77, 78].

$$\text{Cadence} = \frac{\text{steps}}{\text{min}}$$

- **Gait Velocity**: Gait velocity represents the speed at which an individual travels, measured in meters per second (m/s). It serves as a critical indicator of functional status, offering insights into physical, cognitive, and health outcomes [79, 80].

$$\text{Gait Velocity (m/s)} = \frac{\text{distance (m)}}{\text{time (s)}}$$

- **Step Duration**: Step Duration measures the interval between two consecutive occurrences of the same event on opposite feet. This parameter, expressed in seconds (s), is crucial for understanding an individual's walking rhythm.

$$\text{Step Duration (s)} = \frac{1}{\text{Cadence}} \times 60$$

- **Stride Duration or Gait Cycle Time**: Stride Duration (or GC time) is the temporal duration between consecutive initial contacts of the same foot. As a key temporal parameter, it provides insights into the overall rhythm of walking.

$$\text{Stride Duration (s)} = \frac{1}{\text{Cadence}} \times 60 \times 2$$

- **Gait Stability Ratio (GSR)**: The Gait Stability Ratio (GSR) is a critical parameter for assessing walking stability, particularly in older adults. It represents the ratio of cadence to gait velocity and provides dynamic insights into balance during walking [81].

$$\text{Gait Stability Ratio (GSR)} = \frac{\text{Gait Velocity (m/s)}}{\text{Cadence (steps/min)}}$$

- **Stance/Swing Ratio**: The stance/swing ratio measures the percentage of time a foot remains in contact with the ground versus in the air. This parameter typically split into 60% stance and 40% swing in normal gait, can help identify abnormalities caused by neurological or physical impairments.

$$\text{Swing/Stance Ratio} = \frac{\text{Swing Phase Duration (s)}}{\text{Stance Phase Duration (s)}}$$

Integration of Spatiotemporal Parameters in Markerless Systems

Advancements in Marker-Less-Based systems have enabled real-time dynamic assessments of these spatiotemporal parameters. Markerless systems utilize video recordings to estimate parameters like gait velocity, cadence, and stride length, providing valuable feedback to practitioners and healthcare professionals [66, 67].

Integrating STPs into markerless systems enhances their robustness, enabling applications in diverse environments such as clinics, homes, and community settings. These systems are particularly effective for:

- Identifying neuromuscular health indicators and fall risk predictors.

- Supporting long-term monitoring of complex motor disorders like Parkinson's disease and post-stroke impairments [82].

- Providing real-time feedback to improve adherence to therapeutic regimens.

Emerging advancements in AI models and IoT frameworks further enhance the utility of markerless systems. By automating parameter analysis and predicting disease progression, these tools are evolving as indispensable assets in clinical and research settings [83].

2.3 Neurological and Neurodegenerative Disorders

Neurological disorders, such as Stroke and PD, are diverse groups of ailments that cause substantial disability [84]. These disorders often lead to complicated impairments in multiple systems that adversely affect daily activities, exercise, and sports. Walking is commonly affected in most neurological disorders, leading to decreased quality and quantity of performance [85, 86]. For instance, the walking speed of post-stroke patients ranges from 0.18 to 1.03 m/s, much slower than the average walking speed of healthy people of the same age group, around 1.4 m/s [87].

The extent of these motor issues is usually measured in controlled settings by a clinician employing semi-quantitative scales such as the Parkinson's Disease Rating Scale (UPDRS) [88]. While the UPDRS is recognized for its reliable psychometric characteristics [89], its application is hindered by its dependence on an evaluator, time-consuming nature [90], and its intrinsic subjectivity. The inflexible approach of relying on questionnaire-based evaluation tools hampers the

ability to swiftly modify treatments in response to daily fluctuations in the patient's condition. Monitoring these fluctuations requires sensitivity to change and the ability to detect when variations in symptoms reach a minimum clinically important difference—the threshold at which a change is large enough to be considered meaningful in clinical decision-making. For instance, the phenomenon of freezing is more prevalent when medication is not active (Off-state) than when it is (On-state), indicating the need for real-time monitoring of freezing onset, frequency, and duration throughout the day to allow for prompt adjustment of the pharmacological treatment of PD [91].

Neurological conditions affect more than just how well a person can move; they also reduce the amount and type of physical activity a person participates in [92]. Not being physically active enough can seriously affect a person's mental well-being [93], their ability to socialize [94], and their overall quality of life concerning health [95]. The World Health Organization advises that adults with disabilities should engage in 150 to 300 minutes of moderate-intensity physical activity weekly [96]. Nevertheless, people with neurological conditions, such as those who have survived a stroke, often fail to meet these suggested levels of physical activity. For instance, research has shown that stroke patients typically reach only about 60% of the daily steps recommended for disabled individuals [97]. Likewise, individuals in the early stages of PD are reported to take only about 56% of the steps that healthy adults do in a day [98].

Motion analysis involves using advanced equipment that can determine mechanical variables, such as 3D joint kinematics, muscle activation patterns, muscle forces, and coordination patterns, which provide a non-invasive way of understanding the complex human physiology and motor control of human behavior. Research indicates that objective gait assessment, such as IMUs, can capture detailed spatiotemporal and kinematic data crucial for evaluating impairments and treatment efficacy in neurological and neurodegenerative disorders [99, 82]. In addition, recent advancements have enabled the integration of computational intelligence methods, which enhance the interpretation and prediction of gait characteristics, especially in the context of neurological rehabilitation and monitoring neurodegenerative conditions [100]. Such tools support healthcare professionals in precisely quantifying mobility impairments and predicting potential fall risks, a key concern in rehabilitating individuals with disorders like PD [101].

Marker-Less-Based systems have added new dimensions to neurological GAn. These systems leverage DL frameworks to detect subtle, non-cyclic gait irregularities in naturalistic settings. By tracking spatiotemporal parameters in real-time, MLB systems provide clinicians with valuable insights into disease progression and treatment outcomes [66, 67].

Spatiotemporal parameters derived from MLB systems have been particularly effective in identifying early indicators of conditions such as Huntington's disease and Multiple Sclerosis. These technologies allow real-time monitoring in home environments, improving accessibility for patients with mobility challenges [82, 83].

Researchers can identify how neurological disorders affect human behavior by analyzing these variables. For instance, post-stroke patients have a reduced capacity for leg propulsion on their affected limb, contributing to a slower walking speed [102]. However, patients who have suffered a stroke tend to walk using inefficient strategies. They depend more on the hip muscles for moving forward and less on the muscles of their ankle extensors [103, 104]. People with neurological issues, such as those who have had a stroke or have cerebral palsy, often face difficulty in moving their legs while walking [105, 106]. These swinging problems prevent them from moving forward and raise their chances of tripping and falling. In particular, these patients have been found to have a limited ability to bend their knee while swinging, leading to what is known as a 'stiff knee walk' [105, 106]. Several factors contribute to this condition, including a weaker push-off power from the ankle during pre-swing, a slower knee flexion speed at the same phase, and increased quadriceps activity in the thigh muscles [105, 107].

Unlike stroke-related conditions, neurodegenerative disorders such as PD present distinct motor challenges, including freezing, tremors, and rigidity, which interfere with maintaining balance [108]. Recent advancements in DL methods have introduced new opportunities to handle these non-cyclic and complex deviations by analyzing and predicting variations in motor symptoms across a spectrum of movement irregularities. DL-based approaches, particularly those employing Recurrent Neural Network (RNN) and Convolutional Neural Network (CNN), enable a continuous analysis of temporal and spatial gait data, allowing healthcare professionals

to track and interpret subtle, dynamic motor fluctuations in real-time. These models are particularly effective in accommodating inter-patient variability, capturing differences in symptom severity and manifestation across the disease spectrum. For instance, RNN and attention mechanisms have been used effectively to detect and classify freezing episodes, significantly improving the reliability and accuracy of gait assessments in PD [109]. Furthermore, by leveraging feature extraction capabilities, these systems offer enhanced detection of tremors and other motor symptoms, providing precise, automated insights to aid in treatment adjustments [110]. The robustness of DL models to noise and their adaptability to diverse symptom presentations ensure consistent system performance, even under varied conditions. Such DL methodologies improve system reliability through consistent monitoring and the detection of abnormal patterns that might be missed with traditional observational methods, thus enhancing the clinical utility of GAn for PD patients [67].

Future developments in MLB systems include leveraging generative AI models for automated analysis of gait parameters. These advancements aim to provide predictive tools for disease progression, therapy optimization and improved accessibility in low-resource settings [67, 82].

2.4   Artificial Intelligence in Healthcare

Artificial Intelligence is fundamentally reshaping the healthcare landscape, offering a broad set of advantages that significantly enhance patient care and the efficiency of healthcare systems [111, 112]. It employs intricate algorithms and software to replicate human cognition for analyzing complex medical data or inferring diagnoses by observing specific aspects of a subject. AI's capacity to analyze vast datasets enables the early detection of diseases, leading to timely interventions and improved patient outcomes [111]. Personalized analysis of patient data, including genetic information and lifestyle factors, allows AI to tailor treatment plans, increasing their effectiveness [112].

The escalating volume of clinical data and health records poses a significant challenge for healthcare professionals, and AI has emerged as a valuable ally in managing this burgeoning complexity [111]. Its capability to process, analyze, and derive meaningful insights from vast datasets alleviates healthcare professionals' information overload [112]. By leveraging AI-driven algorithms, healthcare providers can sift through extensive electronic health records and clinical data more efficiently, expediting decision-making processes and enabling healthcare professionals to focus on patient care rather than administrative tasks [113]. Furthermore, AI organizes and structures diverse data types, facilitating interoperability between different systems. This interoperability creates a comprehensive and cohesive view of a patient's medical history, leading to more informed diagnoses and personalized treatment plans [111].

Artificial Intelligence has proven transformative in medical imaging. Deep Learning models excel in analyzing radiological images to detect conditions such as tumors and fractures with precision rivaling or surpassing human experts [111]. For example, Convolutional Neural Networks are widely used in mammography to identify early-stage breast cancer, significantly reducing false negatives [112]. Moreover, neural networks classify biomarkers and sensor data to predict diseases, enhancing early intervention strategies [99]. Machine Learning also plays a pivotal role in predictive diagnostics. These models analyze longitudinal patient data to forecast health trajectories, such as survival probabilities or potential complications [114]. Notably, Generative Adversarial Networks (GANs) powered by ML have been employed to predict fall risks in elderly patients, contributing to preventative healthcare measures [115, 116]. Despite these successes, ML-based systems face significant limitations in healthcare applications. An efficient model often requires massive amounts of data, a challenge in fields like neuro telerehabilitation due to limited patient participation [117, 118]. Methods such as data augmentation using MLB biomechanical systems or leveraging smaller datasets with specialized techniques have been explored to address this. However, these approaches still require interdisciplinary collaboration to fully address the issue [119]. Furthermore, deploying AI on resource-constrained devices introduces challenges such as energy efficiency and computational limitations [120]. Techniques like pruning and quantizing have been proposed to reduce model complexity while maintaining acceptable levels of accuracy [121, 122]. Optimizing neural network architecture for specific hardware platforms is another avenue for improving efficiency and usability in constrained environments [122].

Beyond diagnostics, AI is deeply integrated with wearable sensor technologies. Inertial Measurement Unit sensors combined with ML algorithms enable continuous patient mobility monitoring, identifying subtle changes that could signify disease progression [99, 123]. These innovations are critical in advancing telemedicine and remote patient monitoring, extending quality healthcare to underserved areas [124].

Artificial Intelligence has been pivotal in transforming motion analysis, particularly in understanding gait patterns and diagnosing mobility impairments. Convolutional Neural Networks and s have revolutionized this domain, enabling real-time detection of gait abnormalities and enhancing the precision of diagnostic tools. By integrating AI with MLB systems, clinicians can analyze spatiotemporal parameters such as gait velocity, stride length, and cadence in both clinical and naturalistic settings [67, 82]. Artificial Intelligence-driven motion analysis tools are increasingly used in telemedicine and remote monitoring, providing clinicians with real-time data to track disease progression and personalize rehabilitation plans. These tools effectively identify subtle motor impairments in neurodegenerative disorders like PD, Huntington's disease, and Multiple Sclerosis [66, 83]. Additionally, generative AI models predict disease trajectories and optimize therapy outcomes based on patient-specific data.

Despite these advancements, motion analysis technologies face challenges in ensuring equity and accessibility. Variability in lighting conditions, environmental factors, and hardware capabilities can affect data quality and algorithm performance [119]. Emerging technologies hold promise for further advancements. Marker-Less-Based systems combined with wearable devices could enable real-time motion tracking, improving accessibility for patients in remote areas. Addressing variability in lighting conditions, environmental challenges, and algorithmic biases remains essential for ensuring robust and equitable applications across diverse populations. Furthermore, advancements in Explainable Artificial Intelligence (XAI) pave the way for greater transparency, allowing clinicians to understand the rationale behind AI-driven decisions and enhancing trust in these systems [67, 112]. The complexity of AI systems introduces interpretability and privacy concerns, which are critical in healthcare. Explainable Artificial Intelligence methods, such as post-hoc interpretation techniques and intrinsic interpretable models, aim to address these challenges [125, 126]. For example, visualizations of feature importance or local surrogate models provide insights into how decisions are made. Combining interpretable models with more complex neural networks allows for a balance between transparency and predictive power [127]. Techniques like enforcing sparsity in neural networks and using methods such as the Hadamard Product Parameterization enable selective input signal usage, enhancing both transparency and computational efficiency [127]. This is particularly beneficial in multivariate time series networks used for predictive analytics.

Artificial Intelligence's utility is not confined to clinical diagnostics but extends to streamlining hospital operations. It optimizes patient flow and resource allocation and even reduces wait times by dynamically scheduling appointments [128]. Such applications improve operational efficiency and enhance the patient-doctor interaction experience. In drug discovery, AI accelerates the process by analyzing molecular structures, identifying potential drug candidates, and reducing research time and costs [110]. However, significant challenges persist. Ensuring the ethical use of patient data remains paramount, as sensitive information is vulnerable to breaches [83, 112]. Moreover, biases in AI models, often stemming from imbalanced training datasets, can disproportionately affect underrepresented populations, necessitating rigorous validation protocols [111, 112]. Ethical and practical issues, such as integrating AI with existing healthcare infrastructure, also present obstacles. AI deployment can disrupt workflows, necessitating upgrades and training for healthcare professionals [111]. Transparency in AI models, especially through advancements in XAI, is crucial for building trust among clinicians and patients. For example, XAI techniques clarify how AI systems make diagnostic decisions, improving their acceptance in clinical settings [67, 112].

Future advancements must address current limitations. Overcoming challenges like environmental variability and ensuring equitable deployment across diverse populations will be critical for achieving clinical-grade accuracy. Improved ethical frameworks and rigorous data security measures are essential to mitigate concerns about privacy breaches and system reliability [111, 112]. As AI continues to evolve, its potential to revolutionize healthcare depends on addressing these challenges while maximizing its transformative capabilities.

Chapter 3

Technology and Systems

3.1 Wearable Systems

Wearable systems have emerged as a cornerstone of modern gait analysis, offering an alternative to stationary, lab-bound technologies. Equipped with sensors like IMUs, accelerometers, and gyroscopes, these systems provide continuous data on motion patterns, enabling both clinical and everyday applications [129, 130]. Inertial Measurement Unit sensors, in particular, combines accelerometers, gyroscopes, and magnetometers to capture linear acceleration, angular velocity, and orientation. This makes them highly effective for measuring gait parameters in rehabilitation and real-world environments, though challenges like calibration and signal drift persist. Recent innovations include pressure-sensitive insoles and smartphone-integrated accelerometers, which expand the accessibility of gait monitoring. For example, specialized insoles equipped with pressure sensors have demonstrated efficacy in capturing detailed gait metrics such as plantar pressure and force distribution during walking tasks [27]. Similarly, mobile applications utilizing smartphone gyroscopes and accelerometers have made gait analysis more accessible to the general population [131]. In rehabilitation contexts, wearable IMUs have been successfully deployed to monitor asymmetries in gait patterns post-stroke. For instance, during treadmill-based recovery sessions, sensors placed on the lower extremities have provided real-time feedback on stride length and limb coordination, improving rehabilitation outcomes [39]. Despite these advancements, wearable systems face limitations in spatial calibration and susceptibility to signal drift, particularly over extended durations. Advanced algorithms such as Kalman filters and adaptive ML models are being developed to address these issues, ensuring higher data fidelity [132]. Moreover, integrating wearables with IoT frameworks and telemedicine platforms is expected to enhance their utility for remote monitoring and personalized care.

Applications of Wearable Systems

Wearable systems are widely employed in rehabilitation to monitor gait patterns and provide real-time feedback. For instance, IMUs placed on the lower extremities track stride length and cadence during treadmill-based recovery sessions, helping post-stroke patients improve limb coordination [39]. These sensors enable frequent, individualized treatment strategies, even outside clinical settings, enhancing rehabilitation outcomes.

Wearable devices are invaluable for patients with neurological illnesses like PD. Unlike subjective clinical assessments, wearable sensors objectively quantify symptoms such as bradykinesia, tremor, and stride abnormalities [60, 133]. Stride length, a critical gait parameter, correlates with bradykinesia and disease progression, aiding early diagnosis and long-term monitoring [62]. In addition, accelerometers and gyroscopes quantify tremor frequency and amplitude. However, distinguishing between tremors caused by PD and other conditions like essential tremor remains challenging [134]. Mobile apps equipped with accelerometers have been introduced for home monitoring, though further validation is required to ensure diagnostic relevance and patient benefits [135].

Beyond clinical contexts, wearable systems have shown promise in monitoring activities of daily living. Using ML algorithms, these devices classify activities such as standing, walking, sitting, and transitioning between postures [136]. Sensors placed on the lower back, thighs, or feet

enable detailed tracking, supporting independent living and rehabilitation. For example, upper-limb activities like brushing teeth are monitored with wrist-mounted sensors, while lower-limb activities often utilize sensors on the chest or feet. This data informs improved rehabilitation protocols and provides real-time feedback for caregivers and patients.

Challenges, Innovations, and Future Directions

Despite their utility, wearable systems face challenges in user adherence. Studies show significant dropout rates, with 32% of users discontinuing devices within six months and over 50% stopping after a year [64]. Barriers include the inconvenience of wearing devices, proper sensor placement, and regular charging, especially for individuals with physical impairments. For instance, pressure-sensitive insoles require precise placement and consistent maintenance, which can deter long-term use.

To mitigate these issues, sensor technology and data analytics advancements are addressing usability concerns. Miniaturization and extended battery life reduce the inconvenience of wearables, while data imputation algorithms minimize the impact of missing data [64]. Adaptive ML models are also being developed to work with incomplete datasets, improving long-term adherence and ensuring data reliability.

Technical challenges, such as sensor drift and occlusions, are being tackled with innovative solutions. Kalman filters effectively mitigate drift, while generative models for pose estimation enhance accuracy in markerless systems [132, 69]. These innovations pave the way for robust, long-term monitoring and analysis.

Future research should prioritize minimally invasive systems that emphasize user comfort and convenience. Combining advancements in sensor technology, data science, and user-centered design requires a multidisciplinary approach. Integrating wearable systems with IoT and telemedicine platforms promises significant progress in remote healthcare.

Wearable devices hold immense potential for populations with gait-related pathologies, such as PD, enabling early diagnosis, personalized treatment, and long-term care. By addressing existing challenges and incorporating user-friendly features, wearable systems can continue evolving, offering accurate and effective solutions for clinical and everyday applications.

Among the diverse wearable technologies, IMUs sensors have gained significant attention due to their versatility and cost-effectiveness. The following subsection provides a detailed exploration of their components, applications, and challenges.

3.1.1 Inertial Measurement Unit Sensors

Inertial Measurement Unit sensors have emerged as a feasible and cost-effective alternative to traditional MB-MoCap systems used in GAn laboratories. By analyzing the motion signals captured by IMUs, researchers can measure various aspects of human gait and conduct GAn [129, 130]. Inertial Measurement Unit sensors consists of 3D accelerometers, gyroscopes, and magnetometers, which provide a comprehensive understanding of linear acceleration, angular velocity, and magnetic orientation [132, 137]. **Figure 3.1** illustrates the axes and rotational movements of an IMU, showcasing its role in capturing motion dynamics across multiple dimensions.

These components collectively enable the reconstruction of motion patterns and detailed biomechanical analysis. **Figure 3.2** illustrates the axes of measurement for accelerometer, gyroscope, and magnetometer sensors.

Inertial Measurement Unit sensors are preferred over traditional MB-MoCap systems in clinical practice due to their portability and reliability [24]. These sensors are lightweight, wearable, and capable of providing continuous motion data without requiring large, fixed infrastructures. This makes them particularly advantageous for real-world applications, such as remote monitoring of patients or conducting gait assessments outside controlled laboratory settings.

However, the number and placement of IMU sensors are critical considerations that can significantly influence the accuracy and complexity of GAn. Inertial Measurement Unit sensors are typically attached to key anatomical landmarks, such as the lower back, thighs, shins, and feet, to capture a holistic view of movement. Increasing the number of sensors improves the resolution and reliability of the captured data but also raises the computational and logistical
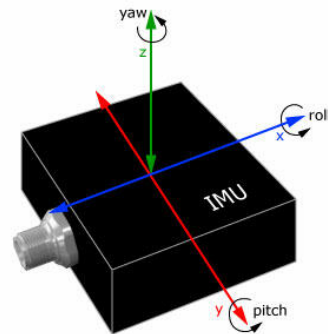
Figure 3.1: Inertial Measurement Unit (IMU) Axes and Rotations. *A schematic representation of an Inertial Measurement Unit (IMU) displaying its three principal axes (X, Y, Z) and corresponding rotational movements: roll, pitch, and yaw. IMUs are widely used in motion analysis to measure orientation, angular velocity, and acceleration, providing critical data for biomechanics, robotics, and navigation systems applications*

Figure 3.2: Components of an Inertial Measurement Unit (IMU). *A diagram illustrating the three primary sensors within an Inertial Measurement Unit (IMU): the accelerometer, gyroscope, and magnetometer. The accelerometer measures linear acceleration along the X, Y, and Z axes, the gyroscope detects angular velocity or rotation around these axes, and the magnetometer provides orientation relative to the Earth's magnetic field. Together, these components enable precise motion tracking and spatial orientation in various applications*

challenges. Each additional sensor node introduces more data streams that require synchronization, calibration, and interpretation, thereby increasing the processing time and the expertise needed to manage the system effectively. In contrast, using fewer sensors simplifies the setup but may compromise the fidelity of the captured data, particularly for complex movements or multi-planar activities. Researchers must, therefore, strike a balance between accuracy and practicality when determining the number of sensors to deploy.

Another limitation of IMUs is their inability to achieve direct spatial calibration. Unlike optoelectronic systems that use camera triangulation to reconstruct 3D coordinates, IMUs rely solely on local acceleration and angular velocity measurements relative to the sensor's position and orientation. This makes it challenging to map motion data onto a global spatial frame, particularly when capturing movements involving significant direction changes or complex trajectories. Moreover, environmental factors, such as magnetic interference, can further affect the reliability of orientation data provided by magnetometers. These spatial calibration issues limit the applicability of IMUs in scenarios requiring high-precision 3D motion reconstruction, such as surgical planning or high-performance sports analysis.

Inertial Measurement Unit sensors are highly sensitive to signal drift, a phenomenon where cumulative errors in gyroscope readings lead to inaccurate estimated orientation over time. This drift arises from integrating small errors in angular velocity measurements, which compound during prolonged recordings. While advanced algorithms such as Kalman filters and complementary filters can mitigate drift, the success of these techniques depends on regular calibration and reliable baseline data [27, 138]. Periodic recalibration is necessary to realign sensor readings with known reference points, which can be time-intensive and impractical in certain clinical or field settings. Additionally, the quality of calibration directly influences the reliability of the data; poor calibration can propagate errors throughout the analysis, potentially compromising the clinical utility of the results.

Despite these challenges, IMUs offer unique advantages in capturing unbiased, real-time evaluations of gait parameters, such as step length, cadence, and walking speed. Wearable sensors can be placed directly on patients during daily activities, enabling data collection in naturalistic environments rather than controlled laboratory conditions. This approach provides valuable insights into functional gait performance, which is often difficult to replicate in clinical settings [139, 140].

However, using IMUs is not without operational trade-offs. The large volume of data generated requires substantial computational power for processing and interpretation, often necessitating specialized software and expertise. Machine Learning algorithms are increasingly employed to automate feature extraction and identify clinically relevant patterns from raw IMU data. Still, these methods also require careful validation and tuning to ensure accuracy and reproducibility. Furthermore, the reliance on wearable sensors introduces challenges related to patient compliance, as improper attachment or detachment during use can affect data quality and consistency.

Integrating AI and ML with IMUs technology could address many of these limitations. Advances in telemedicine and IoT are already expanding the utility of IMUs for remote gait assessment, offering continuous monitoring in diverse settings. With robust validation, AI-driven approaches could unlock deeper insights into clinically relevant gait features, enabling early detection of neurodegenerative conditions and other mobility disorders.

In conclusion, IMUs represent a promising and flexible tool for GAn, offering significant advantages in portability and accessibility. However, their effectiveness depends on addressing key limitations such as spatial calibration, signal drift, and the trade-off between sensor complexity and data fidelity. Ongoing advancements in sensor technology, algorithm development, and user-friendly interfaces will be crucial in enhancing the applicability of IMUs in clinical and research settings.

3.2 Camera-based Systems

Camera-based systems represent a compelling alternative to traditional IMUs for non-intrusive GAn in natural environments. Methods such as Infrared (IR) thermography and depth cameras enable high-resolution tracking of human walking patterns [141, 142]. Moreover, innovative

approaches like the PEM-ID system have addressed challenges like multi-occupant environments and privacy concerns [143, 144]. However, these methods face hurdles, including reliance on line-of-sight clarity and environmental consistency.

Both MB and MLB MoCap systems have undergone significant advancements, addressing their respective limitations and expanding their applications. Recent efforts to integrate the strengths of both MB and MLB systems have led to hybrid models. For instance, sparse marker placement combined with markerless motion capture algorithms has enhanced precision while maintaining MLB systems' flexibility. Such approaches are particularly useful in neurorehabilitation, where both accuracy and ease of use are critical [145]. Innovations in MB systems have focused on minimizing skin motion artifacts and improving real-time data processing. Modern systems now include automated marker placement algorithms and high-speed cameras capable of capturing rapid movements with minimal latency [56]. Marker-Less-Based systems have benefited from advancements in deep learning and computer vision, particularly in human pose estimation. Models like OpenPose and DeepLabCut enable accurate tracking of joint angles and spatiotemporal parameters, even in dynamic and crowded environments [70, 146]. However, challenges such as occlusion and environmental dependencies remain, necessitating further refinement. Developing robust hybrid systems and improved deep learning models is expected to bridge the gap between MB and MLB systems, creating solutions that balance precision, accessibility, and scalability. Edge computing and privacy-preserving algorithms are also poised to enhance the practicality of MLB systems for in-home and community-based applications [48].

Marker-Based systems, including optoelectronic MoCap systems, remain the gold standard for clinical GAn due to their precision [56]. However, their high cost and impracticality in real-world settings limit their adoption. Multi-camera approaches offer a partial solution by reconstructing 3D postures, but their installation complexity and calibration requirements hinder practical implementation. Research continues to explore single-camera systems as a cost-effective alternative. These systems leverage CV and DL advancements to reconstruct 3D human postures from 2D inputs, enabling broader accessibility and reduced costs [147]. **Figure 3.3** compares 3D reconstruction methods: (a) illustrates the use of multi-camera systems for precise posture reconstruction, while (b) demonstrates how 3D data can be derived from 2D camera views, reflecting advancements in MLB motion analysis.

Human Pose Estimation models address challenges like data loss during limb overlapping by predicting joint locations. Algorithms such as the Kalman Filter and Frequency Domain Filter enhance the accuracy of these predictions by mitigating noise and uncertainty [69]. While the Kalman Filter combines noisy measurements with predictive values under a Gaussian model, the Frequency Domain Filter leverages frequency domain energy to recover de-noised signals. Combining these techniques improves joint angle estimations, particularly in low-confidence scenarios.

Despite advancements, privacy concerns and environmental dependencies remain significant obstacles to adopting visual-based methods in residential settings. The balance between technological accuracy and user privacy is crucial for further exploration.

Within the realm of camera-based motion capture, marker-based and markerless systems represent two dominant methodologies, each with unique strengths and limitations. The following subsection explores these approaches in greater detail, comparing their applications, challenges, and future potential.

3.2.1 Marker-based vs Markerless-based Motion Capture Systems

Marker-Based and MLB MoCap systems are two dominant methodologies for capturing and analyzing human motion. Both have unique strengths and limitations, making their selection dependent on the specific application and context. Marker-Based systems, such as optoelectronic MoCap solutions, are considered the gold standard for motion analysis due to their unparalleled accuracy. By attaching reflective markers to the body, these systems track motion with sub-millimeter precision using specialized cameras [56, 148]. Their widespread adoption in clinical and research settings stems from their ability to capture complex movements and provide detailed 3D kinematic data. However, their high cost, complex setup, and dependency on controlled environments make them less suitable for real-world applications. Additionally, the reliance on physical markers can introduce variability due to skin movement artifacts and
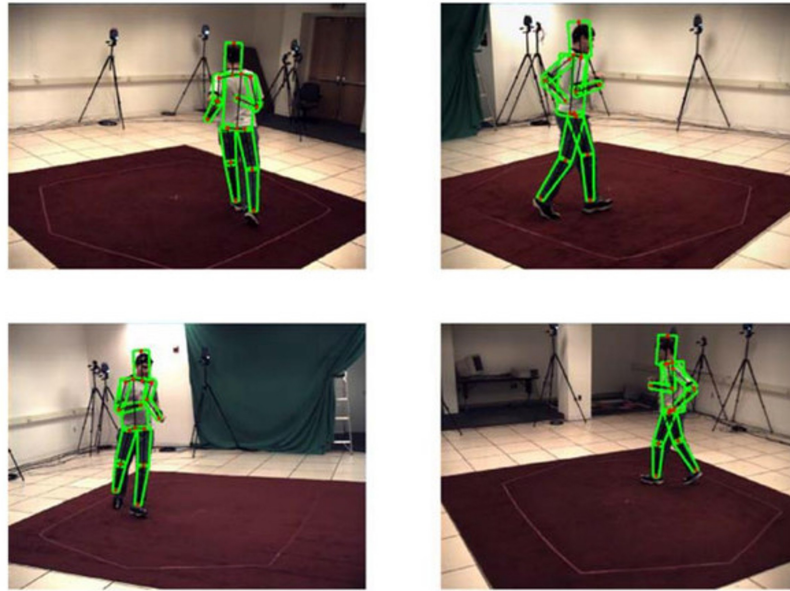
(a) 3D Reconstruction from Multi-Camera Systems
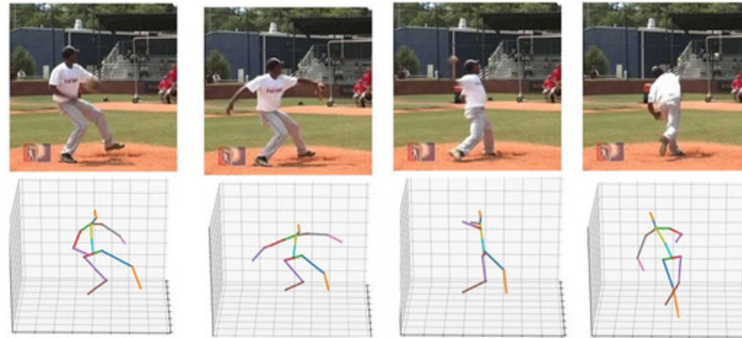
(b) 3D Reconstruction from 2D Camera Views

Figure 3.3: Comparison of 3D reconstruction methods. *(a) using multi-camera systems and (b) deriving 3D data from 2D camera views. These techniques demonstrate the progression from traditional marker-based setups to markerless motion analysis methods. Adapted from [48]*

discomfort for participants [65].

In contrast, Marker-Less-Based systems eliminate the need for physical markers, leveraging CV and DL algorithms to estimate joint positions from video data. These systems offer a less intrusive and more naturalistic approach, making them ideal for real-world and at-home assessments [149, 150]. Marker-Less-Based systems are cost-effective and easier to set up, but their accuracy can be affected by self-occlusion, environmental lighting, and the quality of pose estimation algorithms [151, 152]. While recent advancements in HPE algorithms have closed the gap in precision, MLB systems still struggle in highly dynamic or crowded environments [70, 48].

While MB systems excel in controlled environments requiring high precision, MLB systems prioritize accessibility and scalability. For instance, MB systems are indispensable for applications demanding absolute accuracy, such as surgical planning or high-performance sports analysis. Conversely, MLB systems are better suited for large-scale, cost-sensitive studies or environments where setup constraints make marker placement impractical. Studies have shown that MLB systems are approaching the error rates of MB systems in joint center localization, particularly for sagittal plane movements [153, 154]. However, discrepancies remain, especially at complex joints like the hip, where physical palpation in MB setups provides an advantage [155, 148].

Integrating the strengths of both systems could pave the way for hybrid solutions. For example, combining sparse marker placement with MLB technologies could enhance precision while maintaining ease of use. This approach would be particularly beneficial in applications requiring high accuracy and flexibility, such as neurorehabilitation or biomechanics research [156, 145].

In conclusion, the choice between MB and MLB systems should be guided by the specific requirements of the study or application. While MB systems remain the benchmark for precision, MLB systems are rapidly evolving to meet the demands of cost-effective, scalable, and real-world motion analysis. Continued advancements in computer vision, pose estimation, and dataset quality will further narrow the gap, potentially redefining the gold standard in motion capture.

3.2.2 Markerless Motion Systems Applications

MLB motion capture systems have emerged as a transformative tool in clinical, sports, and research applications. Unlike MB systems, which rely on physical markers and controlled environments, MLB systems use DL algorithms and CV techniques to estimate joint positions from video data. This shift has revolutionized motion analysis by eliminating invasive setups and enabling studies in more naturalistic settings [149, 150]. Marker-Less-Based systems consist of two stages, as depicted in **Figure 3.4**.

- **Stage one**: is the offline stage, where the model is designed and trained using DL-based algorithms considering manually annotated data.

- **Stage two**: the visual information is input into the trained model to estimate the human body pose (so-called human pose estimation) [66].

These stages form the foundation of markerless motion capture systems, enabling their application in diverse scenarios.

Marker-Less-Based MoCap systems can be categorized into two primary families of camera systems, with and without depth-sensing cameras [66, 48]. Systems with depth-sensing cameras record a standard video and simultaneously record the distance between each pixel and the camera. Depth cameras, such as Microsoft Kinect, have demonstrated reliability in capturing key gait parameters, including step time and walking speed, though their performance can be affected by dynamic environments [157, 158]. Depth-sensing cameras have a few drawbacks, such as capture rate, limited working range, and controlled lighting conditions [157, 159, 48]. **Figure 3.5** illustrates the use of depth-sensing technology in markerless motion capture, highlighting its ability to generate precise 3D motion data through an RGB camera, IR sensor, and IR emitter.

Recent advancements include single-camera systems that utilize HPE models like OP, DeepLab-Cut, and AlphaPose, which can estimate 3D joint positions from 2D video frames, significantly
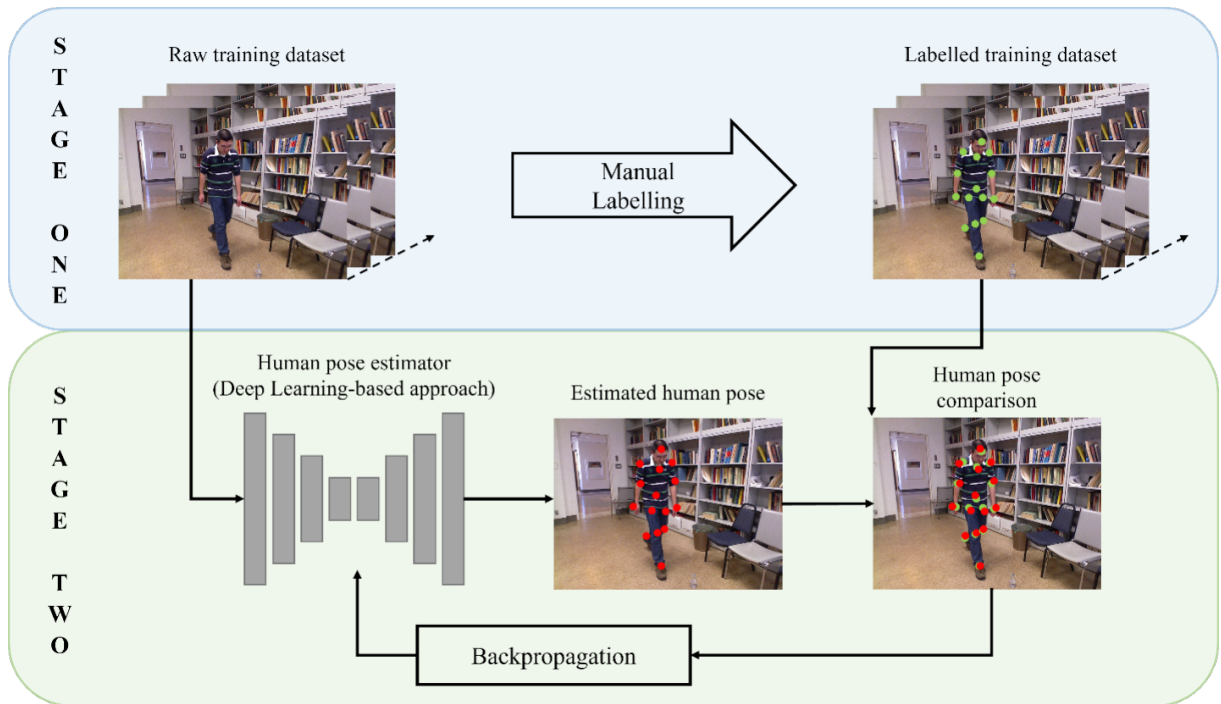
Figure 3.4: Schematic drawings of a general markerless motion capture system overview. *Stage One involves manual labeling of raw training data to create a labeled dataset, while Stage Two utilizes a backpropagation method for human pose estimation. Modified from "Applications and limitations of current markerless motion capture methods for clinical gait biomechanics", by Wade, L., 2022 2007, Developmental Psychology, 43, p. 1515 ([48])*
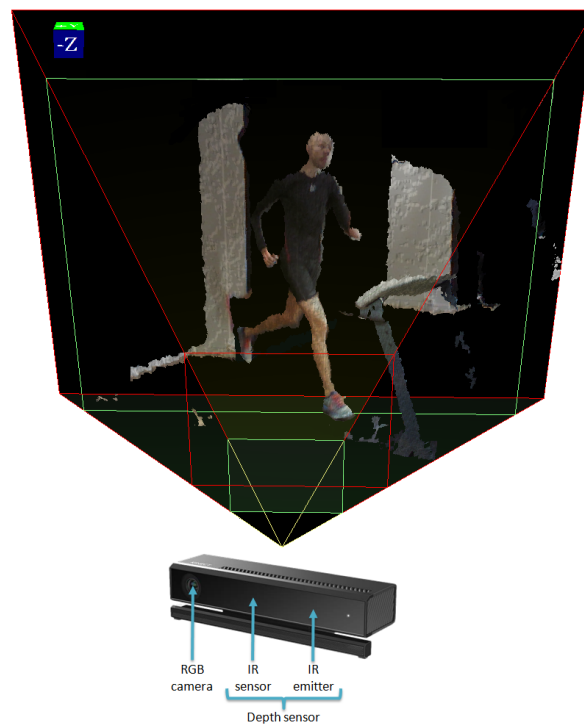
Figure 3.5: Depth Sensor for Markerless Motion Capture. *A representation of depth-sensing technology used in markerless motion capture. The top image illustrates a 3D reconstruction of a runner on a treadmill, captured using a depth sensor. The bottom diagram shows the components of the sensor, including an RGB camera, an IR sensor, and an IR emitter. This system generates depth data for precise motion analysis, enabling tracking body movements without physical markers. Image adapted from [160]*

enhancing accessibility [70, 152]. In clinical settings, MLB systems have been used to monitor rehabilitation progress in stroke patients. For instance, studies utilizing DeepLabCut have shown high accuracy in detecting asymmetries in joint angles during walking tasks, offering valuable insights into recovery trajectories [27, 153]. Similarly, systems like AlphaPose have been applied to analyze gait disturbances in patients with Parkinson's disease, enabling precise tracking of motor symptoms such as bradykinesia and tremors [161]. Marker-Less-Based systems face significant challenges in achieving precision comparable to MB systems, particularly in complex environments or when dealing with occlusions. Techniques such as the Kalman Filter and Frequency Domain Filter have been employed to enhance data accuracy by mitigating noise and improving signal reliability [69]. Future advancements are expected to include the integration of generative AI models and edge computing for real-time, privacy-preserving data analysis.

These advancements have been pivotal in extending the utility of MLB systems into clinical applications, where they play a critical role in assessing and monitoring neurodegenerative and motor impairments. Marker-Less-Based MoCap systems have shown great promise for clinical applications, enabling precise assessment of gait parameters and movement patterns without the constraints of traditional marker-based systems. These systems are particularly valuable for diagnosing and monitoring neurodegenerative diseases, such as PD, Alzheimer's Disease, and stroke-related motor impairments [162, 48]. These systems reduce patient discomfort and streamline the data collection process by eliminating the need for markers.

MLB solutions have demonstrated comparable accuracy in clinical settings to traditional marker-based systems for specific applications. For instance, Eichler et al. (2018) employed a multi-camera system using Microsoft Kinect sensors to assess stroke patients via the Fugl-Meyer Assessment, achieving results consistent with marker-based systems [163]. Similarly, Moro et al. (2020) used DeepLabCut to extract sagittal joint angles in stroke patients, revealing significant differences between affected and unaffected limbs while maintaining high reliability [153]. These findings underscore the potential of MLB solutions to facilitate accessible and cost-effective clinical evaluations.

Emerging technologies like OP, AlphaPose, and DeepLabCut are pivotal in advancing MLB GAn. Martinez et al. (2018) utilized OP to analyze walking cadence and calculate abnormality scores for PD patients, providing clinicians with objective insights into disease progression [164]. Shin et al. (2021) demonstrated that MLB systems could reliably detect subtle gait disturbances in PD patients, offering sensitivity beyond traditional observational methods [161]. These examples highlight the importance of integrating MLB technologies into clinical workflows to improve diagnostic accuracy and treatment planning.

Additionally, 3D HPE has emerged as a critical area of focus, offering a depth dimension to complement 2D joint center locations. Tools like iPi Motion Capture, The Captury, and Theia3D leverage multi-camera setups and depth sensors to achieve high accuracy in kinematic analyses [165, 166, 167]. For example, Kotsifaki et al. (2018) validated the iPi system for assessing sagittal plane knee range and peak angles during functional movement tasks, reporting excellent agreement with marker-based systems [168].

While promising, these systems face limitations, including lower accuracy in detecting hip joint centers and challenges in dynamic or uncontrolled environments. Addressing these gaps requires advancements in dataset labeling, pose estimation algorithms, and system calibration [148, 48]. As technology evolves, integrating MLB MoCap into neurorehabilitation and other clinical domains offers the potential to revolutionize patient care through enhanced accessibility and efficiency.

3.2.3 Commercial Markerless Motion Capture Systems

Several commercial MLB MoCap systems offer diverse clinical, research, and performance application capabilities. These systems leverage advanced computer vision and machine learning techniques to provide reliable, marker-free solutions for motion analysis. Below are key examples of such systems and their applications:

1. iPi Motion Capture: This scalable software supports 1 to 4 depth sensors or 3 to 16 standard cameras to capture 3D human body motions and generate animations. Kotsifaki et al. (2018) validated its application for assessing sagittal plane knee range during functional

movements using a two-camera setup with Microsoft Kinect v2, reporting excellent agreement with marker-based systems [168]. The iPi system requires optimal setup conditions for reliable measurements despite its flexibility.

2. The Captury: This system employs commercial video cameras and sequential computer vision algorithms to estimate human silhouettes and generate 3D motion data. Harsted et al. (2019) found that The Captury produced acceptable agreement levels for variables like jump height and knee flexion but cautioned against interchangeable use with marker-based systems [169]. These findings highlight its potential for applications requiring moderate precision.

3. Theia3D: Using CNN, Theia3D has been validated in controlled laboratory settings for gait analysis. Studies by Riazati et al. (2022) demonstrated low measurement errors for temporospatial parameters and lower extremity kinematics, making it a promising tool for community and clinic-adjacent settings [156]. This system exemplifies how ML models advance 3D pose estimation with greater accessibility and usability.

4. SIMI Shape 3D: This system uses advanced segmentation and tracking algorithms to capture motion without markers. While promising, there is a lack of peer-reviewed studies validating its accuracy or clinical relevance, leaving its potential applications largely unexplored [170].

These commercial systems illustrate the growing diversity and capability of MLB MoCap technologies. However, challenges such as accuracy, environmental dependencies, and high costs remain. As the field progresses, improving system robustness, expanding validation studies, and refining data processing algorithms will be essential to unlocking the full potential of these technologies in clinical and research domains. Addressing gaps in current systems involves improving the labeling of datasets, refining pose estimation algorithms, and enhancing the usability of commercial solutions in dynamic environments. Further development of open-source tools and their integration with commercial systems could democratize access to high-quality gait analysis, especially in resource-limited settings.

3.2.4 Future Perspectives and Technological Advancements in Markerless Motion Capture Systems

Marker-Less-Based MoCap systems hold immense potential to transform clinical, sports, and rehabilitation domains. Despite significant advancements, these systems face challenges in achieving the precision and reliability of MB systems, particularly in complex environments. Future developments aim to address these challenges and broaden the applicability of MLB systems, paving the way for transformative applications.

A key area of innovation lies in integrating artificial intelligence (AI) to enhance human pose estimation algorithms. Deep learning frameworks have already significantly improved the accuracy of joint localization and motion tracking. AI-driven techniques such as automated error correction and robust pose estimation models are expected to mitigate low-confidence predictions and improve performance in challenging environments. Furthermore, AI has the potential to enable real-time motion analysis, making MLB systems more practical for use in clinical and sports settings [48, 147].

The enhancement of datasets is another critical priority. Current systems often rely on open-access datasets with inconsistent labeling and limited biomechanical annotations. High-quality, standardized datasets tailored to clinical applications are essential to training more reliable models. Collaborative efforts to expand datasets to include diverse motion types and demographics will significantly improve the accuracy and applicability of MLB systems across various populations [155, 148].

Hybrid systems that combine the strengths of MLB and MB technologies represent a promising direction for overcoming current limitations. For example, selectively deploying markers with MLB systems can enhance tracking precision in regions like the hip joint, which often experiences significant errors. This approach balances the high accuracy of MB systems with the

accessibility and flexibility of MLB systems, offering practical solutions for contexts where full marker-based setups are impractical [156, 145].

MLB systems must overcome environmental challenges inherent to uncontrolled settings to achieve widespread real-world implementation. Variations in lighting, occlusions, and dynamic backgrounds often compromise system performance. Advances in computer vision, such as 3D reconstruction and improved scene understanding, are critical for addressing these issues. Additionally, the miniaturization of depth cameras and the integration of wearable technologies could expand the usability of MLB systems in real-world scenarios, enabling more naturalistic motion capture [150, 161].

Privacy-centric designs are essential as MLB systems become increasingly prevalent in home and community settings. Privacy concerns, especially in residential applications, can deter users and limit adoption. Innovations in edge computing allow data processing to occur locally, minimizing the need for cloud storage and reducing privacy risks. Anonymization techniques and secure data transmission protocols further enhance trust and usability, ensuring that privacy concerns are adequately addressed [171].

Looking ahead, technological advancements continue to reshape the landscape of gait analysis. Generative AI models and deep learning frameworks are improving accuracy in human pose estimation while addressing persistent issues such as occlusions and noise. Integrating Internet of Things (IoT) technologies with MLB systems enables continuous remote monitoring of gait parameters, supporting telemedicine initiatives and allowing clinicians to receive real-time updates on patient progress. These advancements ensure that gait analysis remains at the forefront of accessible, efficient, and scalable healthcare solutions [69].

In conclusion, MLB motion capture systems are poised for widespread adoption as advancements in AI, dataset quality, hybrid approaches, and privacy-preserving technologies continue to address current limitations. By tackling these challenges and pushing the boundaries of innovation, MLB systems can revolutionize motion analysis, offering accessible, accurate, and non-intrusive solutions for clinical, sports, and rehabilitation applications. As the technology evolves, its readiness for complex, real-world environments will define its success and transformative potential.

3.3 Development of the Marker-less Gait Analysis System

3.3.1 Introduction

Marker-Less-Based human motion tracking systems based on a single RGB camera have been developed to perform HPE and body segments in two dimensions (2D). Open-source CNN like OP [70] and PoseNet [172] have been proposed as effective solutions for 2D single and multi-person pose estimation. These systems can accurately track a person's movements, determine the locations of their body joints, and extract consistent angular information, regardless of the camera's perspective projection, even without depth sensors. For instance, the OP library relies on a two-branch multistage CNN trained with monocular image data to detect multiple people's joints in real-time using an image or video frame as input, achieving both speed and accuracy. Therefore, these systems can estimate human joint points using 2D images or videos with CNNs, representing a valuable tool for various applications such as human-computer interaction, activity recognition, and rehabilitation.

3.3.2 State of the Art

While human skeleton points offer stable and precise 2D positions of body joints in a given scene, they lack information on joint angles. Studies have attempted to estimate body joints using OP. In [173], authors utilized OP, two webcams, and a linear triangulation algorithm to evaluate the accuracy of IMUs using three camera setups. The study discovered discrepancies between an OP-based system and IMUs, with back-lateral and latero-lateral camera configurations yielding better results than back-lateral configuration, which resulted in the worst condition. The variations were attributed to OP's capability to determine joint center coordinates, locomotion activity, and camera position. This could result in occlusion of body joints during the GC. Despite the potential benefits of a 2D knee angle estimation system based on OP, it has been
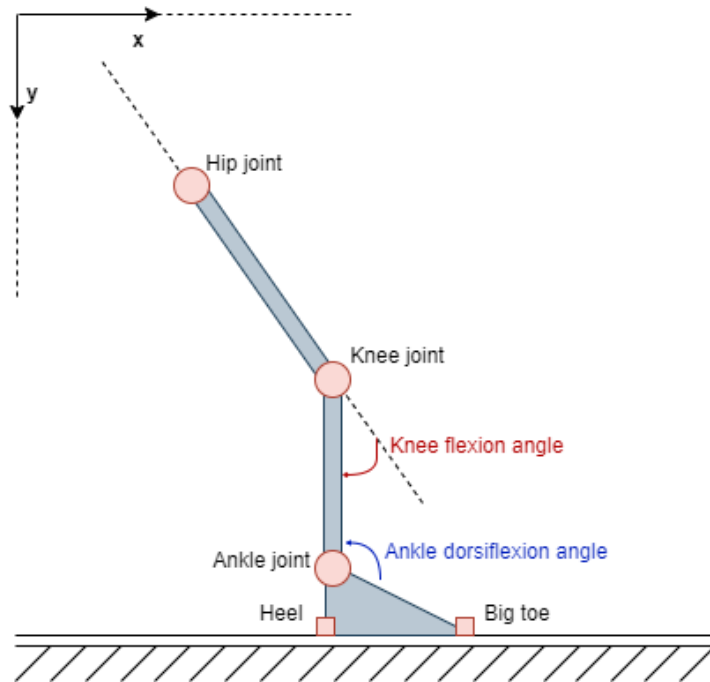
Figure 3.6: Joint Angle Representation. *Visualization of knee flexion and ankle dorsiflexion angles in a biomechanical context. The diagram highlights the hip, knee, ankle, and foot joints with respective angles, showing the relationships between the segments*

reported that only a few researchers have endeavored to verify its accuracy. In [174], the authors effectively validated the performance of such a system. By using a simple phone camera and a personal computer, authors successfully measured knee flexion/extension angles. The method was validated by evaluating the impact of ambient lighting, and it exhibited a high degree of tolerance to considerable changes in lighting conditions. The study concluded that the OP-based system for measuring knee angles is more effective than the Kinect.

3.3.3 Lower Limb Joint Angles Extraction from Video

The 2D position, in pixels, of lower limbs' body joints was extracted using the *body_*25 OP model. This model detects 25 key-points in a human pose, including the head, neck, shoulders, elbows, wrists, hips, knees, and ankles. The 2D position information was used to compute the knee flexion and ankle dorsiflexion angles. The hip, knee, and ankle 2D position information were used to compute the knee flexion angle. The knee, ankle, and toe 2D position information was used to compute the ankle dorsiflexion angle, as shown in **Figure 3.6**.

The knee flexion angle is a biomechanical measurement that quantifies the degree of bending or flexion occurring at the knee joint. It represents the angular displacement between two segments of the lower limb: the thigh and the lower leg. The angle is determined by assessing the positions of key anatomical landmarks, such as the hip joint, knee joint, and ankle joint. The ankle dorsiflexion angle is a biomechanical measure that quantifies the degree of dorsiflexion, which is the upward movement of the foot towards the shin, occurring at the ankle joint. This angle is determined by assessing the positions of key anatomical landmarks, specifically, the knee joint, the ankle joint, and the foot. Knee flexion and ankle dorsiflexion angles were measured by considering the angle between two segments. For knee flexion assessment, the relevant segments included the distance from the hip to the knee joint and from the knee to the ankle joint. In the case of ankle dorsiflexion, the segments considered were the distance from the knee to the ankle joint and from the ankle joint to the proximal end of the big toe. Equation **(3.1)** was used to compute the angles.
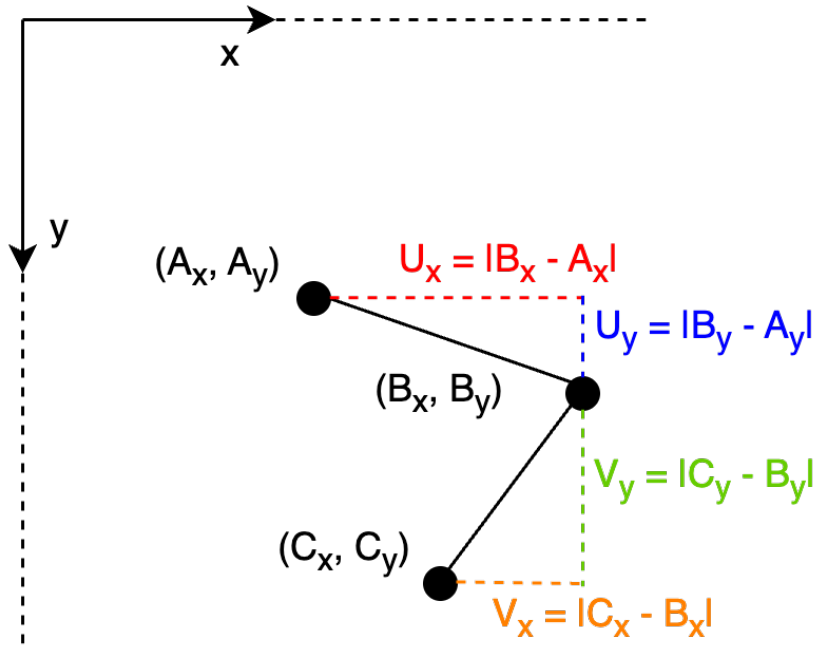
Figure 3.7: Quantitative Representation of Formula Derivation. *Example of how the formula quantities (U_x, U_y, V_x, V_y) are calculated geometrically based on the coordinates of points A, B, and C. The diagram illustrates the mathematical relationships used to compute vector components in a Cartesian coordinate system, providing foundational insights for kinematic analysis*

$$\theta = \arctan\left(\frac{u_y}{u_x}\right) - \arctan\left(\frac{v_y}{v_x}\right) \tag{3.1}$$

The quantities u_x and u_y are defined as the distance in pixels between the x and y coordinates of the joints located at the extremity of the first considered segment. Similarly, the quantities v_x and v_y are defined as the distance in pixels between the x and y coordinates of the joints located at the extremity of the second considered segment. The NumPy Python library $arctan2()$ function was used to compute the θ angle. This upgraded version of the basic $arctan()$ function returns a result in the range $[-\pi, +\pi]$ radians. **Figure 3.7** shows, with an example, how the formula's quantities are computed. Applying the **(3.1)** means computing the clockwise angle from A to C around B.

3.3.4 Software Structure

Figure 3.8 illustrates the flow diagram of the software architecture.
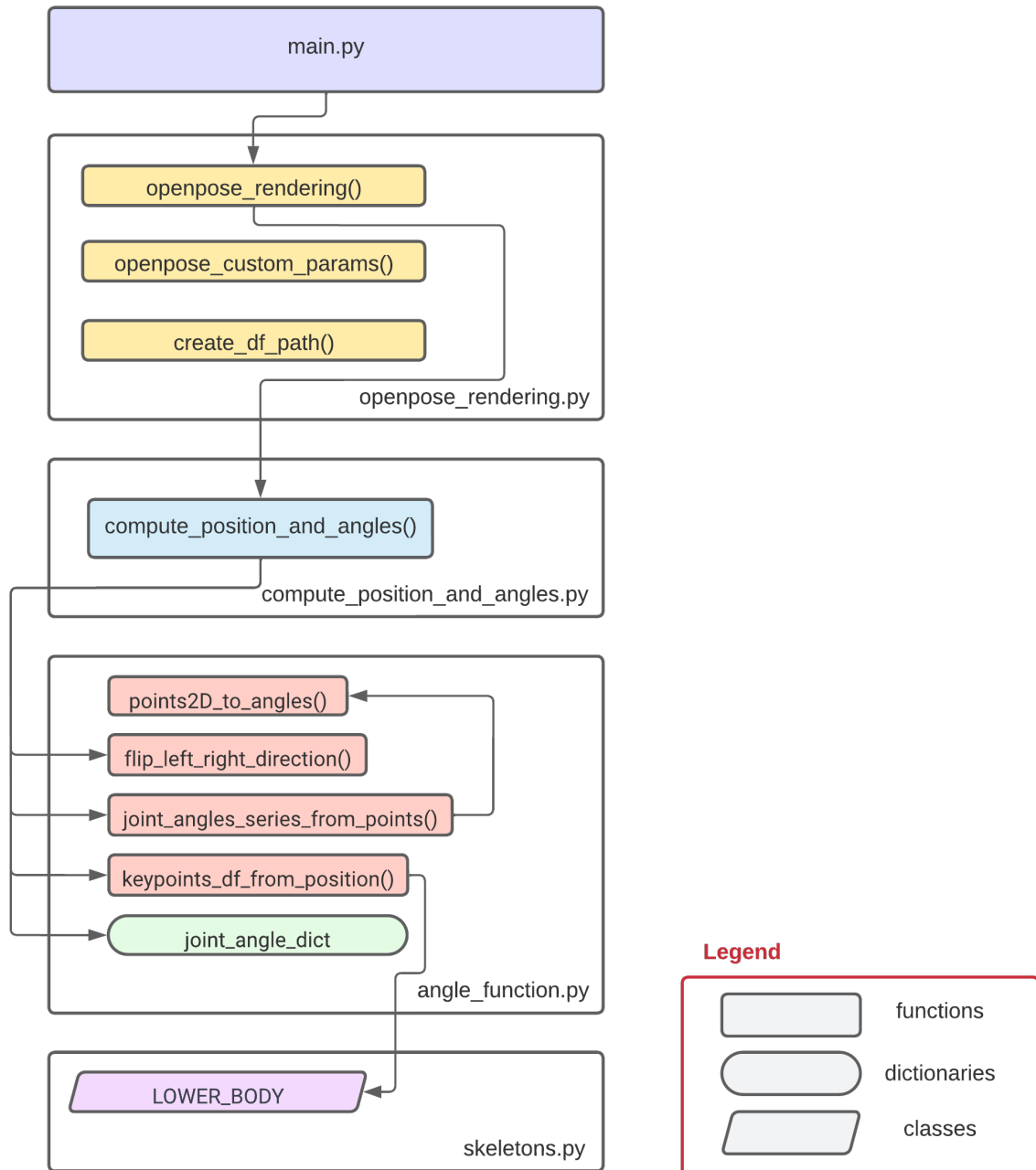
Figure 3.8: Flow Diagram of Software Architecture for Markerless Gait Analysis. *This diagram illustrates the modular structure of a Python-based pipeline for computing joint positions and angles from 2D keypoints. It starts with the main script (`main.py`), which utilizes functionalities from three main modules: `openpose_rendering.py` for rendering keypoints and setting parameters, `compute_position_and_angles.py` for processing angles and positions, and `angle_function.py` for specific angle-related calculations and keypoint transformations*

The primary purpose of the main file (`main.py`) is to read video files and initiate their processing. Upon execution, the script identifies all video files located in a specified folder and constructs their respective file paths. For each video file, the `render_video()` function is invoked. This function, which is defined in the `openpose_rendering.py` file, is responsible for rendering and processing the input video data to extract keypoints or other relevant motion-related details. The modular design of the main file ensures a streamlined workflow, delegating core computational tasks to specialized modules, thereby maintaining clarity and scalability

within the software architecture.

The `openpose_rendering.py` file serves as a crucial component of the software, integrating OP to extract skeletal keypoints and process video data for MLB GAn. It imports and initializes the OP library, setting custom parameters through the `openpose_custom_params()` function, which allows the user to configure model paths, GPU settings, and additional options. For a detailed explanation of the `openpose_custom_params()` function, see **3.3.5.1**. The file also includes the `create_df_path()` function, which constructs the file path for saving the output data, ensuring proper organization of results. The core functionality resides in the `render_-video()` function. This function initializes Open Source Computer Vision Library (OpenCV) to handle video input and streaming frames from the provided video file path. For each frame, OP processes the image to extract pose keypoints, which are formatted into a list containing the x and y coordinates along with their confidence scores. These keypoints are subsequently passed to the `compute_position_and_angles()` function, which calculates relevant biomechanical data. The function compiles these calculations into a DataFrame, aggregating results for all video frames. Once processing is complete, the DataFrame is saved to a CSV file at the designated output path. This modular structure enables seamless video analysis and integration with downstream processing components. Detailed documentation for the `render_video()` can be found in **3.3.5.2**.

The `compute_position_and_angles.py` file defines the `compute_position_and_angles()` function, which is responsible for estimating joint angles from the list of keypoints obtained from OP (**3.3.5.3**). This function serves as a computational backbone, leveraging multiple utilities from the `angle_functions.py` module. The process begins by creating a DataFrame of keypoint positions using the `keypoints_df_from_position()` function (**3.3.5.7**), focusing specifically on the lower body. To handle variations in orientation, the keypoint data is processed with `flip_left_right_direction()` to ensure consistency in the left-right direction (see **3.3.5.5** for an extensive description). Subsequently, joint angles are computed for selected joints, such as the knees and ankles. For each joint, parameters are retrieved from the `joint_angle_-dict` dictionary, and the `joint_angles_series_from_points()` function is used to calculate the angle series. Additional information is provided in **3.3.5.6**. These results are aggregated into a comprehensive list. The computed joint angles are then organized into a DataFrame, with a multi-index structure for better categorization. The DataFrame includes the computed angles for each joint and coordinates, making it ready for further analysis or visualization. This modular approach ensures flexibility and accuracy in processing gait data.

The `angle_functions.py` file is a utility module that provides essential functionalities for computing joint angles from OP keypoints. The `joint_angle_dict` is a predefined dictionary mapping joint names to their respective keypoints and parameters. Each joint specifies the list of keypoints used in the computation, the type of movement (e.g., flexion or dorsiflexion), a reference angle offset, and a multiplier to correct for orientation. This dictionary acts as a lookup table, ensuring consistent and accurate angle computation across different joints. The `points2D_to_angles()` function calculates angles between three points in 2D space. It determines the clockwise angle formed by two vectors around a central point. The function supports individual computations, outputting angles that may range beyond 0° to 360°, depending on the input configuration (see **3.3.5.4** for additional details). The `flip_left_right_direction()` function standardizes the orientation of the dataset. When a person changes direction (e.g., walking leftward instead of rightward), this function flips the x-coordinates of the keypoints to ensure consistent angle calculation regardless of orientation. The flipping is determined by comparing the positions of the toes and heels (**3.3.5.5**). The `joint_angles_series_from_points()` function generates a time series of joint angles for a given joint. It retrieves the relevant keypoints from the DataFrame, computes angles using the `points2D_to_angles()` function, and applies corrections based on the parameters from the `joint_angle_dict`. The resulting series represents the computed angles for the joint across all frames in the dataset (**3.3.5.6**). The `key-points_df_from_position()` function creates a structured DataFrame from the raw keypoint data. Using a hierarchical multi-index, it organizes the keypoints by body part and coordinate (x, y, likelihood). This format facilitates efficient processing and ensures compatibility with downstream computations, such as angle estimation. This module's functions and dictionary collectively enable precise and efficient computation of joint angles from markerless motion capture data. A comprehensive explanation of the `keypoints_df_from_position()` is available in

3.3.5.7.

The `skeletons.py` file defines hierarchical skeleton structures using the `anytree` library. Among these, the `LOWER_BODY` model focuses on the lower extremities, providing a structured representation of the body parts involved in motion analysis. The `LOWER_BODY` model is created using the `Node` class from the `anytree` library. It starts with a root node, `"CHip"`, representing the central hip joint. The model branches out to include both right and left limbs, defining the hierarchical relationship between joints and keypoints. For the right side, the `"RHip"` node leads to `"RKnee"`, which further connects to `"RAnkle."` From there, it extends to finer details like `"RBigToe"` and `"RHeel"`, representing the toe and heel, respectively. Similarly, the left side follows the same structure, starting from `"LHip"` and branching to `"LKnee"`, `"LAnkle"`, `"LBig-Toe"`, and `"LHeel."` This hierarchical representation ensures that all keypoints are organized systematically, facilitating efficient traversal and referencing during computations. The `LOWER_BODY` model is particularly useful for analyzing gait, as it isolates the key joints and segments critical for lower-body movement dynamics. By leveraging the `anytree` library, the model's structure can be easily visualized and manipulated, ensuring adaptability for various motion analysis tasks. The software's main functions are described in detail, each accompanied by a relevant code snippet.

3.3.5 Functions Description

3.3.5.1 openpose_custom_params()

```python
# Set OpenPose parameters
def openpose_custom_params():
    params = dict()
    params["model_folder"] = project_path + "models/"
    params["number_people_max"] = 1
    # params["model_pose"] = 'COCO'
    # params["model_pose"] = 'BODY_25B'
    params["num_gpu"] = 1

    return params
```

Purpose:

Configures and returns a dictionary of parameters for OP, which is used to process video data and detect human keypoints. The function standardizes the configuration for consistency and flexibility across the software.

Input Arguments:

None. This function does not take any input arguments.

Output:

A dictionary containing the OP configuration parameters such as the path to model files, the maximum number of people to detect, and the number of GPUs to use.

Logic:

1. **Initialize Parameters Dictionary:**

   - Create an empty dictionary `params`.

2. **Set Required Parameters:**

   - Set the `model_folder` path using the global `project_path`.

> - Limit detection to one person by setting `number_people_max` to 1.
> - Specify that one GPU should be used via `num_gpu`.

3. **Optional Parameters (Commented Out):**

> - Include commented-out lines for `model_pose`, which can be enabled and customized for specific pose models (`COCO`, `BODY_25B`, etc.).

4. **Return the Parameters Dictionary:**

> - Return the constructed dictionary `params`.

Key Notes:

- The function assumes that the global variable `project_path` is correctly set before calling.

- It focuses on single-subject scenarios by default, which is suitable for most analyses.

- Optional parameters are provided for flexibility but are not active in the current implementation.

Example Usage:

```
params = openpose_custom_params()
print(params)
# Output:
# {'model_folder': '/path/to/project/models/',
#   'number_people_max': 1,
#   'num_gpu': 1}
```

Key Dependencies:

- Relies on the global variable `project_path` to correctly define the `model_folder` path.

3.3.5.2 render_video()

```python
def render_video(video_filepath):
    print("\nPerforming Video Rendering...")

    # Output file_path
    output_path = create_df_path(video_filepath)

    # Custom Params
    params = openpose_custom_params()

    # Starting OpenPose
    opWrapper = op.WrapperPython()
    opWrapper.configure(params)
    opWrapper.start()

    # Process Image
    datum = op.Datum()

    #Creates a video capture object, which would help stream or display the video.
    cap = cv2.VideoCapture(video_filepath)

```

```python
21      df_angles_list = []
22
23    while cap.isOpened():
24
25          # Returns a tuple bool and frame, if ret is True then there's a video frame
          ↪   to read
26          ret, frame = cap.read()
27
28          if not ret:
29              print("Can't receive frame (stream end?). Exiting ...")
30              break
31
32          else:
33              # "datum.cvOutputData" is the output frame, the processed one
34              datum.cvInputData = frame
35              opWrapper.emplaceAndPop([datum])
36
37              # opframe = datum.cvOutputData
38              network_output = datum.poseKeypoints
39
40              # Cast all the OpenPose identified keypoints into a list like:
              ↪   [x_keypoint_coordinate, y_keypoint_coordinate, likelihood]
41              kpts = network_output[0].tolist()
42
43              # Take the angles df global variable and save it into a df list
44              df_angles = compute_position_and_angles(kpts)
45
46              df_angles_list.append(df_angles)
47
48              if cv2.waitKey(1) & 0xFF == ord('q'):
49                  break
50
51    cap.release()
52    cv2.destroyAllWindows()
53
54    df_angles_video = pd.concat(df_angles_list)
55    df_angles_video.to_csv(output_path, index=False)
```

Purpose:

This function is the core of the video processing pipeline. It takes an input video file, processes each frame using OP to extract keypoints, computes joint angles, and saves the results in a CSV file.

Input Arguments:

video_filepath (string): The file path of the input video to be processed.

Output:

A CSV file containing the computed joint angles for each frame of the video.

Logic:

1. **Initialize Output and OP Configuration:**

   - The output file path is created using create_df_path().
   - OP is configured with custom parameters obtained from openpose_custom_params().

- An OP wrapper (`opWrapper`) is initialized, configured, and started.

2. **Video Processing:**

   - A video capture object is created using OpenCV to read the input video frame by frame.
   - A loop processes each frame:
     - If a frame is available, it is sent to OP via `opWrapper.emplaceAndPop()` for keypoint detection.
     - The keypoints are extracted as a list of [`x`, `y`, `likelihood`] coordinates.
     - The keypoints are passed to `compute_position_and_angles()` to calculate joint angles.
     - The resulting data frame is appended to a list.

3. **Finalize and Save Results:**

   - Once the video processing is complete, the list of data frames is concatenated into a single data frame.
   - The consolidated data frame is saved as a CSV file to the specified output path.

Key Notes:

- If no frame is available (e.g., at the end of the video), the loop exits gracefully.

- Pressing the 'q' key during processing interrupts the video rendering.

- OpenCV ensures proper resource management by releasing the video capture object and closing all display windows after processing.

Example Usage:

```
video_filepath = "input_video.mp4"
render_video(video_filepath)
# Output: A CSV file containing joint angles saved to the specified output path.
```

Key Dependencies:

- The `openpose_custom_params()` function to configure OP.

- OpenCV (`cv2`) for video capture and processing.

- `compute_position_and_angles()` to calculate joint angles from detected keypoints.

- Pandas (`pd`) to handle data frames.

3.3.5.3 compute_position_and_angles()

```
def compute_position_and_angles(keypoints):
    # Select joint angles
    joint_angles = ['Right ankle', 'Left ankle', 'Right knee', 'Left knee']

    # Create a dataframe with the position keypoints
    keypoints_df = keypoints_df_from_position(keypoints, 'LOWER_BODY')

    # Flip along x when feet oriented to the left
    df_points = flip_left_right_direction(keypoints_df)

```

```
11      # Joint angles
12      joint_angle_series = []
13      for j in joint_angles:
14          angle_params = joint_angle_dict.get(j)
15          j_ang_series = joint_angles_series_from_points(df_points, angle_params)
16          joint_angle_series += [j_ang_series]
17
18      # Creating df with the joint angles
19      angs = joint_angles
20
21      coords = [joint_angle_dict.get(j)[1] for j in joint_angles]
22      tuples = list(zip(angs, coords))
23      index_angs_csv = pd.MultiIndex.from_tuples(tuples, names=['angs', 'coords'])
24
25      angle_series = joint_angle_series
26
27      df_angles = pd.DataFrame(angle_series, index=index_angs_csv).T
28      return df_angles
```

Purpose:

This function processes the keypoints detected by OP to compute joint angles. It returns a structured data frame containing the calculated angles for selected joints.

Input Arguments:

`keypoints` (`list`): A list of keypoints detected by OP. Each keypoint includes the `x` and `y` coordinates and a confidence score.

Output:

A Pandas data frame containing the computed joint angles. Each row represents a set of angles for the given frame of input keypoints.

Logic:

1. **Filter Keypoints for the Lower Body:**

   - A data frame of position keypoints is created using the `keypoints_df_from_position()` function.

   - The keypoints are flipped along the x-axis if the feet are oriented to the left using the `flip_left_right_direction()` function.

2. **Select and Compute Angles:**

   - The joint angles to compute are pre-defined as [`'Right ankle'`, `'Left ankle'`, `'Right knee'`, `'Left knee'`].

   - For each joint:
     - Retrieve parameters from the `joint_angle_dict`.
     - Compute the joint angles using the `joint_angles_series_from_points()` function.

3. **Structure Angles into a Data Frame:**

   - Combine the calculated joint angles into a multi-indexed data frame.

   - The index specifies both the angle (e.g., `Right knee`) and its corresponding coordinates (e.g., `x, y`).

41

Key Notes:

- The function focuses on lower-body joints (`Right ankle`, `Left ankle`, `Right knee`, `Left knee`) by default.

- The keypoints are flipped when the feet are oriented leftward to ensure consistent angle calculations.

Example Usage:

```
keypoints = [...]  # Detected keypoints from OpenPose
df_angles = compute_position_and_angles(keypoints)
print(df_angles)
# Output: A Pandas data frame containing joint angles for the given keypoints.
```

Key Dependencies:

- `keypoints_df_from_position()` to generate the keypoints data frame.

- `flip_left_right_direction()` to ensure consistent orientation of the keypoints.

- `joint_angles_series_from_points()` for calculating the joint angles.

- `joint_angle_dict` for retrieving parameters associated with each joint.

- Pandas (`pd`) to handle data frames and perform transformations.

3.3.5.4 points2D_to_angles

```python
def points2D_to_angles(points_list):

    ax, ay = points_list[0]
    bx, by = points_list[1]

    cx, cy = points_list[2]
    ux, uy = ax-bx, ay-by
    vx, vy = cx-bx, cy-by

    ang = np.array(np.degrees(np.arctan2(uy, ux) - np.arctan2(vy, vx)))

    return ang
```

Purpose:

This function computes angles based on input points in 2D space. It handles:

- Clockwise angles between three points.

Input Arguments:

`points_list` (`list`): A list containing 3 points, each represented as (`x, y`) coordinates.

Output:

A float representing the computed angle in degrees. The output may range beyond `0.0` to `360.0` depending on the input configuration.

Logic:

1. For a **3-point list**:

    - Two vectors are computed:
        - One from the first point (`a`) to the second point (`b`).
        - Another from the third point (`c`) to the second point (`b`).
    - The angle between these vectors is computed.

2. The angle is calculated using the arctangent difference between the vectors' orientations, adjusted for the OpenCV coordinate system where the y-axis points downward.

Key Notes:

- The function computes clockwise angles between three points.

- The computation adjusts for OpenCV's downward-pointing y-axis, ensuring correct clockwise angles.

- The returned angle is in degrees, making them directly interpretable.

Example Usage:

```python
# Example with three points
points_list = [(1, 2), (4, 5), (7, 8)]
angle = points2D_to_angles(points_list)
print(angle)  # Output: Angle between vectors in degrees
```

Key Dependencies:

- NumPy (`np`) for numerical operations and angle computation.

3.3.5.5 flip_left_right_direction

```python
def flip_left_right_direction(df_points):

    righ_orientation =
    ↪   df_points.iloc[:,df_points.columns.get_level_values(0)=='RBigToe'].iloc[:,0]
    ↪   -
    ↪   df_points.iloc[:,df_points.columns.get_level_values(0)=='RHeel'].iloc[:,0]

    left_orientation =
    ↪   df_points.iloc[:,df_points.columns.get_level_values(0)=='LBigToe'].iloc[:,0]
    ↪   -
    ↪   df_points.iloc[:,df_points.columns.get_level_values(0)=='LHeel'].iloc[:,0]

    orientation = righ_orientation + left_orientation

    df_points.iloc[:,2::3] = df_points.iloc[:,2::3] * np.where(orientation>=0, 1,
    ↪   -1).reshape(-1,1)

    return df_points
```

Purpose:

This function flips the x-coordinates of keypoints when the detected person changes direction to the left. This ensures consistency in angle computations.

Input Arguments:

df_points (DataFrame): A Pandas DataFrame containing pose detection keypoints. The keypoints are structured with hierarchical indexing, where the x-coordinates are adjusted based on direction.

Output:

A Pandas DataFrame with flipped x-coordinates for keypoints when the direction changes.

Logic:

1. **Compute Orientation:**

   - The relative positions of the RBigToe and RHeel are used to calculate the right-side orientation.
   - Similarly, the relative positions of the LBigToe and LHeel are used to calculate the left-side orientation.
   - The combined orientation (right_orientation + left_orientation) is calculated to determine the overall direction.

2. **Flip X-Coordinates:**

   - The x-coordinates of all keypoints (df_points.iloc[:, 2::3]) are multiplied by -1 when the orientation indicates a leftward direction (orientation < 0).
   - This ensures consistent keypoint alignment regardless of the detected person's orientation.

Key Notes:

- The flipping logic is based on the relative positions of toes and heels for both sides of the body.

- This function is particularly useful for maintaining consistency in subsequent computations, such as joint angles.

- The adjustments are performed in-place, modifying the x-coordinates directly in the input DataFrame.

Example Usage:

```python
# Example DataFrame with pose keypoints
df_points = pd.DataFrame({
    # Simulated hierarchical indexing for keypoints (simplified for clarity)
    'RBigToe_x': [5, 6], 'RHeel_x': [3, 2],
    'LBigToe_x': [7, 8], 'LHeel_x': [5, 6]
}, index=[0, 1])

# Apply the flipping function
flipped_df = flip_left_right_direction(df_points)
print(flipped_df)
# Output: DataFrame with adjusted x-coordinates based on orientation.
```

Key Dependencies:

- NumPy (`np`) for element-wise operations and vectorized computations.

- Pandas (`pd`) for handling hierarchical DataFrame structures.

3.3.5.6 `joint_angles_series_from_points`

```python
def joint_angles_series_from_points(df_points, angle_params):

    # Retrieve points
    keypt_series = []
    for k in angle_params[0]:
        keypt_series +=
        ↪ [df_points.iloc[:,df_points.columns.get_level_values(0)==k].iloc[:,:2]]

    # Compute angles
    points_list = [k.values.T for k in keypt_series]
    ang_series = points2D_to_angles(points_list)
    ang_series += angle_params[2]
    ang_series *= angle_params[3]
    ang_series = np.where(ang_series>180,ang_series-360,ang_series)
    ang_series = np.where((ang_series==0) | (ang_series==90) | (ang_series==180),
    ↪ +0, ang_series)

    return ang_series
```

Purpose:

This function computes a time series of joint angles from pose keypoints.

Input Arguments:

df_points (`DataFrame`): A Pandas DataFrame containing pose detection keypoints.

angle_params (`list`): Specifies the points to use for angle computation, as well as offsets and scaling factors for adjusting the angles.

Output:

A NumPy array of computed angles for the selected joint over time.

Logic:

1. **Retrieve Keypoints:**

   - Keypoints specified in `angle_params[0]` are extracted from the DataFrame.
   - The selected keypoints are stored as a series of 2D points.

2. **Compute Angles:**

   - The extracted keypoints are passed to `points2D_to_angles()` to compute angles.
   - Angle adjustments are applied:
     - Add offsets specified in `angle_params[2]`.
     - Scale angles using `angle_params[3]`.
   - Angles are normalized to ensure they fall within a consistent range:
     - Angles greater than 180 are adjusted to the $[-180, 180]$ range.

− Specific angles (0°, 90°, 180°) are set to 0° to handle edge cases.

3. **Return Result:**

- The processed angles are returned as a NumPy array.

Key Notes:

- The function includes angle adjustments (offsets and scaling factors) for increased accuracy and flexibility.

- Normalization ensures angles are within a consistent range, facilitating further analysis.

- The function leverages `points2D_to_angles()` for the core angle computations.

Example Usage:

```python
# Example DataFrame and angle parameters
df_points = pd.DataFrame({
    'Joint1_x': [1, 2, 3], 'Joint1_y': [4, 5, 6],
    'Joint2_x': [7, 8, 9], 'Joint2_y': [10, 11, 12]
}, index=[0, 1, 2])
angle_params = [['Joint1', 'Joint2'], 0, 0, 1]  # Example params

# Compute joint angle series
angle_series = joint_angles_series_from_points(df_points, angle_params)
print(angle_series)
# Output: NumPy array of angles over time
```

Key Dependencies:

- `points2D_to_angles()` for calculating angles based on the input keypoints.

- NumPy (`np`) for numerical operations.

- Pandas (`pd`) for handling keypoint data frames.

3.3.5.7 keypoints_df_from_position

```python
def keypoints_df_from_position(keypoints, pose_model):
    model = eval(pose_model)
    keypoints_ids = [node.id for _, _, node in RenderTree(model)]
    keypoints_names = [node.name for _, _, node in RenderTree(model)]

    keypoints_names_rearranged = [y for x,y in
        ↪  zip(keypoints_ids,keypoints_names)]

    keypoints_nb = len(keypoints_ids)

    keypoints_model = []

    for id in keypoints_ids:
        keypoints_model += [keypoints[id]]

    keypoints_model = [item for sublist in keypoints_model for item in sublist]
```

46

```
17            bodyparts = [[p]*3 for p in keypoints_names_rearranged]
18            bodyparts = [item for sublist in bodyparts for item in sublist]
19            coords = ['x', 'y', 'likelihood']*keypoints_nb
20
21            tuples = list(zip(bodyparts, coords))
22            index_csv = pd.MultiIndex.from_tuples(tuples, names=['bodyparts', 'coords'])
23
24            # Create dataframe
25            df = pd.DataFrame(keypoints_model, index=index_csv).T
26
27            return df
```

Purpose:

This function creates a Pandas DataFrame of pose detection keypoints. The structure is designed to maintain compatibility with other functions in the pipeline.

Input Arguments:

`keypoints` (`list`): Keypoints detected by OP. Each keypoint includes `x`, `y`, and likelihood values.

`pose_model` (`str`): The pose model used (e.g., `LOWER_BODY`). This specifies the body parts and structure for reordering the keypoints.

Output:

A Pandas DataFrame with a multi-level index (`bodyparts`, `coords`) representing the detected keypoints.

Logic:

1. **Retrieve Pose Model:**

   - Evaluate the `pose_model` string to obtain the hierarchical pose structure.
   - Extract keypoint IDs and names using the `RenderTree` function.

2. **Reorder Keypoints:**

   - Keypoints are rearranged to match the order defined by the pose model.
   - Flatten the nested keypoint list into a single sequence for DataFrame creation.

3. **Create Multi-Level Index:**

   - Generate a multi-level index with `bodyparts` (e.g., `Right knee`, `Left ankle`) and `coords` (x, y, `likelihood`).

4. **Construct DataFrame:**

   - Populate the DataFrame with the rearranged keypoints and apply the multi-level index.

Key Notes:

- The function ensures keypoints are ordered according to the pose model structure, facilitating compatibility with other processing steps.

- The multi-level index simplifies subsequent operations such as filtering and angle computation.

47

- The input pose model must be compatible with the expected hierarchical structure for correct DataFrame construction.

Example Usage:

```
1   # Example keypoints and pose model
2   keypoints = [[[1, 2, 0.9], [3, 4, 0.8]], [[5, 6, 0.85], [7, 8, 0.95]]]   # Simulated
    ↪   data
3   pose_model = "LOWER_BODY"   # Example pose model
4
5   # Generate DataFrame
6   df_keypoints = keypoints_df_from_position(keypoints, pose_model)
7   print(df_keypoints)
8   # Output: Pandas DataFrame with multi-level index for body parts and coordinates.
```

Key Dependencies:

- `RenderTree` for extracting the hierarchical pose model structure.

- Pandas (`pd`) for creating and managing the DataFrame.

Chapter 4

Data

4.1 Data Collection Campaigns

During my PhD, two acquisition campaigns were conducted between 2021 and 2023 to collect data for markerless motion analysis. Data from both campaigns included tri-axial accelerometer and gyroscope readings, sampled at 100 Hz. For the first campaign, these readings were used to calculate 102 kinematic features. The second campaign also included 2D video-derived joint angles. The second campaign introduced synchronized video data to complement IMU readings. This allowed for markerless motion analysis, leveraging IMU and video data to enhance the scope of kinematic evaluations.

All data were anonymized in compliance with ethical guidelines. Faces in videos were blurred to protect participants' privacy. The studies adhered to the Declaration of Helsinki and received ethics committee approval from the IRCCS "Bonino Pulejo" Neurolesi Center.

4.1.1 First Acquisition Campaign

The first acquisition campaign was conducted within the IRCCS "Bonino Pulejo" Neurolesi Center in Messina, Italy. Thirty-seven young, healthy participants were recruited via email and provided information about the study. They signed a written consent form before participation. Each testing session lasted approximately one hour and a half.

Inclusion and Exclusion Criteria

Participants were required to meet the following criteria:

- **Inclusion Criteria:**
  - Age between 18 and 40
  - No pain experienced in the past month
  - No ongoing health management or therapies (e.g., physiotherapy) in the past three months

- **Exclusion Criteria:**
  - Gait impairments due to neurological, cardiovascular, orthopedic, or rheumatologic conditions
  - Pregnancy for female participants

Protocol

Participants performed two walking tasks at their natural speed, barefoot, for five minutes on a treadmill (Gait Trainer 3; Biodex Medical Systems, Shirley, New York). The order of tasks was randomized to avoid bias. Motion data were captured using 9 IMUs (MyoMotion, NORAXON, USA) sampling at 100 Hz. The sensors were placed as follows:

- **Upper Body**: Fixed to the upper thoracic (below C7) and lower thoracic (T12/L1) regions

- **Lower Body**: Placed on the pelvis, thighs, shanks, and feet using elastic belts and skin-safe tape (Hypafix, BSN medical GmbH)

Data collected included tri-axial accelerometer and gyroscope readings, resulting in 102 features. After completing the tasks, participants filled out the International Physical Activity Questionnaire (IPAQ) long version. Responses were translated into a categorical physical activity level (PAL) score ("Low," "Moderate," or "High") using a Python script.

4.1.2 Second Acquisition Campaign

The second acquisition campaign involved 31 young, healthy participants in a single-session study conducted at the IRCCS "Bonino Pulejo" Neurolesi Center in Messina, Italy. Recruitment followed a similar protocol: initial contact via email, online eligibility screening, and written informed consent. Each session lasted approximately two hours.

Inclusion and Exclusion Criteria

Participants were required to meet the following criteria:

- **Inclusion Criteria:**

  - Age between 18 and 55
  - No neurological, cardiovascular, orthopedic, or rheumatologic conditions causing significant pain (5/10) or impairing gait or posture within the last three weeks
  - No ongoing health management or therapies in the past three months

- **Exclusion Criteria:**

  - Pregnancy for female participants

Protocol

Participants walked on the treadmill for five minutes at a natural speed while wearing shoes. Lower body motion data were recorded using 7 IMUs (MyoMotion, NORAXON, USA) at 100 Hz. Additionally, a high-definition camera (Logitech Brio 4K Stream Edition) synchronized with the IMU software was employed to capture videos at 60 fps and 720×1280 pixels resolution. Synchronization was achieved using an LED triggered by the IMU software.

IMU placement followed a protocol similar to the first campaign, with sensors on the pelvis, thighs, shanks, and feet. Calibration was performed in a designated area free from ferromagnetic interference. The camera was positioned 2.80 meters from the treadmill at a 45-degree angle to optimize joint visibility and minimize occlusion issues.

The recorded videos were segmented into 15 twenty-second trials. Each trial was analyzed using custom OP-based software to extract 2D knee and ankle joint angles for both legs.

4.2 Data Cleaning

After data collection, MATLAB® (The MathWorks Inc., Natick, MA, USA) and the Python 3 Pandas library were used to analyze and clean the motion data. The IMUs recorded data, which includes body 3D linear accelerations [mG], anatomical segments and joint angles [deg], and 3D orientation of the IMUs at a sampling frequency of 100 Hz, were imported in MATLAB® for a preliminary graphical inspection.

As part of the initial preprocessing steps, negative times before zero were trimmed from the data to ensure all recordings started at $t = 0$, maintaining consistency across subjects. Additionally, acquisitions exceeding five minutes (more than 3000 samples) were excluded, as these were deemed outliers due to the standardized protocol duration of five minutes per trial.

Shorter acquisitions were retained, even if not exceeding five minutes, provided they adhered to the recording protocol.

An initial analysis of the signals revealed inaccuracies in several trigonometric features caused by gyro-offset problems inherent to the IMUs. These inaccuracies manifested as sudden phase shifts of ± 360, occurring sporadically throughout the recordings. The shifts varied in duration and appeared in random time series segments. Significantly, the signals reverted to their original, unshifted patterns following each erroneous phase shift. These errors were likely due to hardware limitations or improper calibration of the gyroscopic sensors within the IMUs, a known challenge in motion capture studies.

4.2.1 Correction Methodology

To preserve the quality of the data, a dedicated MATLAB$^{\circledR}$ function was developed to correct these phase shift errors systematically. This function followed a series of steps, ensuring both precision and automation:

1. **Identification of Shift Windows**: The algorithm first differentiated the time-varying features of the signals to emphasize abrupt changes. Peaks in the resulting derivatives corresponded to the boundaries of the shift windows. These peaks marked the start and end points of the erroneous segments. If no peaks were detected, indicating the absence of shifts, the algorithm returned the feature unchanged.

2. **Automatic Detection of Shift Direction**: Both upward ($+360$) and downward (-360) phase shifts were observed, often without a consistent pattern. Logical conditions within the algorithm automatically determined the direction of each shift by analyzing the trend of the derivatives within the identified windows.

3. **Handling Edge Cases**: For shifts extending to the end of a signal without completing before the final sample, the last data point of the time series was used as the terminal point of the shift window. This ensured that no portion of the signal was left uncorrected.

4. **Phase Shift Adjustment**: Once the shift windows were identified, the affected segments of the signals were isolated. The algorithm applied a phase correction of ± 360, effectively restoring the original patterns within these windows. This correction preserved the data's integrity by retaining the signals' underlying trends.

5. **Outlier Correction Near Extrema**: Occasionally, data points near the boundaries of the shift windows were not captured during detection, appearing as outliers when compared to the corrected segments. To address this, the built-in MATLAB$^{\circledR}$ "`filloutliers`" function was employed, using piecewise cubic spline interpolation as the fill method. This step ensured a smooth transition between corrected and uncorrected segments.

Figure 4.1 provides a visual representation of a trigonometric feature before and after applying this correction method, illustrating the effectiveness of the approach.

The preprocessing and cleaning steps described above significantly improved the quality and reliability of the data, reducing noise and ensuring the integrity of the trigonometric features. These improvements were critical for enhancing the performance and interpretability of the machine learning models built using this dataset. The corrected data were further reviewed for residual issues, such as drift, distortion, or noise. For signals where these issues were localized to the beginning or end of the recordings, the affected portions were trimmed to maintain data quality. In cases where the distortions rendered the entire signal unusable, the corresponding data file was excluded from further analysis. This rigorous quality control ensured that only high-quality data were included in subsequent analyses.
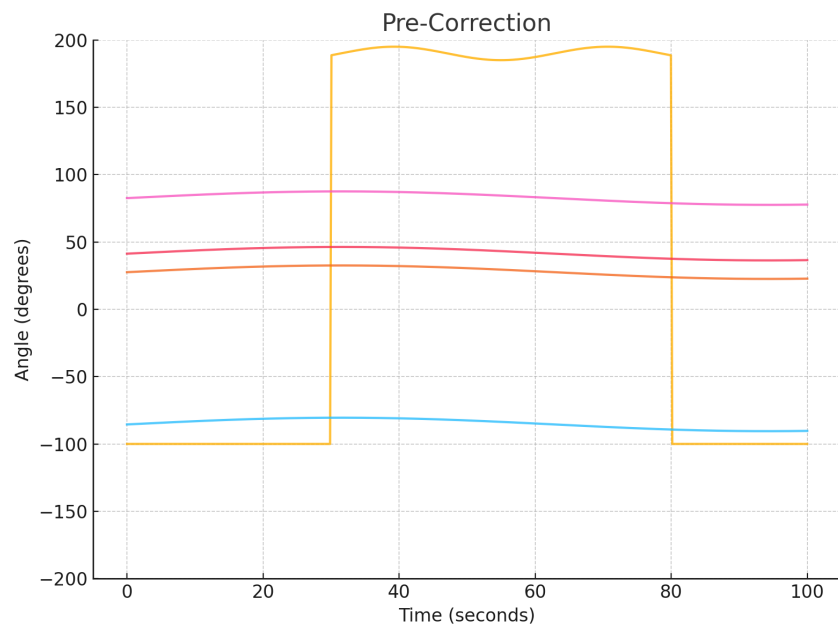
(a) Pre-Correction
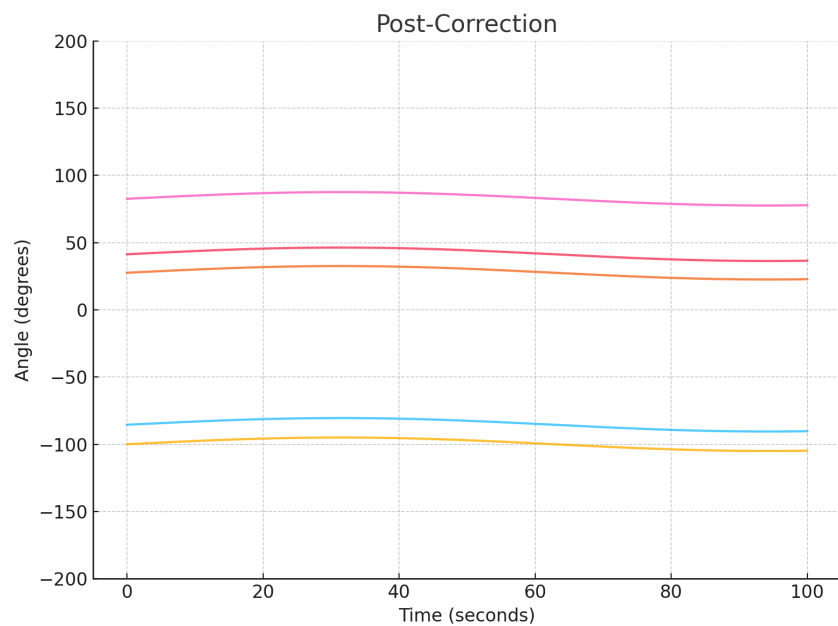
(b) Post-Correction

Figure 4.1: Correction of Drifting Signal in Angle Measurements Over Time. *The Pre-Correction plot (a) highlights a drifting signal (yellow line) alongside other stable signals. The drifting signal exhibits a rectangular shape with a flat section between 30 and 80 seconds, reflecting uncorrected measurement drift. The Post-Correction plot (b) presents the same signals, except the previously drifting signal has been corrected to follow a smooth sinusoidal shape, ensuring consistency with the stable signals. This demonstrates the effectiveness of the correction method in stabilizing the signal*

Chapter 5

Methodology

5.1 Predicting Physical Activity Level using Motion Features

5.1.1 Introduction

This Section will present a classification task using motion data provided by IMUs. Specifically, the aim was to correctly classify subjects' Physical Activity Level using a self-reported questionnaire (International Physical Activity Questionnaire) via kinematic features provided by wearable wireless IMUs sensors as ground truth. From the acquired data, velocity, acceleration, jerk, and smoothness were calculated and used to perform statistical feature extraction. The Neighborhood Component Analysis (NCA) algorithm processed the statistical features space and selected the most significant ones. Several ML models have been trained and tested before and after the feature selection to validate the approach's effectiveness. **Figure 5.1** shows the procedure implemented from the raw IMUs data to the training of several ML classifiers to validate the proposed approach, going through data pre-processing and the statistical feature extraction.
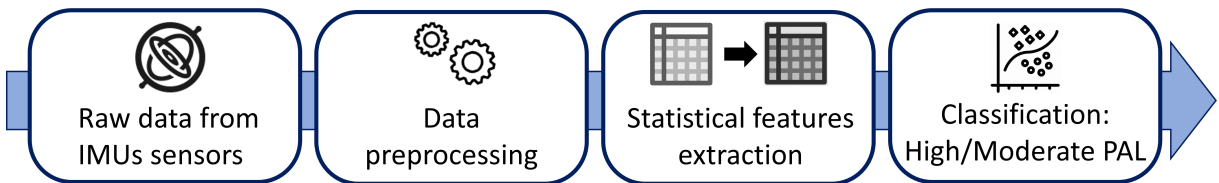
Figure 5.1: Overall Methodology followed. *A flowchart depicting the methodology for classifying physical activity levels (PAL) using IMU sensor data. The process involves four main steps: (1) collection of raw data from IMU sensors, (2) data preprocessing to clean and organize the input, (3) statistical feature extraction to identify meaningful metrics, and (4) classification into high or moderate PAL based on the extracted features. This structured approach ensures a reliable and systematic analysis*

5.1.2 State of the Art

Gait Analysis has become an essential tool for quantitatively assessing human motion, with significant applications in healthcare, rehabilitation, and diagnostics. Gait Analysis facilitates evaluating walking ability and overall physical performance by extracting clinically relevant parameters. These parameters are crucial for timely medical interventions and tracking recovery progress, offering insights into a patient's biomechanical and neuromuscular functions [175, 176, 177]. Physical Activity Level is closely linked to gait characteristics, influencing parameters such as balance control, propulsion, and walking speed[178, 179].

Traditional methods for assessing PAL, such as the IPAQ, provide a validated and globally recognized framework for estimating physical activity [180, 181]. However, their reliance on self-reported data introduces subjective variability, which can affect the accuracy of GAn-derived insights. This underscores the need for objective measures to eliminate inconsistencies and enhance the reliability of clinical evaluations [27].

Inertial Measurement Unit sensors have emerged as a robust solution to address these challenges. Inertial Measurement Unit sensors, comprising accelerometers, gyroscopes, and magne-

tometers, are lightweight, portable, and cost-effective devices that capture detailed motion data, including linear acceleration, angular velocity, and magnetic orientation [137, 132]. Due to their portability and ease of use, IMUs are increasingly preferred in clinical settings for GAn [129, 130, 139, 182, 140]. Despite these advantages, the extensive volume of data generated by IMUs in full-body analysis presents significant challenges in data processing and interpretation.

Recent ML advances have shown promise in addressing these complexities by efficiently analyzing large datasets, identifying patterns, and making predictions [183, 184]. Specifically, ML algorithms have been applied to process IMU data for tasks such as gait phase identification, biometric authentication, and the detection of pathological gait patterns [185, 186, 187, 188, 189]. These developments highlight the potential of ML to revolutionize GAn by enhancing accuracy and scalability in clinical applications.

Integrating NCA with ML models has further advanced this field. Neighborhood Component Analysis facilitates the identification of discriminative features, streamlining data processing while improving model performance. By focusing on kinematic features such as 3D joint range of motion, researchers aim to achieve accurate PAL classification with reduced computational burden. This approach aligns with clinical priorities, suggesting time-efficient IMU setups that improve the interpretability of GAn results.

Despite these advancements, gaps remain in predicting outcomes of clinically validated questionnaires using motion data, such as the IPAQ. While ML applications in GAn have explored diverse datasets and methodologies, leveraging these techniques to predict questionnaire outcomes remains underexplored [190, 191, 192]. Bridging this gap could significantly enhance the clinical utility of GAn by providing more actionable insights for patient care.

In summary, advancements in wearable sensor technology and ML are transforming GAn into a versatile and accessible tool for real-world clinical applications. The current study aims to optimize sensor configurations and reduce data complexity while preserving clinical relevance by integrating IMU-derived kinematic features and predictive ML models.

5.1.3 Study Design

The study recruited 37 young, healthy participants whose characteristics are summarized in **Table 5.1**.

	Male	**Female**	**Overall**
Number (%)	24 (65%)	13 (35%)	37
Age (mean±std_dev)	24 ± 3	22 ± 2	23 ± 3
Height (mean±std_dev, cm)	177 ± 9	167 ± 7	173 ± 10
Body Mass (mean±std_dev, Kg)	73 ± 9	63 ± 8	69 ± 10

Table 5.1: Subjects' Characteristics. A summary of the demographic and anthropometric characteristics of the study participants, grouped by gender and overall. Metrics include the number of participants (percentage), age (mean ± standard deviation), height in centimeters (mean ± standard deviation), and body mass in kilograms (mean ± standard deviation). These characteristics provide an overview of the sample population's distribution

Data were collected using IMUs to capture full-body motion during treadmill walking tasks, and participants' physical activity levels were assessed using the IPAQ long version (**Table 5.2**).

Details of the experimental setup and sensor placements are provided in **Chapter 4**. **Figure 5.2** shows the full body IMUs setup. Upper body sensors were securely fixed directly to the skin via a skin-safe tape (Hypafix, BSN medical GmbH) on the upper thoracic and lower thoracic (respectively below C7 and T12/L1). Lower body sensors were placed on the pelvis and both

IPAQ Level	Number of Subjects
Low	0
Moderate	11
High	26

Table 5.2: IPAQ Level Distribution. *A table summarizing the distribution of subjects across different IPAQ (International Physical Activity Questionnaire) levels. The levels include Low, Moderate, and High, with corresponding counts of subjects in each category. This distribution highlights the activity levels within the study population*

legs. Elastic belts were used on the sacrum, thighs, and shanks. The remaining sensors were taped to the feet. The participant acquisition file reported all the information provided by each IMU's tri-axial accelerometer and tri-axial gyroscope, resulting in 102 features.
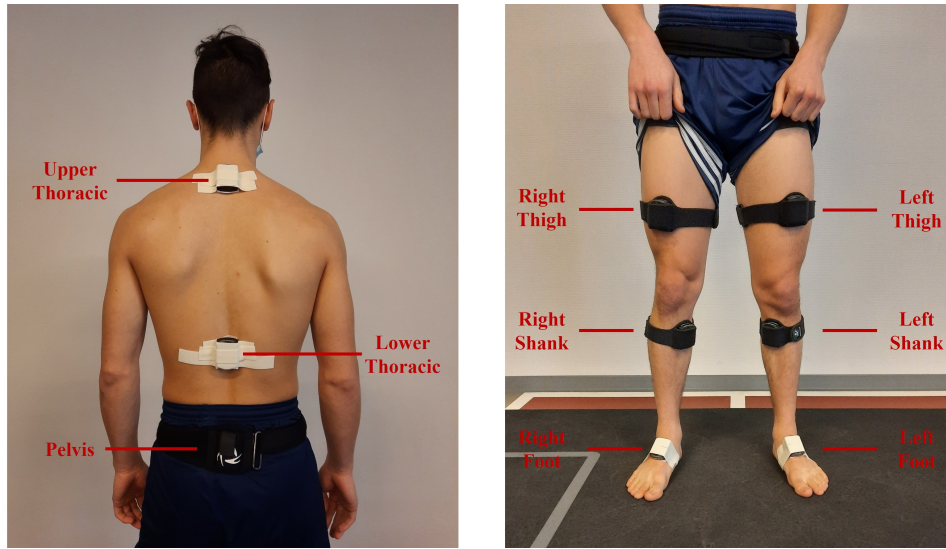
Figure 5.2: IMUs sensors placement. *The placement of Inertial Measurement Units (IMUs) on key body segments for motion analysis. Sensors are positioned at the upper thoracic, lower thoracic, pelvis, thighs (left and right), shanks (left and right), and feet (left and right). This configuration ensures comprehensive data collection for assessing movement patterns and joint kinematics*

5.1.4 Data Processing

MATLAB® R2019b and Python 3's Pandas library were used for data processing. Data augmentation was performed by identifying the participants' gait cycles to increase the number of pares considered in the ML approach. Gait Cycle and heel strike detection were realized via acceleration peak detection of the right-foot IMU sensor. Triaxial accelerometer and gyroscope data were zero-lag filtered using a 4th-order low-pass Butterworth filter with a cut-off frequency of $\omega_c = 4$Hz to remove undesirable sensor noise [193, 194]. The acceleration magnitude was calculated from the filtered accelerometer signals using the (**5.1**), and shown in **Figure 5.3**.

$$\sqrt{(right\_foot\_a_x)^2 + (right\_foot\_a_y)^2 + (right\_foot\_a_z)^2} \qquad (5.1)$$

For each participant, consecutive windows of 6 gait cycles were considered. In this way, each gait cycle window was equated with an instance of the resulting dataset. Six gait cycles are sufficient to perform averaging procedures and thus minimize artifacts caused by natural gait variability [195]. The MATLAB "findpeaks" function, with `MinPeakProminence` = 200 and `MinPeakDistance` = 80, automatically identified the heel strike. Single gait cycle detection was based on two consecutive peaks [196, 197] (**Figure 5.4**).
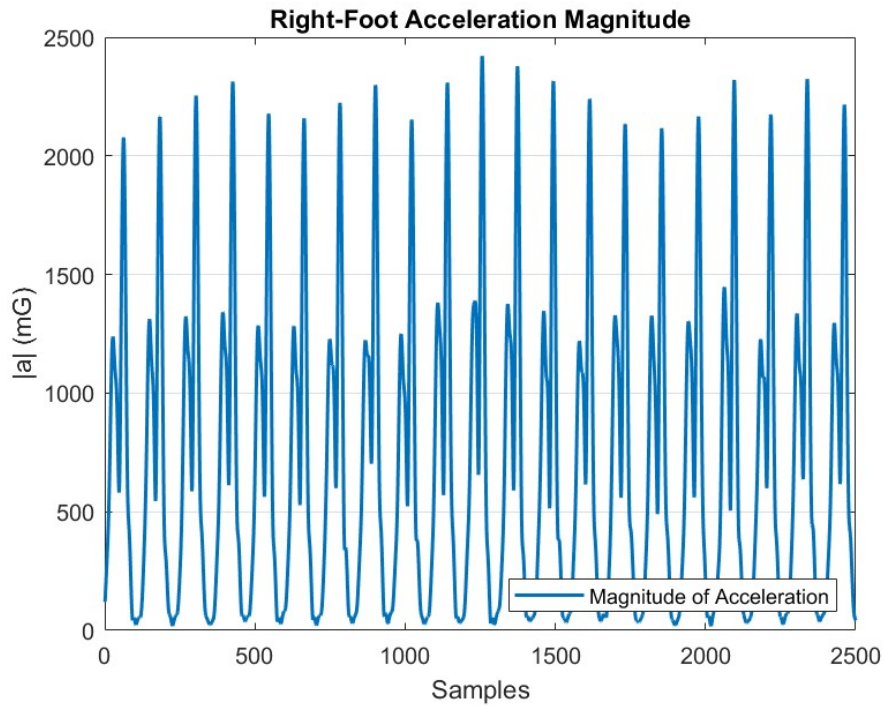
Figure 5.3: Magnitude of Right-Foot IMU Acceleration Signal. *A plot illustrating the magnitude of the acceleration signal recorded by the IMU sensor placed on the right foot. The x-axis represents the number of samples, while the y-axis shows the acceleration magnitude in milli-g (mG). The periodic oscillations correspond to the dynamic movement patterns during gait cycles, highlighting the sensor's ability to capture fine-grained motion data*
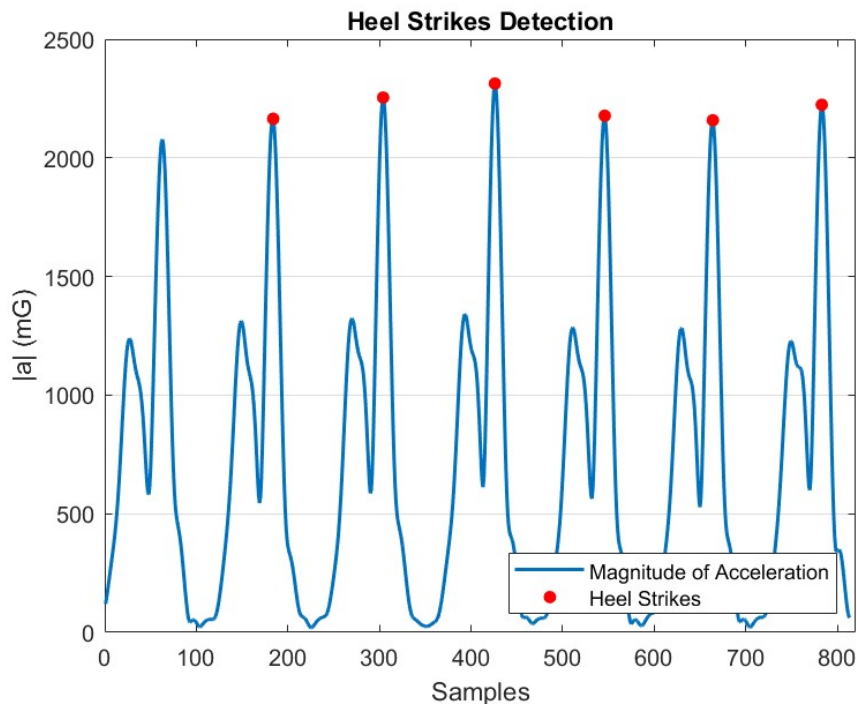
Figure 5.4: Heel Strike Detection for Gait Cycle Identification. *A plot demonstrating six consecutive gait cycles identified through heel strike detection (indicated by red markers). The magnitude of the right foot IMU acceleration signal is shown on the y-axis (in milli-g), with the x-axis representing the number of samples. The red markers correspond to heel strike events, which are key points in analyzing gait patterns and extracting temporal gait parameters*

After data augmentation, a dataset of 1520 instances was created from the 37 participants' acquisition dataset. Each of the instances contained 102 kinematic features provided by the

sensors. Considering the absence of participants' laterality, only the right-sided 3D Joints' Range of Motion was considered, resulting in 30 kinematic features (**Table 5.3**).

Anatomical Angles (deg)	
Upper Body Sensors	**Lower Body Sensors**
Lumbar Flexion	Hip Flexion
Lumbar Lateral	Hip Abduction
Lumbar Axial	Hip Rotation
Thoracic Flexion	Ankle Dorsiflexion
Thoracic Lateral	Ankle Inversion
Thoracic Axial	Ankle Abduction
Orientations (deg)	
Upper Body Sensors	**Lower Body Sensors**
Upper Spine Course	Pelvis Course
Upper Spine Pitch	Pelvis Pitch
Upper Spine Roll	Pelvis Roll
Lower Spine Course	Thigh Course
Lower Spine Pitch	Thigh Pitch
Lower Spine Roll	Thigh Roll
	Shank Course
	Shank Pitch
	Shank Roll
	Foot Course
	Foot Pitch
	Foot Roll

Table 5.3: 3D Joints Range of Motion Features. A table detailing the anatomical angles and orientations measured using upper and lower body sensors. The anatomical angles include lumbar and thoracic movements (flexion, lateral, axial) for the upper body and hip, ankle (flexion, abduction, rotation), and lower body joint movements. Orientations include the course, pitch, and roll for the upper and lower spine, pelvis, thighs, shanks, and feet. These features provide a comprehensive representation of 3D joint kinematics for motion analysis

Velocity, acceleration, and jerk were computed for each the 30 considered features, resulting in 120 new signals (30 initial features × 4). The smoothness [198] was computed by calculating the jerk magnitude, resulting in a total of 130 signals ([(30 initial features × 4) + 10 smoothness]). Statistical features, such as mean, root mean square, maximum, and standard deviation, were extracted from the 130 new features. Statistical extraction resulted in 520 derived features (130 new features × 4 statistic measures) (**Figure 5.5**).

The described procedure allows to move from a time series dataset, in which each subject was characterized by 130 signals (considered as features), to a tabular dataset, in which each subject is represented by a row in the table and characterized by 520 columns (considered as features).

After data augmentation and statistical feature extraction, the resulting dataset consisted of 1520 instances described by 520 statistical features with the PAL (IPAQ outcomes) as ground
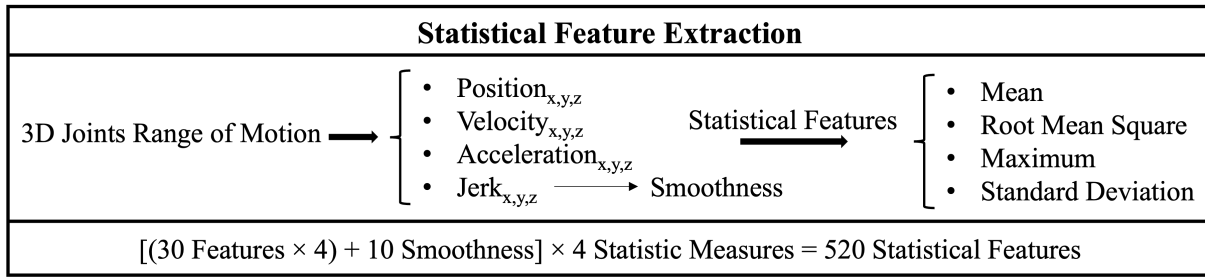
Statistical Feature Extraction		
3D Joints Range of Motion ⟶	• Position$_{x,y,z}$ • Velocity$_{x,y,z}$ • Acceleration$_{x,y,z}$ • Jerk$_{x,y,z}$ ⟶ Smoothness Statistical Features ⟶	• Mean • Root Mean Square • Maximum • Standard Deviation
[(30 Features × 4) + 10 Smoothness] × 4 Statistic Measures = 520 Statistical Features		

Figure 5.5: Summary of Statistical Feature Extraction Procedure. *A flowchart summarizing the procedure for statistical feature extraction from raw IMU sensor data. The process involves preprocessing the data, segmenting it into relevant intervals, and calculating statistical metrics such as mean, variance, skewness, and kurtosis. These features serve as inputs for classification models to analyze motion patterns and activity levels effectively*

truth for the supervised learning application. The provided dataset was used to train several ML models to classify the PAL of input instances, identifying which features are most significant for discrimination. The NCA was used to explore the discrimination power of the selected features and reduce the number of features considered. NCA is a supervised learning non-parametric technique that uses the gradient ascent technique to maximize the average leave-one-out (LOO) classification performance in the transformed space. The goal is to "learn" a distance metric by finding a linear transformation of the input data. NCA proves to be an effective method for both metric learning and linear dimensionality reduction [199]. As reported in [200], NCA provides a feature ranking by learning a feature weighting vector based on features' statistical distribution and discriminatory power. The algorithm is almost insensitive to the increase in the number of irrelevant features. It performs better than the neighbor-based feature weighting state-of-the-art methods in most cases, such as Simba (Iterative Search Margin Based Algorithm) [201], LMFW (Large Margin Feature Weighting method) [202] and FSSun [203]. Waikato Environment for Knowledge Analysis – WEKA 3.8.6 (Waikato University, New Zealand) was used to test the efficiency of the approach [204]. Several ML models were trained before and after NCA, and performance was compared using Accuracy, the Area Under the Curve (AUC), Precision, and Recall (Sensitivity) (**Figure 5.6**).
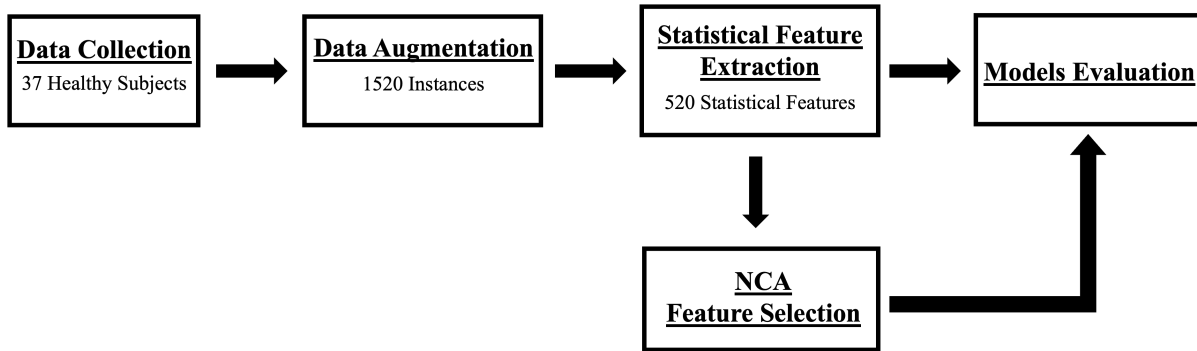
Figure 5.6: Summary Diagram of the Data Analysis Process. *A comprehensive flowchart summarizing the data analysis process. It outlines the key stages, including data acquisition, preprocessing, feature extraction, and subsequent analysis. This diagram provides an overview of the systematic approach used to process raw sensor data into actionable insights, emphasizing the integration of statistical and machine learning techniques*

The 70% and 30% of the statistical instances dataset were manually assigned to the training and test sets, respectively. Careful data splitting was realized to keep all instances related to a single subject in one set to avoid biasing the classification results. Precision, recall, accuracy [205], and AUC [206] scores were considered for performance evaluation. Those measures are all commonly used metrics in ML to evaluate the performance of a classification model. Each of these metrics provides different information about the model's performance, and together, they can give a more complete picture of how well the model is working. Precision measures the percentage of instances classified as positive that are actually positive. Recall (Sensitivity)

measures the percentage of positive instances that are correctly classified as such by the model. Accuracy measures the percentage of all instances that are classified correctly. AUC score measures the model's overall performance in terms of its ability to distinguish between the two classes. These metrics are important because they provide a way to objectively evaluate the performance of a model and compare it to other models. By looking at these metrics, it is possible to identify areas where the model performs well and needs improvement. For example, a model with high precision but low recall may be good at identifying positive instances but is missing many.

5.1.5 Results

From the initial 520 statistical features, the NCA algorithm identified 20 as the most relevant (**Table 5.4**). Features with a higher weight correspond to the most relevant features for classification. Features with lower values than the 20th represent irrelevant features discarded from the initial dataset.

Rank	Features Selected by NCA	Weight
1	RTFootRoll_deg_MAXIMUM	0.693
2	RTHipFlexion_deg_MAXIMUM	0.607
3	RTShankRoll_deg_MEAN	0.540
4	LumbarFlexion_deg_MEAN	0.502
5	RTThighCourse_deg_MAXIMUM	0.460
6	RTAnkleDorsiflexion_deg_MEAN	0.390
7	RTShankCourse_deg_MAXIMUM	0.382
8	RTFootCourse_deg_MEAN	0.375
9	RTFootCourse_deg_MAXIMUM	0.282
10	RTShankRoll_deg_MAXIMUM	0.188
11	RTHipRotation_Out_deg_MAXIMUM	0.117
12	RTFootCourse_deg_STD_DEV	0.091
13	LumbarFlexion_deg_RMS	0.058
14	RTShankCourse_deg_MEAN	0.043
15	RTAnkleInversion_deg_MAXIMUM	0.042
16	PelvisPitch_deg_MEAN	0.035
17	RTHipAbduction_deg_MAXIMUM	0.035
18	RTAnkleAbduction_deg_MEAN	0.032
19	LowerSpineCourse_deg_MEAN	0.027
20	LowerSpineCourse_deg_RMS	0.020

*Table 5.4: **The 20 Most Relevant Features Selected by NCA.** A ranked list of the top 20 features selected by Neighborhood Component Analysis (NCA) for their importance in motion classification. Each feature is associated with a specific body segment and motion parameter, including metrics such as maximum, mean, standard deviation, and root mean square (RMS) values. The weight column quantifies the relative importance of each feature, with higher weights indicating greater relevance to the analysis. This table highlights the features most influential in the study's data modeling and classification tasks*

Each ML model was trained and tested 10 times, normalizing the data and shuffling the

training and test sets to avoid bias. The mean and standard deviation were evaluated for each performance measure. The overall performance of the models is summarized in **Table 5.5**, considering all the features and those selected by the NCA.

All Features				
Classifier	**Precision)**	**Recall**	**Accuracy**	**AUC**
	(mean±std_dev)	(mean±std_dev)	(mean±std_dev)	
AdaBoost	0.811±0.000	0.820±0.000	81.978±0.000	0.905±0.000
REPTree	0.660±0.046	0.643±0.050	64.286±5.051	0.607±0.048
KNN	0.632±0.009	0.631±0.006	63.055±0.577	0.528±0.011
Logistic Regression	0.778±0.000	0.758±0.000	75.824±0.000	0.868±0.000
MLP	0.586±0.014	0.604±0.012	60.440±1.167	0.635±0.007
Random Forest	0.709±0.071	0.745±0.028	74.505±2.823	0.801±0.024
Random Tree	0.680±0.109	0.687±0.097	68.681±9.679	0.588±0.128
RSesLib KNN	0.661±0.000	0.648±0.000	64.835±0.000	0.568±0.000
SGD	0.624±0.011	0.654±0.008	65.407±0.788	0.516±0.013
SVM	0.821±0.000	0.763±0.000	76.264±0.000	0.554±0.000
NCA Selected Features				
Classifier	**Precision)**	**Recall**	**Accuracy**	**AUC**
	(mean±std_dev)	(mean±std_dev)	(mean±std_dev)	
AdaBoost	0.751±0.000	0.752±0.000	75.165±0.000	0.733±0.000
REPTree	0.726±0.034	0.679±0.050	67.846±5.566	0.670±0.058
KNN	0.834±0.008	0.820±0.003	81.978±0.368	0.675±0.003
Logistic Regression	0.626±0.000	0.618±0.000	61.758±0.000	0.590±0.000
MLP	0.787±0.052	0.799±0.049	79.846±4.508	0.766±0.051
Random Forest	0.843±0.043	0.841±0.035	84.044±3.409	0.901±0.041
Random Tree	0.726±0.092	0.697±0.090	69.736±9.768	0.639±0.118
RSesLib KNN	0.868±0.000	0.840±0.000	83.956±0.000	0.698±0.000
SGD	0.710±0.004	0.734±0.004	73.429±0.302	0.609±0.006
SVM	0.506±0.000	0.589±0.000	58.901±0.000	0.401±0.000

Table 5.5: Models Classification Performance. A comprehensive comparison of classification performance across various machine learning models. Metrics include precision, recall, accuracy (mean ± standard deviation), and the area under the curve (AUC). The table compares models using all features versus features selected by Neighborhood Component Analysis (NCA). The results highlight how feature selection impacts the performance of classifiers such as AdaBoost, KNN, Random Forest, and others, with metrics reflecting the effectiveness of each model in predicting outcomes

Table 5.6 shows the confusion matrix related to the Random Forest, which was found to be the best-performing classifier.

Following the study's secondary aim, a further analysis was executed to find the best-accuracy-retrieving combination of the minimum set of selected features. The accuracy as a function of the number of features selected by the NCA was analyzed to assess the best classifier

		Predicted	
		High	**Moderate**
Ground Truth	**High**	326	8
	Moderate	59	62

Table 5.6: Confusion Matrix of the Random Forest Classifier. *A confusion matrix summarizing the performance of the Random Forest classifier in distinguishing between high and moderate activity levels. The rows represent the ground truth, and the columns represent the predicted classifications. The matrix indicates 326 true positives (high activity correctly classified), 62 true negatives (moderate activity correctly classified), 59 false positives (moderate activity misclassified as high), and 8 false negatives (high activity misclassified as moderate). This visualization provides insights into the classifier's accuracy and error distribution*

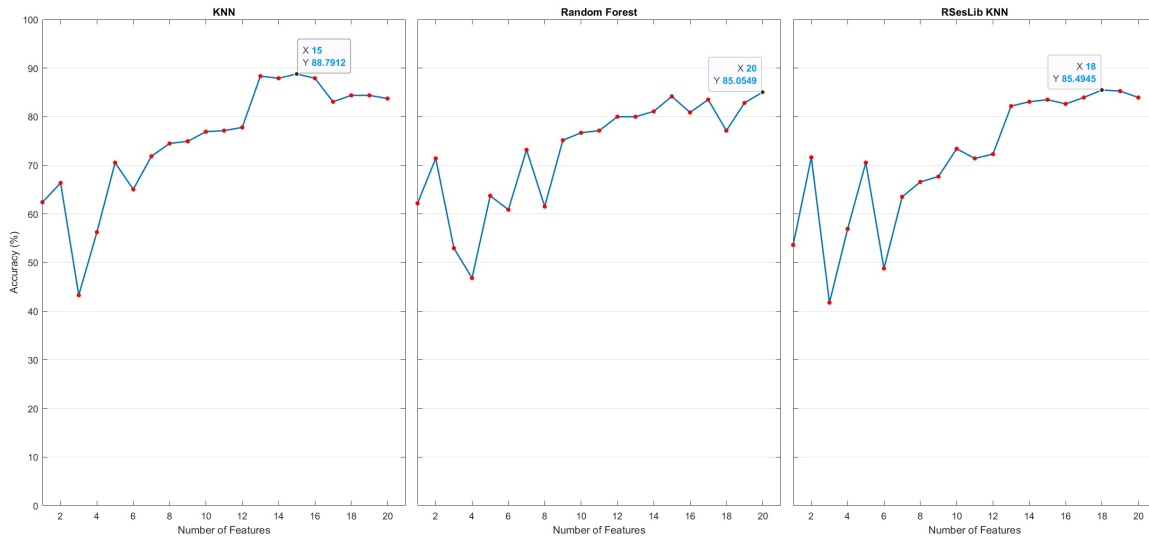with the fewest features (**Figure 5.7**).

Figure 5.7: Accuracy Trend of Best-Performing Classifiers. *A comparison of the accuracy trends for three classifiers (KNN, Random Forest, and RSesLib KNN) as a function of the number of features selected by Neighborhood Component Analysis (NCA). The x-axis represents the number of features used, while the y-axis indicates classification accuracy in percentage. Each classifier shows different performance patterns, with highlighted points indicating peak accuracies for specific feature counts, providing insights into the optimal feature selection for each algorithm*

5.1.6 Discussion and Conclusions

In the present study, the performance of different classifiers in predicting PAL was analyzed by considering statistical features extracted from kinematic gait data. The results show that walking with a linear trajectory at natural speed is sufficient to predict PAL with good accuracy without administering any questionnaire. Specifically, 9 IMUs were used to acquire kinematic data, and 6 gait cycles (recording only 8 seconds of walking) were considered to validate the methodology. In addition, the NCA algorithm was used to rank the derived statistical features and understand which IMUs are found to be most discriminating and to which body segment they belong. The NCA results showed that considering only four sensors is sufficient to predict PAL, as the algorithm recognized only features derived from lower body IMUs as relevant. The behavior of the best-performing classifiers was then analyzed by varying the 20 most relevant features selected by NCA.

Table 5.4 shows how the NCA algorithm considers features derived from position data of the lower body sensors more discriminating than those derived from velocity, acceleration, jerk, and

smoothness. In [207], the authors used NCA to identify the body segments and corresponding significant features with the greatest discriminatory power in classifying asymptomatic individuals from those with chronic neck pain while performing linear and nonlinear gait trajectories. Although nonlinear walking trajectories provided the best classification performance, a comparison can be made between the results obtained from the linear walking trajectory and the results presented in this study. It is reported that for a linear walk path, the most representative body segments appear to be those related to the upper body sensors, such as the head and trunk, while the characteristics related to jerk smoothness and speed turn out to be the most discriminative (higher feature weight). The differences between the studies result from having a similar walking direction with possibly different kinematic characteristics since walking overground is not limited by maintaining a constant gait speed. As reported in [208], statistically significant differences exist between overground and treadmill walking in healthy subjects for some joint kinematic and temporal variables. Specifically, significant increases were seen during treadmill walking in hip range of motion, maximum hip flexion joint angle, and cadence. Differences between overground and treadmill walking in temporal gait parameters were also reported [209]. The authors reported a lower pelvic obliquity motion for treadmill walking compared to overground walking, and the pelvic rotation movement pattern showed the most significant difference between walking modes. Moreover, the systematic review [210] reported significant differences in kinematic parameters such as reduced pelvic range of motion, maximum hip flexion angle for females, maximum knee flexion angle for males, and cautious gait pattern.

Considering the accuracy reported in **Table 5.5** the classifiers that benefited most from feature reduction were the KNN (81.978 ± 0.368), Random Forest (84.044 ± 3.409), and RSesLib KNN (83.956 ± 0). Previous studies have addressed ML classification problems using kinematic data from IMUs. However, it was shown by [211] that no ML model is the best for activity classification, as differences in sensor placement, IMU specifications, and pre-processing decisions can affect model performance. In [212, 213], the authors achieved 87.75% accuracy in classifying cerebral palsy and 98.60% in classifying upper limb exercises with the Random Forest classifier, respectively. Similar to what was found in this study, the results suggest that the Random Forest classifier demonstrates the highest classification accuracy using kinematic data from IMUs. The confusion matrix of the Random Forest is presented in **Table 5.6**, revealing that a significant number of misclassifications occur when instances are labeled as "High" instead of "Moderate" (59 misclassified instances). This result is not surprising, given the prevalence of the "High" category. However, a less noticeable effect was expected since the class imbalance was not as obvious.

In [214], the authors developed a Deep Neural Network model to detect stroke from kinematic gait data. They achieved 99.36% of accuracy in identifying stroke gaits. Further analysis of the identified stroke gaits shows that the drop foot gait, the circumduction gait, the hip hiking gait, and the back knee gait are stroke patients' four common gait abnormalities. As described in the articles reviewed above, several ML applications on kinematic data have been developed. Still, none have aimed to predict the result of a clinically validated questionnaire such as the IPAQ. This study represents the first step towards developing ML algorithms based on kinematic gait data able to predict clinically validated outcomes in different clinical populations, e.g., predicting the Motor Section 3 of the UPDRS in Parkinson's disease patients [215].

Of all the models analyzed, only those that performed best were selected for further analysis. It can be seen from **Figure 5.7** that, except for the Random Forest classifier, the highest value of accuracy is obtained with fewer features than those selected by the NCA. This suggests that some of the features selected by the algorithm are redundant in that they do not provide additional discriminatory information. The KNN classifier achieves the highest accuracy with only 15 features. The KNN and RSesLib KNN overall performance deteriorates after reaching the maximum accuracy value considering the first 15 and 18 features reported in **Table 5.4**, respectively.

One of the main limitations of this study was the small number of samples considered (37 participants). Although the data augmentation technique provided us with 1520 instances, it still limits the use of typical statistical techniques for ML model evaluation. Data augmentation forced manual perform of data splitting to ensure that all instances related to a single subject were present in the train or test set to avoid biasing classification results. For this reason, techniques such as cross-validation should be avoided, as it could not be guaranteed that instances

of the same participants would be limited to the train or test set.

Another limitation is represented by the statistical features derived from the original kinematic features. With the performed statistical feature extraction, the conducted analysis moved from a time series classification problem to a standard classification problem. These problems are easier to address because they require less computing power, making it possible to use tools such as WEKA for the testing part. On the other hand, working with derived features reduces the explicability of the models, making them less interpretable for clinicians. Instead of extracting statistical features, in [216, 217] the authors deal with time series data by making them all of the same lengths and then applying functional data boosting (FDboost) [218].

This study investigated the classification performance of different ML classifiers in discriminating PAL from motion data. It was shown that reducing the feature space increased performance for most considered classifiers. Analysis of the best-performing classifiers (KNN, Random Forest, and RSesLib KNN) showed the behavior of accuracy by varying the number of features considered, suggesting that some of the features are redundant.

Future work should focus on extending the proposed results by comparing NCA with other feature selection techniques and analyzing and testing additional ML classifiers based on time-varying data. In addition, a more in-depth analysis of performance behavior concerning the number of features considered is needed. To this end, shuffling the features to find the best minimum set of relevant features will be executed.

5.2 A novel measurement procedure for error correction in single camera gait analysis

5.2.1 Introduction

Gait Analysis plays a pivotal role in the quantitative assessment of human movement, offering vital insights for rehabilitation and health diagnostics. Despite the widespread application of optoelectronic systems as the clinical "gold standard," their expense and complexity limit broader implementation. Integrating IMUs and MLB MoCap advancements promises a more accessible alternative. This study aims to validate the accuracy of a novel, cost-effective MLB software developed using the OP library to measure knee flexion and ankle dorsiflexion angles.

5.2.2 State of the Art

The evolution of GAn methodologies reflects the pursuit of accurate, efficient, and practical solutions for assessing human motion. Gait Analysis is a critical diagnostic tool in rehabilitation and health diagnostics, providing quantitative insights into gait biomechanics and enabling timely interventions by extracting clinically relevant parameters to assess walking ability [175, 176, 177].

Historically, optoelectronic systems have been considered the "gold standard" for GAn. These systems, which track three-dimensional (3D) marker-based motion using multiple cameras, deliver highly accurate kinematic data [219, 220, 221]. However, their reliance on controlled environments, extensive setup requirements, and technical expertise limit their practicality for widespread clinical use [222]. To overcome these limitations, IMUs have emerged as a portable and cost-effective alternative. Inertial Measurement Unit sensors, comprising accelerometers, gyroscopes, and magnetometers, facilitate motion analysis outside traditional gait laboratories and are particularly suited for applications requiring accessibility and quick setups [223, 132, 224]. Despite their advantages, IMUs face challenges such as calibration issues in ferromagnetic environments and the significant technical expertise required for data processing [225].

Marker-Less-Based systems have further transformed GAn by leveraging camera-based technology and HPE algorithms to track body movement without needing physical markers. These systems simplify experimental setups, eliminate the need for specialized laboratories, and have been applied in clinical assessments and sports biomechanics [226, 149, 227].

Two-dimensional (2D) single-camera systems based on CNN have gained popularity in parallel. Open-source models like OP and PoseNet estimate human joint positions directly from 2D images or videos, providing a cost-effective and flexible solution for GAn [70, 172]. These

systems offer stable joint location estimates while reducing the technical barriers associated with traditional methods. However, their focus on positional data limits their ability to capture critical 3D kinematic parameters needed for biomechanical analysis.

Advances in CV and DL have further enhanced MLB systems. Custom-trained models, particularly those based on OP, now demonstrate precision in joint angle estimation and are increasingly viable for clinical applications. Studies validating these methods against IMUs have shown promising results, with certain configurations achieving accuracy sufficient for clinical assessments [173]. For example, single-camera setups have been successfully applied to estimate knee flexion and ankle dorsiflexion angles, offering streamlined and cost-effective approaches to GAn.

Despite these innovations, challenges remain in optimizing MLB systems for real-world applications. Controlled environments are often required, and limitations in capturing fast joint movements or subtle kinematic details persist. Researchers focus on refining experimental setups and integrating advanced algorithms to address these issues to enhance accuracy and reliability.

Building on this foundation, the current study aims to validate a cost-effective MLB software for estimating knee flexion and ankle dorsiflexion angles using a single-camera setup. By comparing OP-derived estimations with IMUs data, this approach seeks to refine the precision of GAn while reducing complexity and costs, advancing the feasibility of clinical and research applications.

5.2.3 Study Design

Thirty-one young, healthy subjects (mean age 24.07 ± 6.42 years, 20 females) participated in this study. Their characteristics are summarized in **Table 5.7**.

	Male	**Female**	**Overall**
Number (%)	11 (35%)	20 (65%)	31
Age (mean±std_dev)	25 ± 5.8	23 ± 6.7	24 ± 6.42

Table 5.7: Participant Demographics and Characteristics. A table summarizing the demographics of the study participants, grouped by gender and overall. It includes the number of participants (with percentages) and their ages represented as mean ± standard deviation. This table provides an overview of the sample population's composition and age distribution

Data collection involved two five-minute treadmill walking tasks, during which lower-body motion data were recorded using 7 IMUs (MyoMotion, NORAXON, USA) sampling at 100 Hz. Additionally, a high-definition camera (Logitech Brio 4K Stream Edition) captured synchronized video data at 60 fps and 720 × 1280 pixels resolution. Details of the experimental setup and IMU placement are described in **Chapter 4**.

IMU sensors were positioned on the pelvis, thighs, shanks, and feet using elastic belts and skin-safe tape (Hypafix, BSN Medical GmbH), as illustrated in **Figure 5.8**. Calibration was conducted in a ferromagnetic interference-free zone before each task. Participants were instructed to maintain an upright posture during calibration to ensure accurate measurements.

The camera was mounted on a fixed tripod 2.80 meters away from the treadmill at a 45-degree angle, optimizing joint visibility and minimizing occlusion issues (**Figure 5.9**).

The orientation angle was chosen to optimize the visibility of body joints and to exclude any possible occlusion problem that affects 2D videos [228, 174]. Subjects were then recorded while walking for five minutes at a comfortable speed on the treadmill. The recorded videos were analyzed and segmented into fifteen twenty-second trials. Each trial was processed with self-made OP-based software to obtain both legs' 2D knee and ankle joint angles. OP is an open-source processing framework developed by a research group at Carnegie Mellon University [70], implemented in C++ and utilizing OpenCV and Convolutional Architecture for Fast Feature Embedding (Caffe). OpenPose can perform real-time multi-person 2D joint detection, providing the 2D coordinates of anatomical keypoints for each person in the input RGB images

Figure 5.8: Placement of Sensors on Lower Limbs. *This image shows the front and back views of sensor placement on the lower limbs. Sensors are affixed to key anatomical landmarks, including the thighs, shanks, and feet, to accurately capture motion data during gait analysis. Proper placement ensures reliable and consistent measurements for biomechanical evaluations*
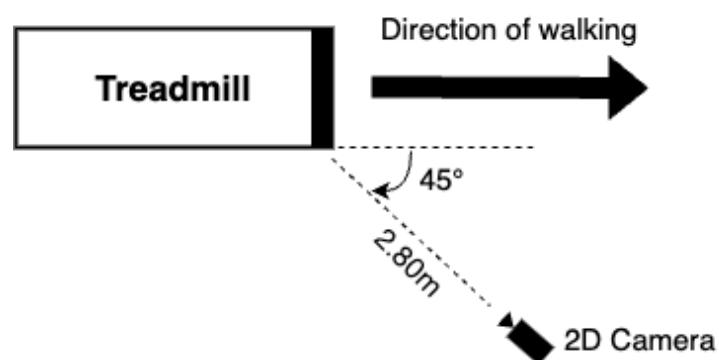

Figure 5.9: Protocol's Experimental Setup. *Schematic representation of the experimental setup for motion capture during treadmill walking. A 2D camera is positioned at a distance of 2.80 meters from the treadmill, angled at 45 degrees relative to the walking direction. This configuration minimizes occlusion while capturing comprehensive gait data*
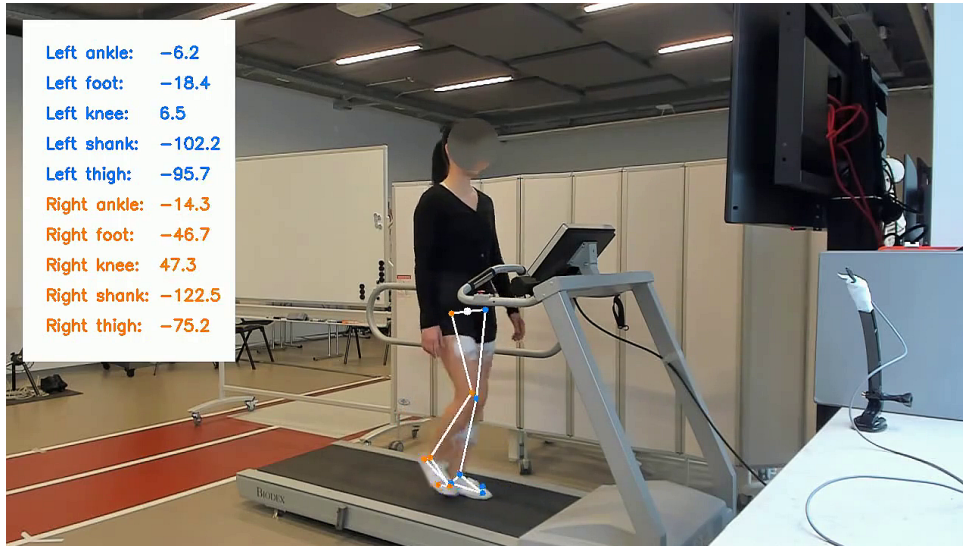
Figure 5.10: Output of Custom OP-Based Software. *The image illustrates the output of the custom-built OpenPose-based (OP-based) software, showcasing the estimation of joint angles from a video input during treadmill walking. Joint angles for both left and right limbs are displayed alongside skeletal tracking, highlighting the system's capability for real-time biomechanical analysis.*

captured from standard webcams. In the initial step, a feed-forward network predicts 2D confidence maps of body part locations and 2D vector fields encoding limb location and orientation [229]. These confidence maps represent the likelihood of a particular body part occurring at the location of each pixel. Furthermore, for each pixel, OP provides a 2D vector representing the limb position and orientation. The last stage associates the confidence maps and affinity fields using greedy inference to generate 2D keypoints for all individuals in the image. The CNN is trained on the Common Objects in Context (COCO) dataset [230], augmented by a foot dataset comprising 15,000 annotations from the COCO dataset. These datasets contain RGB images depicting various real-world scenarios and challenges, such as object detection, segmentation, image capturing, person keypoints detection, and recognition in context [229]. Instead of using the standard OP library, which allows the extraction of the 2D position in pixels for each frame, we developed self-made software that utilizes the OP position information as a reference for detecting the lower limbs.

5.2.4 Data Processing

Videos were analyzed with developed software to obtain each frame's knee and ankle joint angles. To validate the proposed approach and ensure robustness, we systematically segmented the initial five-minute acquisition for each participant into fifteen trials, each lasting twenty seconds. This choice aligns with the minimum number of steps to consider, as taking at least twelve steps is considered sufficient to perform averaging procedures and thus minimize artifacts caused by natural gait variability [195]. Segmenting the data in this way allowed us to analyze the data in manageable segments, significantly reducing the extensive processing time required for the full acquisition. This optimization of data processing not only facilitated detailed assessments across various conditions within the study but also enhanced the accuracy of our evaluations, thereby contributing significantly to the reliability of our findings. Due to erratic IMUs signals, two of the initial thirty-one subjects were excluded from the data analysis, resulting in twenty-nine participants being considered.

Figure 5.10, shows the output of the custom-built OP-based software. By giving a 2D video as input, the software can estimate both legs' knee flexion and ankle dorsiflexion angles, which are also printed in the output video.

The data set for the GAn was created using both the camera and the IMUs of the twenty-nine considered participants, and from these, the angles of the joints, particularly the knee and ankle joints, were derived. The study aimed to compare the angles estimated by camera-based and IMU approaches, both in terms of signal correlation and measurement compatibility, and to
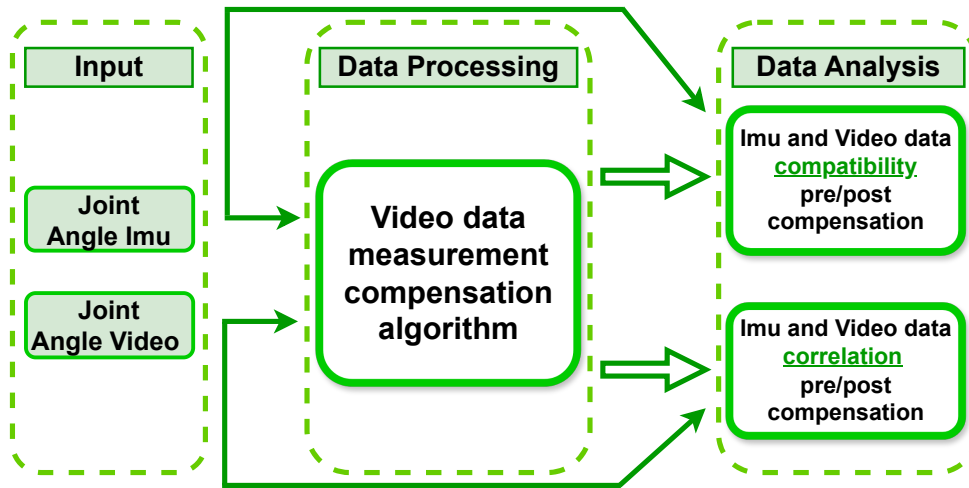
Figure 5.11: Block Diagram of Data Processing and Analysis. The block diagram summarizes the logical steps used to process and compare the data acquired from inertial sensors and video input. It outlines the data flow through input acquisition, processing, measurement compensation, and correlation analysis, ensuring compatibility between the two data sources for accurate biomechanical evaluation.
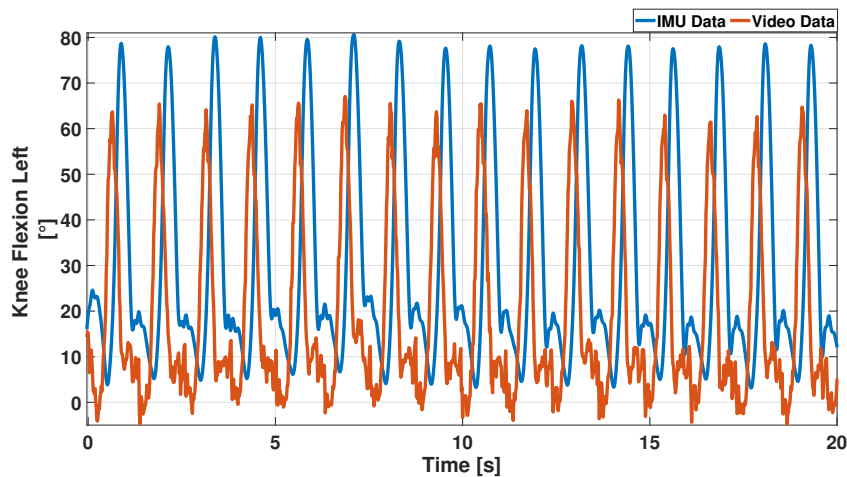

Figure 5.12: Comparison of Knee Flexion Signals (Pre-Compensation). The graph compares the knee flexion signals obtained from inertial measurement units (IMUs) and video-based motion capture systems in the pre-compensation case. Time-series data demonstrate discrepancies between the two methods, highlighting the necessity for signal alignment and compensation to ensure accurate biomechanical analysis

find suitable compensation mechanisms to make camera-based measurements compatible with a reference case, i.e., the IMU-based data. The block diagram in **Figure 5.11** explains how the data were processed and managed; in particular, the process inputs were the raw joint angles from the IMUs and the video, respectively.

Figure 5.12 shows an example of knee flexion acquired from one participant: the orange line (video data) is delayed and offset from the blue line (IMUs data); these differences have to be compensated to make data comparable. A suitable compensation algorithm has been developed to achieve this goal.

The compensation algorithm pseudo-code was described in **Algorithm 1**, particularly correction factors were calculated based on a frequency study. The dataset was split into two parts:

- data from 19 participants were used to compute the compensation coefficients (training group)

- data from 10 participants were used to apply the correction coefficients previously computed (test group)

The compensation coefficients were intentionally applied uniformly across all participants. This approach demonstrated that the coefficients are independent of individual subjects, ensuring the method's generalization ability across different populations. By applying the same coefficients universally, we validate the robustness and reproducibility of the method, confirming its applicability in diverse scenarios beyond the specific subjects used for training.

Once the training group was set up, IMUs and video data were loaded for each participant and each joint angle, on which a Fast Fourier Transform (`FFT`) was performed to obtain the signal module and phase. Two vectors are created, one defined by the difference between the IMUs and video tracks' modules and the other by the difference between the phases calculated on the IMUs and video signals. The compensation coefficient was computed by the maximum occurrences of difference vectors Diff_{Mod}, Diff_{Ph} and added to the video `FFT` traces of the test group. Finally, an Inverse Fast Fourier Transform (`IFFT`) was applied to the corrected video trace to return to the time domain signal. The algorithm was run for all participants in the test group and for the four joint angles considered in this study (left and right knee flexion, left and right ankle dorsiflexion).

Algorithm 1 Video Data Compensation

1: **Input**: Raw IMU-Video Signals
2: **Output**: Compensated Video Signals
3: N_{angle} = Total number of joint angles
4: N_{ID} = Total number of training group participants
5: **for** $y = 1, \ldots, N_{angle}$ **do**
6:     **for** $k = 1, \ldots, N_{ID}$ **do**
7:         $Imu = \texttt{load}(Imu_{data}(y,k))$
8:         $Video = \texttt{load}(Video_{data}(y,k))$
9:         $I_{Mod}(:,k) = \texttt{abs}(\texttt{fft}(Imu))$
10:        $I_{Ph}(:,k) = \texttt{angle}(\texttt{fft}(Imu))$
11:        $V_{Mod}(:,k) = \texttt{abs}(\texttt{fft}(Video))$
12:        $V_{Ph}(:,k) = \texttt{angle}(\texttt{fft}(Video))$
13:        $Diff_{Mod}(:,k) = I_{Mod}(:,k) - V_{Mod}(:,k)$
14:        $Diff_{Ph}(:,k) = I_{Ph}(:,k) - V_{Ph}(:,k)$
15:     **end for**
16: **end for**
17: **Compensation coefficients**: Maximum occurrences of vectors $Diff_{Mod}$ and $Diff_{Ph}$
18: **For test group participants:**
19: $V_{ModComp} = V_{Mod} + \texttt{MaxOcc}(Diff_{Mod})$
20: $V_{PhComp} = V_{Ph} + \texttt{MaxOcc}(Diff_{Ph})$
21: $V_{Final} = \texttt{real}(\texttt{ifft}(V_{ModComp} \cdot \texttt{exp}(1j \cdot V_{PhComp}))) = 0$

Figure 5.13 displays an example of the compensation effect on the video signal: compared to **Figure 5.12**, the offset and delay of the orange signal were balanced. This gives better tracking of the IMUs signal. Two features were computed to evaluate the compensation's effect: the measurement's compatibility and the correlation between the signals. Measurements of the same quantity can be different but compatible, i.e., not statistically discrepant, if the absolute value of their difference falls within the expanded standard uncertainty interval, given a target confidence level: the rigorous definition from International Vocabulary of Metrology can be found in [231]. Specifically, to evaluate the compatibility, the mean and standard deviation of the mean (Type A computed standard uncertainty) of 15 trials of 20 s each for both video and IMUs data were considered for the test group. On the other hand, the correlation coefficient was used to analyze the linear dependence between IMUs and video signals. Particularly, the Pearson correlation was applied (eq. (**5.2**)).

$$\rho(V, I) = \frac{1}{N-1} \sum_{i=1}^{N} \left(\frac{V_i - \mu_V}{\sigma_V} \right) \cdot \left(\frac{I_i - \mu_I}{\sigma_I} \right) \tag{5.2}$$

Where V and I are the video and IMUs signals, respectively, μ_V and σ_V are the mean and
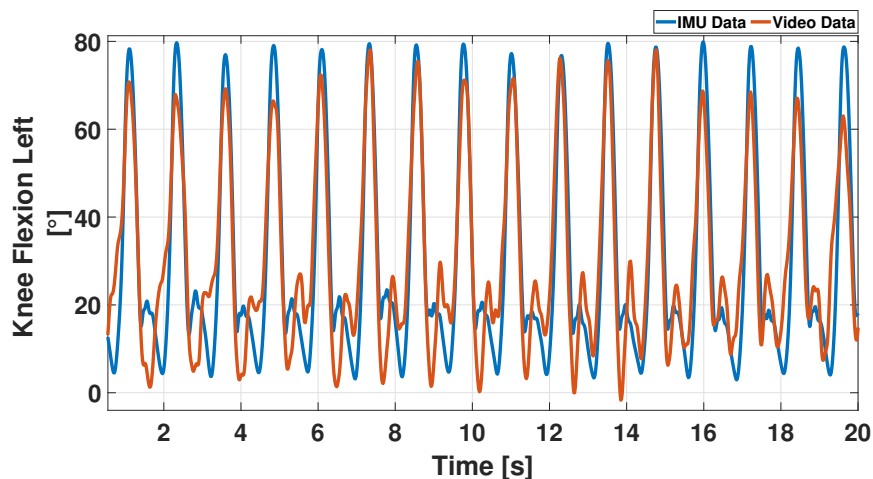
Figure 5.13: Comparison of Knee Flexion Signals (Post-Compensation). *The graph illustrates the alignment of knee flexion signals obtained from inertial measurement units (IMUs) and video-based motion capture systems after applying a compensation algorithm. The time-series data demonstrate improved agreement between the two methods, ensuring enhanced accuracy and compatibility for biomechanical analysis*

standard deviation of the video signal, while μ_I and σ_I are the mean and standard deviation of IMUs signal. Both the compatibility and the correlation are carried out on the IMUs/video data of the test group pre- and post-compensation.

5.2.5 Results

The feature's data processing and computation were obtained using MATLAB® environment. The compatibility between the video and IMUs signals was assessed pre and post-compensation, and it is shown graphically in **Figure 5.14** and **Figure 5.15**. The blu and purple bars indicate the compatibility obtained pre/post compensation for the Knee Flexion Left (KL, **Figure 5.14a**) and Right (KR, **Figure 5.14b**). In contrast, the green and yellow bars represent the compatibility pre/post compensation of the Ankle Dorsiflexion Left (AL, **Figure 5.15a**) and Right (AR, **Figure 5.15b**). In the case of the knee, it is clear how compensation has improved compatibility in most cases. In particular, as described in **Table 5.8** for the KL, an improvement of 80% is achieved, while for the KR, it is 90%. It should be noted, however, that compatibility pre-compensation is over 70%.

|	**Knee Left**	**Knee Right**	**Ankle Left**	**Ankle Right**
Compatibility	8/10	9/10	8/10	10/10
Correlation	9/10	8/10	10/10	7/10

Table 5.8: Improvement Rate for Post-Compensation Performance. *A table summarizing the improvement rates of post-compensation performance compared to pre-compensation for each joint. The metrics include compatibility and correlation, evaluated across four joints: Knee Left, Knee Right, Ankle Left, and Ankle Right. The improvement rate is represented as the number of participants with better post-compensation results out of 10 total participants, demonstrating the effectiveness of the compensation algorithm*

The **Table 5.9** shows the average of the compatibility coefficients calculated for each participant. In the case of the knee, an improvement of 5% (KL) and 6%(KR) is observed between the period pre and post-compensation. An enhancement of 16% (AL) and 57% (AR) is observed for the ankle from pre-post compensation. The clearing operation brings the average compatibility values above 91% in three out of four cases.

Moving on to the correlation, the main obtained results are reported in **Figure 5.16** and **Figure 5.17**. Similarly to how it was done for compatibility, the blue and purple bars indicate the pre/post compensation correlation for the knees (**Figure 5.16a - 5.16b**), while the green
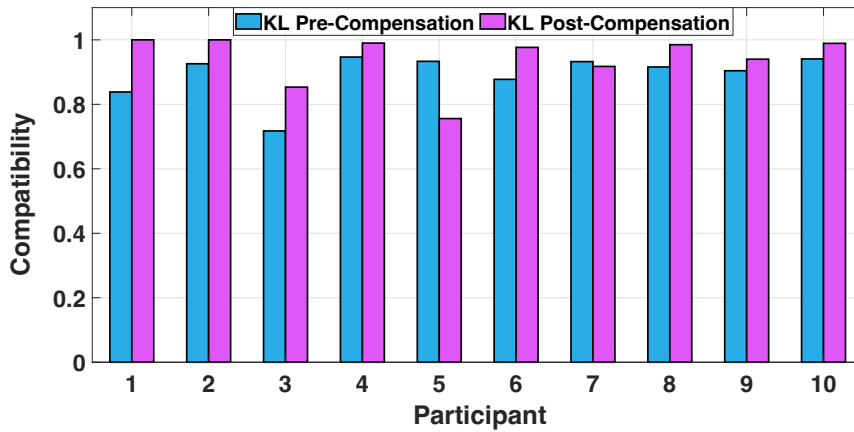
(a) Knee flexion left
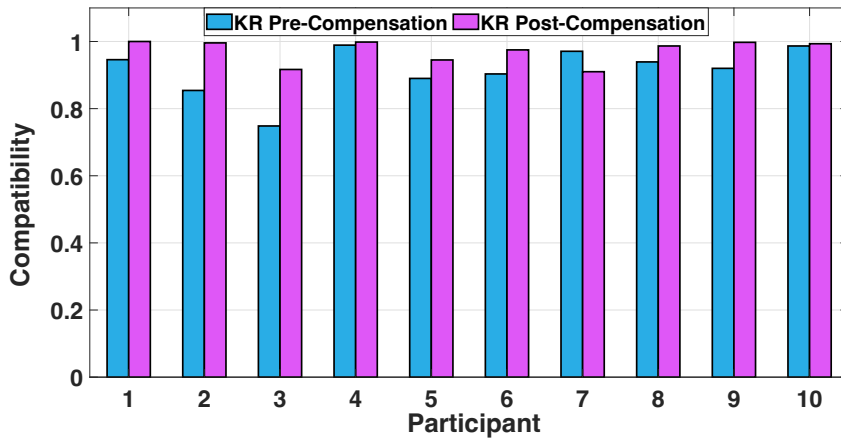
(b) Knee flexion right

Figure 5.14: Pre- and Post-Compensation Compatibility for Knee Flexion. *Two bar plots comparing the compatibility between IMU and video-based signals for knee flexion before and after compensation, calculated across participants. (a) Knee Flexion Left: Illustrates compatibility metrics for the left knee, showing substantial improvement after compensation. (b) Knee Flexion Right: Demonstrates compatibility metrics for the right knee, similarly reflecting enhanced alignment of signals post-compensation. These results highlight the effectiveness of the compensation algorithm in aligning IMU and video signals for biomechanical analysis*
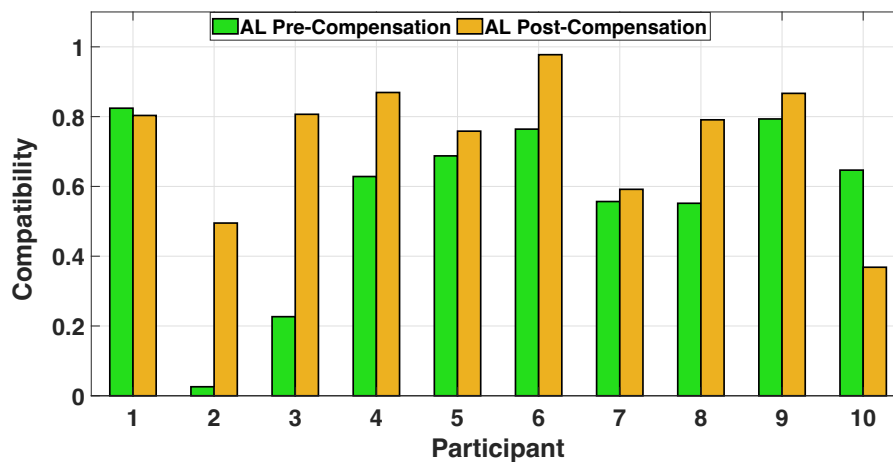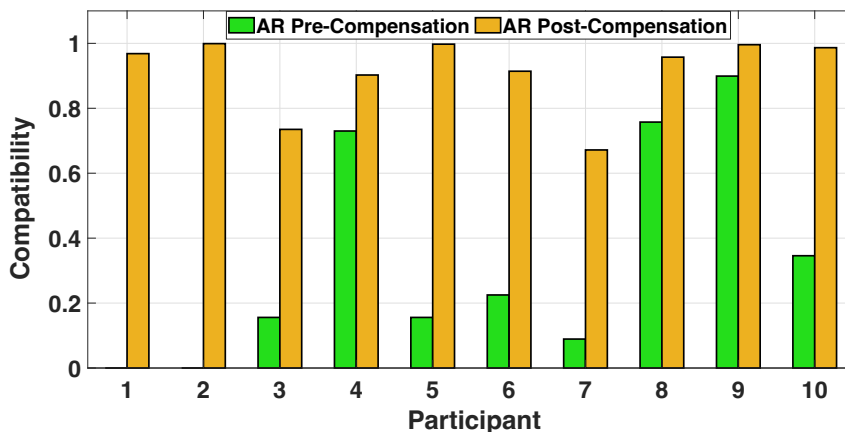
(a) Ankle dorsiflexion left

(b) Ankle dorsiflexion right

Figure 5.15: Pre- and Post-Compensation Compatibility for Ankle Dorsiflexion. *Two bar plots comparing the compatibility between IMU and video-based signals for ankle dorsiflexion before and after compensation, calculated across participants. (a) Ankle Dorsiflexion Left: Depicts compatibility metrics for the left ankle, showing significant improvements post-compensation. (b) Ankle Dorsiflexion Right: Displays compatibility metrics for the right ankle, highlighting enhanced signal alignment after compensation. These findings emphasize the effectiveness of the compensation algorithm in harmonizing IMU and video signals for accurate biomechanical assessments*

	Compatibility Knee Left	Compatibility Knee Right	Compatibility Ankle Left	Compatibility Ankle Right
Pre-Compensation	0.89	0.91	0.57	0.34
Post-Compensation	0.94	0.97	0.73	0.91

Table 5.9: Mean Compatibility Coefficients Across Joints. *This table displays the mean compatibility coefficients for each participant, evaluated across four joints: Knee Left, Knee Right, Ankle Left, and Ankle Right. The coefficients are presented for both pre-compensation and post-compensation scenarios. Significant improvements are observed post-compensation, particularly in the ankle joints, where compatibility values increased substantially. These results demonstrate the effectiveness of the compensation algorithm in aligning IMU and video-based motion data*

(a) Knee flexion left
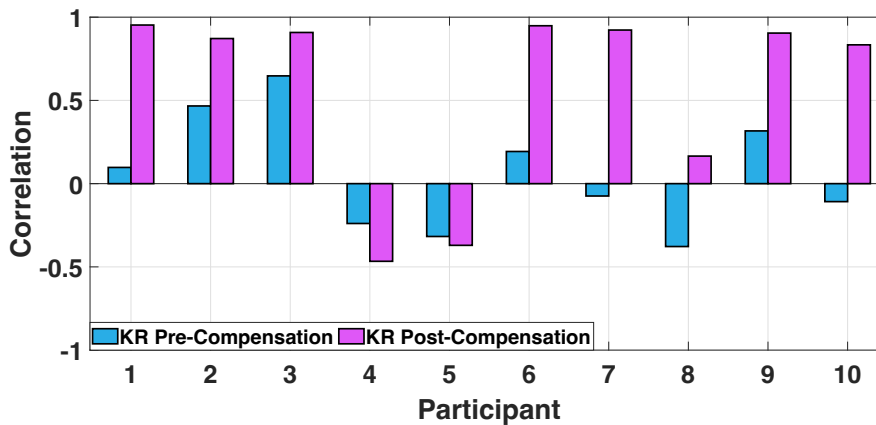
(b) Knee flexion right

Figure 5.16: Pre- and Post-Compensation Correlation for Knee Flexion. *Two bar plots comparing the correlation coefficients of IMU and video-based signals for knee flexion before and after compensation, evaluated across participants. (a) Knee Flexion Left: Displays the correlation coefficients for the left knee, showing significant improvements post-compensation. (b) Knee Flexion Right: Illustrates the correlation coefficients for the right knee, highlighting enhanced alignment of signals after applying the compensation algorithm. These results demonstrate the effectiveness of the compensation algorithm in improving signal correlation for accurate biomechanical evaluations*

and yellow bars represent the pre/post compensation correlation for the ankles (**Figure 5.17a - 5.17b**).

Compensation of video data ensures a clear improvement in the correlation parameter. This result is also underlined in the second row of the **Table 5.8**: an improvement of 90% is obtained in the case of the KL and 80% in the KR. Concerning the AL, all participants get an improvement in the correlation coefficient, while in the case of the right ankle, 70%.

(a) Ankle dorsiflexion left
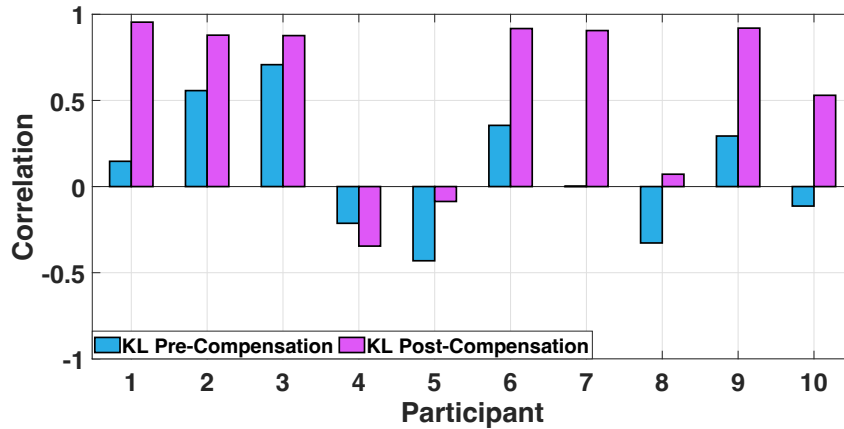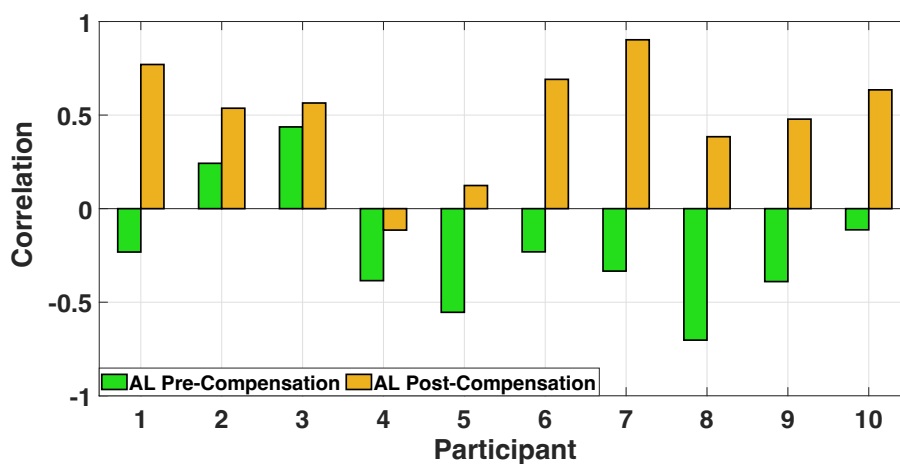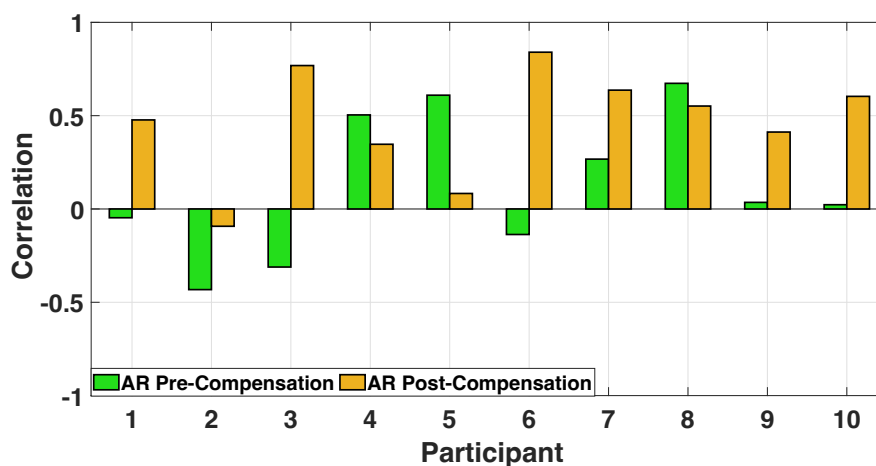

(b) Ankle dorsiflexion right

Figure 5.17: Pre- and Post-Compensation Correlation for Ankle Dorsiflexion. *Two bar plots comparing the correlation coefficients of IMU and video-based signals for ankle dorsiflexion before and after compensation, evaluated across participants. (a) Ankle Dorsiflexion Left: Displays the correlation coefficients for the left ankle, indicating significant improvements post-compensation. (b) Ankle Dorsiflexion Right: Illustrates the correlation coefficients for the right ankle, showing enhanced alignment of signals after applying the compensation algorithm. These results highlight the algorithm's effectiveness in improving signal correlation for accurate biomechanical analysis of ankle motion*

Looking at the **Table 5.10**, the mean of the correlation coefficient in pre-compensation is below 11% in all 4 cases; this indicates that before the correction, the trends of the IMUs and video tracks were uncorrelated. Turning to the post-compensation correlation values, it can be observed that in 3 cases out of 4 (KL-KR AL), it goes above 50%. The greatest increase is recorded for AL, from a negative correlation value of -0.22 to 0.50. Correcting the video data improves performance relative to the correlation coefficient.

	Correlation Knee Left	Correlation Knee Right	Correlation Ankle Left	Correlation Ankle Right
Pre-Compensation	0.10	0.06	-0.22	0.11
Post-Compensation	0.56	0.57	0.50	0.46

Table 5.10: Mean Correlation Coefficients Across Joints. This table presents the mean correlation coefficients for each participant across four joints: Knee Left, Knee Right, Ankle Left, and Ankle Right. The values are shown for both pre-compensation and post-compensation scenarios. Post-compensation results indicate a substantial improvement in correlation, demonstrating the algorithm's effectiveness in aligning IMU and video-based motion data. Negative correlations in the pre-compensation case (e.g., Ankle Left) were successfully resolved, further validating the robustness of the compensation approach

After assessing the impact of the compensation on the measurements, the mean error of the angle amplitude pre and post-correction is compared. **Figure 5.18** shows a bar chart between the mean error obtained as the difference between the video trace and the IMU trace pre- (blue bar) and post-correction (orange bar).
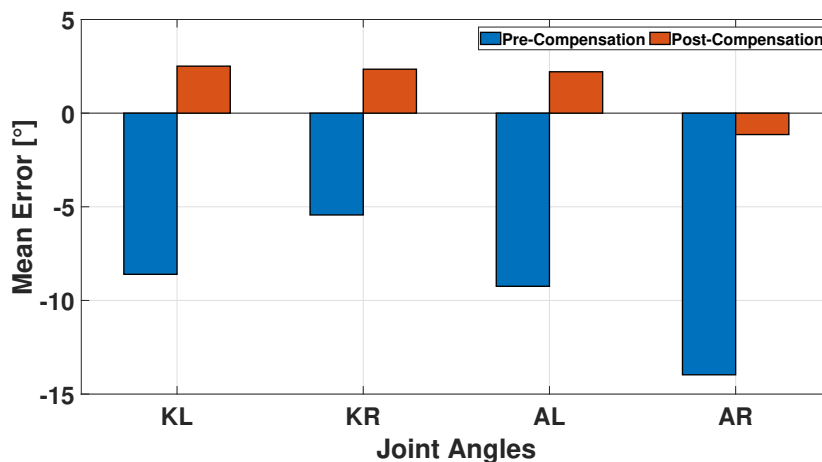
Figure 5.18: Mean Error Between IMU Reference and Video Data. A bar plot illustrating the mean error (in degrees) between IMU reference data and video-based motion data for pre- and post-compensation scenarios. The error is evaluated across four joint angles: Knee Left (KL), Knee Right (KR), Ankle Left (AL), and Ankle Right (AR). Post-compensation results show a significant reduction in error, demonstrating the effectiveness of the compensation algorithm in aligning IMU and video data for biomechanical analysis

Before compensation, the video signal is underestimated relative to the reference IMU signal, and the worst mean error obtained is around 15°. Conversely, after correction, the error is reduced to 2° relative to the reference, although there is a slight overestimation in all three-quarters of the cases studied.

Finally, to make our evaluation more robust, we also computed the waveform distortion, adopting the IMU trace as a baseline and evaluating its discrepancy with respect to the video trace with and without applying the compensation algorithm. In particular, we obtain that the distortion of the compensated video data is much lower than the same value calculated without applying our compensation algorithm in 92.72% of the training cases (82.67% in the test).

5.2.6   Discussion and Conclusions

The main aim of this study is to compare knee and ankle joint angle assessment in the sagittal plane, evaluating the accuracy of the measurement of the video data vs the IMUs-based data. An algorithm was implemented and applied to a training group to calculate the compensation coefficient based on frequency analysis. Particularly, the compensation coefficient is computed considering a subgroup of participants (training group) by evaluating and comparing the module and phase of the IMUs and Video track. This operation is necessary to compensate for time delay and amplitude offset. The observed delay may be attributed to the different sampling frequencies between the two technologies. Specifically, the IMUs operate at 100 Hz, whereas the camera captures at 60 FPS (60 Hz), leading to a potential mismatch in data synchronization. Subsequently, these factors were used to correct video data from the test group. Regarding the amplitude offset, it is likely due to the precision limitations of the developed software when processing the video data, which could impact the accuracy of the results. After applying the developed algorithm, the results show how video data compared with IMUs obtained an accuracy improvement of more than 80% for compatibility and more than 70% for correlation. Specifically, the mean pre/post compatibility for KL went from 0.89 to 0.94, KR from 0.91 to 0.97, AL from 0.57 to 0.73, and AR from 0.34 to 0.91. Looking at the mean values of the pre/post correction correlation coefficients, it can be seen that for KL they ranged from 0.097 to 0.56, for KR from 0.060 to 0.57, while for AL the mean correlation went from -0.22 to 0.50 and for AR from 0.11 to 0.46. These results demonstrate how the compensation made on the video data positively impacts the measurements, improving the quality of the video data compared to the IMUs signal in terms of compatibility and correlation. Moreover, the average error calculated on the post-compensation data (**Figure 5.18**) is also significantly reduced compared to the pre-case, in particular for KL, KR, AL, a slight overestimation and an error of about 2° is obtained, while in the case of AR, a slight underestimation with an error of 1° is obtained.

Several studies have assessed the application of single-camera markerless motion capture systems in analyzing movements by comparing these techniques with manual labeling or traditional marker-based systems. Specifically, these studies have concentrated on analyzing limb movements closest to the camera. In [232] and [153], the authors found that while markerless approaches yielded greater joint center deviations (10-20 mm) compared to marker-based systems, they did not exhibit significant differences in temporospatial and joint angle outcomes in activities like underwater running and walking among stroke survivors. This suggests that single-camera markerless methods can be practical alternatives to traditional systems, achieving temporo-spatial and planar 2D joint angle measurements with accuracy comparable to traditional marker-based systems, particularly when assessments are conducted on the side of the body closest to the camera [233].

A recent study compared the accuracy of a markerless system to that of a marker-based system for spatiotemporal parameters and joint angles. While the markerless system slightly underestimated maximum flexion for knee and ankle angles, the overall performance in gait analysis was comparable to marker-based systems, with only minor discrepancies in sagittal plane movements, demonstrating the potential of markerless systems to serve as a practical alternative in clinical settings [234]. In another systematic review, researchers found that markerless systems performed well in measuring spatiotemporal gait parameters, with good-to-excellent accuracy and reliability compared to marker-based systems. However, for joint angles, the results were more variable, with higher accuracy in measuring hip and knee movements in the sagittal plane but lower accuracy in the transverse and frontal planes. This highlights that while markerless systems are improving, there are still challenges in capturing complex multi-plane movements with the same precision as marker-based systems [47].

[66] highlight that markerless systems are finding crucial applications in sports biomechanics and rehabilitation. However, their ability to measure complex movements accurately, particularly in varying environments, has not been fully validated. Some systems can measure sagittal plane angles with reasonable accuracy (within 2°–3° during walking gait), but comprehensive validation across different movements and settings is lacking.

Previous studies on markerless GAn tried to assess the feasibility of such approaches by validating them with IMUs. In [173], authors have explored the feasibility of using dual-camera systems and linear triangulation algorithms. While the angular trajectories recorded by the

markerless system generally matched the IMUs waveform trajectories, they reported significant inaccuracies, particularly in ankle and knee angle estimations. Additionally, the system often failed to track foot coordinates effectively across most frames and from all camera positions, exacerbated by the complex relative rotation of the ankle with the foot and shank and the lower visibility of the foot segment to cameras compared to larger body segments like the pelvis, thigh, and tibia [235, 236].

This study aims to build upon the foundation set by previous research in markerless motion analysis, such as the work by [173]. While the referenced study utilized a dual-camera system, our research demonstrates the potential of a single-camera system paired with an advanced compensation algorithm based on frequency analysis. This approach has shown promise in reducing computational complexity and costs while maintaining high accuracy in measuring joint angles. In contrast to earlier studies that reported substantial inaccuracies with errors up to $14° \pm 1.8$ in ankle and knee angle estimations, our methodology has been shown to reduce these errors significantly. The mean post-compensation errors in our study are approximately 2° for knee angles and 1° for ankle angles. This improvement is substantial regarding numerical values and reflects a meaningful advancement in the accuracy and reliability of video-based joint angle measurements. Applying the compensation algorithm has facilitated an 80% improvement in compatibility and a 70% increase in correlation between the video data and IMUs measurements. These improvements underscore the potential of our single-camera, algorithmically-enhanced system to provide accurate assessments of knee and ankle joint angles, even in comparison to systems using more complex and costly dual-camera setups.

Markerless motion analysis systems, particularly those utilizing single-camera setups, are emerging as promising tools in biomechanical research despite their relative infancy and the current limitations in capturing the full range of three-dimensional human motion. Studies such as those by [236] have demonstrated the potential for clinical applications, showing effectiveness in observing major joint movements with ease and reduced preparation time. However, these systems often fall short in accurately tracking smaller or more complex joints like the ankle, especially during faster movements, compared to marker-based systems, which remain the gold standard in many biomechanical and clinical settings.

Our research builds upon these findings by simplifying the hardware setup without compromising the quality of data, which proves particularly beneficial in environments requiring minimalistic setups. Through algorithmic enhancements, we have refined the capabilities of single-camera systems, extending their applicability in clinical settings and sports environments. This work emphasizes the potential for these technologies to become more accessible and practical, driven by lower equipment and processing requirements.

However, several limitations of the current study should be acknowledged. First, the method is validated only on healthy subjects, which may limit its applicability in populations with altered gait patterns, such as individuals with neurological or musculoskeletal disorders. Further testing is required to evaluate the robustness of this approach in these populations. Additionally, the study was conducted in a controlled environment using a treadmill, which may not fully represent real-world conditions. Gait on a treadmill can differ from overground walking, potentially affecting the generalizability of our findings to everyday scenarios. Another limitation is the accuracy of the single-camera setup in dynamic and multi-plane movements. While promising for knee flexion and ankle dorsiflexion, the system may struggle with more complex three-dimensional joint angles, particularly during fast or irregular movements. This suggests further enhancements in the algorithm's tracking ability for more intricate motion patterns. Finally, while the compensation algorithm used in this study improves accuracy, it may still require refinements to ensure compatibility with various camera setups and different environmental conditions.

This study represents the initial phase in the broader research trajectory, aiming to develop a model capable of automatically correcting raw video data to closely match IMUs data trends. The insights garnered here set the foundational work necessary for the future creation of such a model, intending to capture the same IMUs features from acquired 2D video data. This preliminary work is designed to make the acquisition setup faster and less intrusive, offering significant benefits over more complex multi-camera systems.

Future research should focus on expanding the applicability of this method to diverse populations, including individuals with abnormal gait patterns or clinical conditions. This would

involve collecting data from various age groups and clinical populations and performing testing in more natural, overground walking environments. Furthermore, advancements in deep learning techniques could be explored to improve the accuracy and adaptability of the single-camera system in capturing complex multi-plane movements.

As we refine these methodologies, we aim to reduce error margins further and enhance the practicality of single-camera systems in conducting dynamic and complex motion analyses. These advancements contribute significantly to the ongoing dialogue in biomechanical research, providing a robust alternative to traditional systems and paving the way for broader adoption in diverse settings.

In conclusion, this study provides compelling evidence for the viability of markerless GAn using a single-camera setup integrated with the OP framework. Our findings suggest that this approach holds potential for clinical applications and challenges traditional methods by offering a cost-effective, accessible, and less cumbersome alternative. Importantly, the enhancements in measurement accuracy through the compensation algorithm underline the practical applicability of this method in real-world settings. Using a universal compensation algorithm demonstrates the method's ability to generalize across different subjects, confirming its robustness and reproducibility in diverse scenarios. Although a direct comparison with the gold standard optoelectronic systems was not conducted in this study, future research will focus on validating the proposed methods against these established systems to ensure their accuracy and reliability. Future research should aim to refine these algorithms further, explore the integration of machine learning techniques for dynamic adjustment during live analysis, and expand the system's applicability to varied demographic and clinical populations. This could greatly enhance GAn's diagnostic and rehabilitative capabilities, potentially transforming patient care by providing high-fidelity insights into human locomotion with minimal setup and investment.

Chapter 6

Conclusions and Future Perspective

This thesis has delved into the evolving domain of GAn, highlighting the integration of MLB MoCap systems and wearable IMUs as transformative tools for clinical applications. These advancements bridge the gap between traditional laboratory-based assessments and more accessible, modern methodologies. By exploring both technological and clinical dimensions, this work emphasizes the potential of these systems while addressing their limitations.

Inertial Measurement Unit sensors offer distinct advantages, particularly their portability and ability to capture movement patterns in real-world environments. Their non-invasive nature facilitates natural and unrestricted movements, making them highly effective for assessing pathological gait in various clinical and non-clinical contexts. Furthermore, their affordability and accessibility have broadened their applicability, with spatiotemporal and kinematic data proving invaluable for diagnosing and monitoring conditions such as PD's disease, stroke, and osteoarthritis. However, IMUs are not without challenges. They face limitations in detecting subtle gait deviations, particularly in individuals with severe motor impairments, and prolonged use may cause user fatigue, affecting data accuracy and compliance. Moreover, distinguishing between gait events in complex settings remains a significant obstacle.

Marker-Less-Based MoCap systems, on the other hand, represent a paradigm shift in GAn. These systems leverage advanced CV and ML algorithms to provide a non-invasive alternative to traditional MB approaches. By eliminating the need for physical markers, these technologies minimize the risk of data bias introduced by unnatural movement patterns. Marker-Less-Based systems have demonstrated comparable accuracy in measuring STPs and extend their applications beyond controlled environments to real-world settings. Despite these advances, they remain sensitive to environmental factors such as lighting and occlusion. The reliance on 2D data also introduces potential inaccuracies in joint angle estimations, especially in complex motion sequences.

Building on these findings, several future directions emerge for advancing GAn methodologies. Integrating multiple camera systems for 3D reconstruction offers a promising path forward. By capturing gait parameters from multiple perspectives, these systems can address the limitations of 2D data, enabling richer kinematic insights and more precise joint angle estimations. Additionally, initiating a data acquisition campaign at Rehazenter in Luxembourg presents a valuable opportunity to validate and refine these methodologies in a clinical setting. Collaborating with healthcare professionals to gather diverse datasets will enhance the robustness and generalizability of ML models.

Translating research findings into clinical practice remains a critical challenge. Future efforts should focus on developing user-friendly applications that seamlessly integrate IMUs and MLB systems into routine workflows. These tools must provide real-time data visualization and feedback to empower clinicians during assessments and interventions. The role of AI and ML is particularly significant in this context. Advanced models capable of real-time error correction and prediction can enhance the reliability of GAn systems. Explainable Artificial Intelligence techniques, which promote transparency in diagnostic processes, will be crucial for fostering trust and adoption in clinical settings.

Equally important is prioritizing accessibility and scalability in developing GAn technologies. Cost-effective solutions that can be deployed in resource-limited environments will ensure broader adoption. Collaborations with industry partners can help produce affordable, portable systems without compromising functionality. Ethical considerations regarding data privacy and

security must also remain at the forefront of technological advancements. Establishing standardized protocols for anonymization and secure data transmission will safeguard patient trust.

Finally, integrating advanced GAn systems into personalized rehabilitation protocols represents a transformative opportunity. Combining detailed spatiotemporal data with patient-specific clinical insights will enable tailored interventions, optimizing recovery outcomes. Real-time feedback mechanisms during rehabilitation exercises can further enhance the effectiveness of these interventions, promoting better patient engagement and adherence.

In conclusion, this thesis lays the groundwork for a new generation of GAn tools, combining the strengths of IMUs and MLB systems with the capabilities of AI. By addressing existing challenges and pursuing these future directions, the field of GAn has the potential to revolutionize clinical outcomes, ultimately improving the quality of life for individuals with gait-related disorders.

Bibliography

[1]   Huanhuan Zhang and Yufei Qie. "Applying Deep Learning to Medical Imaging: A Review". In: *Applied Sciences 2023, Vol. 13, Page 10521* 13 (18 Sept. 2023), p. 10521. ISSN: 2076-3417. DOI: 10.3390/APP131810521. URL: https://www.mdpi.com/2076-3417/13/18/10521/htmhttps://www.mdpi.com/2076-3417/13/18/10521.

[2]   Yanbu Wang, Linqing Liu, and Chao Wang. "Trends in using deep learning algorithms in biomedical prediction systems". In: *Frontiers in Neuroscience* 17 (Nov. 2023), p. 1256351. ISSN: 1662453X. DOI: 10.3389/FNINS.2023.1256351/BIBTEX.

[3]   Ryad Zemouri, Noureddine Zerhouni, and Daniel Racoceanu. "Deep Learning in the Biomedical Applications: Recent and Future Status". In: *Applied Sciences 2019, Vol. 9, Page 1526* 9 (8 Apr. 2019), p. 1526. ISSN: 2076-3417. DOI: 10.3390/APP9081526. URL: https://www.mdpi.com/2076-3417/9/8/1526/htmhttps://www.mdpi.com/2076-3417/9/8/1526.

[4]   S uk Ko et al. "Differential gait patterns by history of falls and knee pain status in healthy older adults: Results from the Baltimore Longitudinal Study of Aging". In: *Journal of Aging and Physical Activity* 26 (Apr. 2018), pp. 577–582.

[5]   A Ardalan et al. "Analysis of gait synchrony and balance in neurodevelopmental disorders using computer vision techniques". In: *Health informatics journal* 27 (2021), p. 14604582211055650.

[6]   S Rupprechter et al. "A clinically interpretable computer-vision-based method for quantifying gait in Parkinson's disease". In: *Sensors* 21 (Apr. 2021), p. 5437.

[7]   Charissa Ann Ronao and Sung Bae Cho. "Human activity recognition with smartphone sensors using deep learning neural networks". In: *Expert Systems with Applications* 59 (Oct. 2016), pp. 235–244. ISSN: 0957-4174. DOI: 10.1016/J.ESWA.2016.04.032.

[8]   Bjoern M. Eskofier et al. "An Overview of Smart Shoes in the Internet of Health Things: Gait and Mobility Assessment in Health Promotion and Disease Monitoring". In: *Applied Sciences 2017, Vol. 7, Page 986* 7 (10 Sept. 2017), p. 986. ISSN: 2076-3417. DOI: 10.3390/APP7100986. URL: https://www.mdpi.com/2076-3417/7/10/986.

[9]   Yao Guo et al. "Detection and assessment of Parkinson's disease based on gait analysis: A survey". In: *Frontiers in Aging Neuroscience* 14 (Aug. 2022), p. 916971. ISSN: 16634365. DOI: 10.3389/FNAGI.2022.916971/BIBTEX.

[10] Dylan Kobsar et al. "Wearable Inertial Sensors for Gait Analysis in Adults with Osteoarthritis—A Scoping Review". In: *Sensors 2020, Vol. 20, Page 7143* 20 (24 Dec. 2020), p. 7143. ISSN: 1424-8220. DOI: 10.3390/S20247143. URL: https://www.mdpi.com/1424-8220/20/24/7143.

[11] Walter Pirker et al. "Gait disorders in adults and the elderly A clinical guide". In: *Wien Klin Wochenschr* 129 (2017), pp. 81–95. DOI: 10.1007/s00508-016-1096-4.

[12] Lone Jørgensen, Torgeir Engstad, and Bjarne K. Jacobsen. "Higher incidence of falls in long-term stroke survivors than in population controls: depressive symptoms predict falls after stroke". In: *Stroke* 33 (2 2002), pp. 542–547. ISSN: 1524-4628. DOI: 10.1161/HS0202.102375. URL: https://pubmed.ncbi.nlm.nih.gov/11823667/.

[13] Bastiaan R. Bloem et al. "Prospective assessment of falls in Parkinson's disease". In: *Journal of neurology* 248 (11 2001), pp. 950–958. ISSN: 0340-5354. DOI: 10.1007/S004150170047. URL: https://pubmed.ncbi.nlm.nih.gov/11757958/.

[14] Joseph O Nnodim, Chinomso V Nwagwu, and Ijeoma Nnodim Opara. "Nnodim Opara I (2020) Gait Disorders in Older Adults-A Structured Review and Approach to Clinical Assessment". In: *Nnodim et al. J Geriatr Med Gerontol* 2020 (2020), p. 101. ISSN: 2469-5858. DOI: 10.23937/2469-5858/1510101.

[15] B Moreland, R Kakara, and A Henry. "Trends in nonfatal falls and fall-related injuries among adults aged 65 years - United States, 2012-2018". In: *MMWR. Morbidity and mortality weekly report* 69 (Apr. 2020), pp. 875–881.

[16] C S Florence et al. "Medical costs of fatal and nonfatal falls in older adults". In: *Journal of the American Geriatrics Society* 66 (2018), pp. 693–698.

[17] Y K Haddad, G Bergen, and C S Florence. "Estimating the economic burden related to older adult falls by state". In: *Journal of Public Health Management and Practice* 25 (Apr. 2019), E17–E24.

[18] M Yamada and N Ichihashi. "Predicting the probability of falls in community-dwelling elderly individuals using the trail-walking test". In: *Environmental health and preventive medicine* 15 (Apr. 2010), pp. 386–391.

[19] E Schönfelder et al. "Costs of illness in amyotrophic lateral sclerosis (ALS): A cross-sectional survey in Germany". In: *Orphanet Journal of Rare Diseases* 15 (Apr. 2020), p. 149.

[20] G Palestra et al. "Evaluation of a rehabilitation system for the elderly in a day care center". In: *Information* 10 (Apr. 2018), p. 3.

[21] M W Whittle. "Normal gait". In: *Gait analysis: An introduction* (1991).

[22] Stéphane Armand et al. "Current practices in clinical gait analysis in Europe: A comprehensive survey-based study from the European society for movement analysis in adults and children (ESMAC) standard initiative". In: *Gait posture* 111 (June 2024), pp. 65–74. ISSN: 1879-2219. DOI: 10.1016/J.GAITPOST.2024.04.014. URL: https://pubmed.ncbi.nlm.nih.gov/38653178/.

[23] Richard Baker. "The history of gait analysis before the advent of modern computers". In: *Gait Posture* 26 (3 Sept. 2007), pp. 331–342. ISSN: 0966-6362. DOI: 10.1016/J.GAITPOST.2006.10.014.

[24] Sheldon R. Simon. "Quantification of human motion: gait analysis-benefits and limitations to its application to clinical problems". In: *Journal of biomechanics* 37 (12 Dec. 2004), pp. 1869–1880. ISSN: 0021-9290. DOI: 10.1016/J.JBIOMECH.2004.02.047. URL: https://pubmed.ncbi.nlm.nih.gov/15519595/.

[25] Grazia Cicirelli et al. "Human Gait Analysis in Neurodegenerative Diseases: A Review". In: *IEEE Journal of Biomedical and Health Informatics* 26 (1 Jan. 2022), pp. 229–242. ISSN: 21682208. DOI: 10.1109/JBHI.2021.3092875.

[26] Tishya A.L. Wren et al. "Efficacy of clinical gait analysis: A systematic review". In: *Gait posture* 34 (2 June 2011), pp. 149–153. ISSN: 1879-2219. DOI: 10.1016/J.GAITPOST.2011.03.027. URL: https://pubmed.ncbi.nlm.nih.gov/21646022/.

[27] Alvaro Muro de-la Herran, Begoña García-Zapirain, and Amaia Méndez-Zorrilla. "Gait Analysis Methods: An Overview of Wearable and Non-Wearable Systems, Highlighting Clinical Applications". In: *Sensors (Basel, Switzerland)* 14 (2 Feb. 2014), p. 3362. ISSN: 14248220. DOI: 10.3390/S140203362. URL: https://www.ncbi.nlm.nih.gov/pmc/articles/PMC3958266/.

[28] L Lonini et al. "Video-based pose estimation for gait analysis in stroke survivors during clinical assessments: A proof-of-concept study". In: *Digital Biomarkers* 6 (Apr. 2022), pp. 9–18.

[29] J Perry and J M Burnfield. *Gait analysis: Normal and pathological function.* Vol. 9. 1992.

[30] D. H. Sutherland. "The evolution of clinical gait analysis: Part II kinematics". In: *Gait and Posture* 16 (2 Oct. 2002), pp. 159–179. ISSN: 09666362. DOI: `10.1016/S0966-6362(02)00004-8`. URL: `https://pubmed.ncbi.nlm.nih.gov/12297257/`.

[31] Richard. Baker. "Measuring walking : a handbook of clinical gait analysis". In: (2013), p. 229. URL: `https://www.wiley.com/en-ca/Measuring+Walking%3A+A+Handbook+of+Clinical+Gait+Analysis-p-9781908316660`.

[32] Shuqi Jia et al. "The prediction model of fall risk for the elderly based on gait analysis". In: *BMC Public Health* 24 (1 Dec. 2024), pp. 1–10. ISSN: 14712458. DOI: `10.1186/S12889-024-19760-8/FIGURES/5`. URL: `https://bmcpublichealth.biomedcentral.com/articles/10.1186/s12889-024-19760-8`.

[33] Hanatsu Nagano. "Gait Biomechanics for Fall Prevention among Older Adults". In: *Applied Sciences 2022, Vol. 12, Page 6660* 12 (13 June 2022), p. 6660. ISSN: 2076-3417. DOI: `10.3390/APP12136660`. URL: `https://www.mdpi.com/2076-3417/12/13/6660/htmhttps://www.mdpi.com/2076-3417/12/13/6660`.

[34] Aisha Cobbs. *Gait and Balance Dysfunction in Older Adults: Challenges and Interventions — Lower Extremity Review Magazine.* Feb. 2019. URL: `https://lermagazine.com/article/gait-and-balance-dysfunction-in-older-adults-challenges-and-interventions`.

[35] F I MAHONEY and D W BARTHEL. "Functional evaluation: The Barthel index". In: *Maryland state medical journal* 14 (Apr. 1965), pp. 61–65.

[36] *Motion Capture Technology and Systems — Qualisys — Qualisys.* URL: `https://www.qualisys.com/`.

[37] Lars Mündermann, Stefano Corazza, and Thomas P. Andriacchi. "The evolution of methods for the capture of human movement leading to markerless motion capture for biomechanical applications". In: *Journal of NeuroEngineering and Rehabilitation* 3 (Mar. 2006), p. 6. ISSN: 17430003. DOI: `10.1186/1743-0003-3-6`. URL: `https://www.ncbi.nlm.nih.gov/pmc/articles/PMC1513229/`.

[38] Erika Rovini, Carlo Maremmani, and Filippo Cavallo. "How wearable sensors can support parkinson's disease diagnosis and treatment: A systematic review". In: *Frontiers in Neuroscience* 11 (OCT Oct. 2017), p. 288959. ISSN: 1662453X. DOI: `10.3389/FNINS.2017.00555/BIBTEX`. URL: `www.frontiersin.org`.

[39] Catherine P. Adans-Dester et al. "Wearable Sensors for Stroke Rehabilitation". In: *Neurorehabilitation Technology, Third Edition* (Jan. 2022), pp. 467–507. DOI: `10.1007/978-3-031-08995-4_21`. URL: `https://link.springer.com/chapter/10.1007/978-3-031-08995-4_21`.

[40] Pablo MacEira-Elvira et al. "Wearable technology in stroke rehabilitation: towards improved diagnosis and treatment of upper-limb motor impairment". In: *Journal of neuroengineering and rehabilitation* 16 (1 Nov. 2019). ISSN: 1743-0003. DOI: `10.1186/S12984-019-0612-Y`. URL: `https://pubmed.ncbi.nlm.nih.gov/31744553/`.

[41] Enrica Papi, Woon Senn Koh, and Alison H. McGregor. "Wearable technology for spine movement assessment: A systematic review". In: *Journal of biomechanics* 64 (Nov. 2017), pp. 186–197. ISSN: 1873-2380. DOI: `10.1016/J.JBIOMECH.2017.09.037`. URL: `https://pubmed.ncbi.nlm.nih.gov/29102267/`.

[42] P W Tipton. "Dissecting parkinsonism: cognitive and gait disturbances". In: *Neurologia i Neurochirurgia Polska* 55 (Apr. 2021), pp. 513–524.

[43] K.-D. Ng et al. "Measuring gait variables using computer vision to assess mobility and fall risk in older adults with dementia". In: *IEEE journal of translational engineering in health and medicine* 8 (2020), p. 2100609.

[44] Muhammad Imran Sharif et al. "Human Gait Recognition using Deep Learning: A Comprehensive Review". In: (Sept. 2023). URL: https://arxiv.org/abs/2309.10144v1.

[45] Chuanfu Shen et al. "A Comprehensive Survey on Deep Gait Recognition: Algorithms, Datasets and Challenges". In: (June 2022). URL: https://arxiv.org/abs/2206.13732v2.

[46] Denise M. Peters et al. "Utilization of wearable technology to assess gait and mobility post-stroke: a systematic review". In: *Journal of NeuroEngineering and Rehabilitation* 18 (1 Dec. 2021). ISSN: 17430003. DOI: 10.1186/S12984-021-00863-X.

[47] Sofia Scataglini et al. *Accuracy, Validity, and Reliability of Markerless Camera-Based 3D Motion Capture Systems versus Marker-Based 3D Motion Capture Systems in Gait Analysis: A Systematic Review and Meta-Analysis*. June 2024. DOI: 10.3390/s24113686.

[48] Logan Wade et al. "Applications and limitations of current markerless motion capture methods for clinical gait biomechanics". In: *PeerJ* 10 (Feb. 2022), e12995. ISSN: 21678359. DOI: 10.7717/PEERJ.12995/FIG-5. URL: https://peerj.com/articles/12995.

[49] Koen Wishaupt et al. "The applicability of markerless motion capture for clinical gait analysis in children with cerebral palsy". In: *Scientific Reports 2024 14:1* 14 (1 May 2024), pp. 1–10. ISSN: 2045-2322. DOI: 10.1038/s41598-024-62119-7. URL: https://www.nature.com/articles/s41598-024-62119-7.

[50] *Abnormal Gait: Gait Disorder Types, Causes Treatments*. URL: https://my.clevelandclinic.org/health/diseases/21092-gait-disorders.

[51] Donald A.. Neumann et al. "Kinesiology of the musculoskeletal system : foundations for rehabilitation". In: (2017), p. 766.

[52] R A Mann and J Hagy. "Biomechanics of walking, running, and sprinting". In: *The American Journal of Sports Medicine* 8 (Apr. 1980), pp. 345–350.

[53] *Gait Cycle*. URL: https://www.angelfire.com/la/Ivan/gait.html.

[54] Gentaro Taga. "A model of the neuro-musculo-skeletal system for human locomotion. II Real-time adaptability under various constraints". In: *Biological cybernetics* 73 (2 July 1995), pp. 113–121. ISSN: 0340-1200. DOI: 10.1007/BF00204049. URL: https://pubmed.ncbi.nlm.nih.gov/7662764/.

[55] Subhra Chowdhury and Neelesh Kumar. "Estimation of Forces and Moments of Lower Limb Joints from Kinematics Data and Inertial Properties of the Body by Using Inverse Dynamics Technique". In: *Journal of Rehabilitation Robotics* (2013). DOI: 10.12970/2308-8354.2013.01.02.3.

[56] Matt Topley and James G. Richards. "A comparison of currently available optoelectronic motion capture systems". In: *Journal of biomechanics* 106 (June 2020). ISSN: 1873-2380. DOI: 10.1016/J.JBIOMECH.2020.109820. URL: https://pubmed.ncbi.nlm.nih.gov/32517978/.

[57] Christoph Schärer et al. "Energy Transformation on Vault in Elite Artistic Gymnastics: Comparisons between Simple and Difficult Tsukahara and Yurchenko Vaults". In: *Applied Sciences* 11.20 (2021). ISSN: 2076-3417. DOI: 10.3390/app11209484. URL: https://www.mdpi.com/2076-3417/11/20/9484.

[58] Théo Jourdan, Noëlie Debs, and Carole Frindel. "The Contribution of Machine Learning in the Validation of Commercial Wearable Sensors for Gait Monitoring in Patients: A Systematic Review". In: *Sensors (Basel, Switzerland)* 21 (14 July 2021). ISSN: 1424-8220. DOI: 10.3390/S21144808. URL: https://pubmed.ncbi.nlm.nih.gov/34300546/.

[59] Feng Lin et al. "Smart Insole: A Wearable Sensor Device for Unobtrusive Gait Monitoring in Daily Life". In: *IEEE Transactions on Industrial Informatics* 12 (6 Dec. 2016), pp. 2281–2291. ISSN: 15513203. DOI: 10.1109/TII.2016.2585643.

[60] Luigi Battista and Antonietta Romaniello. "A novel device for continuous monitoring of tremor and other motor symptoms". In: *Neurological Sciences* 39 (8 Aug. 2018), pp. 1333–1343. ISSN: 15903478. DOI: `10.1007/S10072-018-3414-2/METRICS`. URL: `https://link.springer.com/article/10.1007/s10072-018-3414-2`.

[61] Jeffrey M. Hausdorff. "Gait dynamics in Parkinson's disease: Common and distinct behavior among stride length, gait variability, and fractal-like scaling". In: *Chaos* 19 (2 June 2009). ISSN: 10541500. DOI: `10.1063/1.3147408/909419`. URL: `/aip/cha/article/19/2/026113/909419/Gait-dynamics-in-Parkinson-s-disease-Common-and`.

[62] Christiana Ossig et al. "Wearable sensor-based objective assessment of motor symptoms in Parkinson's disease". In: *Journal of Neural Transmission* 123 (1 Jan. 2016), pp. 57–64. ISSN: 14351463. DOI: `10.1007/S00702-015-1439-8/METRICS`. URL: `https://link.springer.com/article/10.1007/s00702-015-1439-8`.

[63] Tyler M. Wiles et al. "Pattern analysis using lower body human walking data to identify the gaitprint". In: *Computational and Structural Biotechnology Journal* 24 (2024), pp. 281–291. ISSN: 2001-0370. DOI: `10.1016/j.csbj.2024.04.017`. URL: `https://doi.org/10.1016/j.csbj.2024.04.017`.

[64] Alberto J. Espay et al. "Technology in Parkinson's disease: Challenges and opportunities". In: *Movement disorders : official journal of the Movement Disorder Society* 31 (9 Sept. 2016), pp. 1272–1282. ISSN: 1531-8257. DOI: `10.1002/MDS.26642`. URL: `https://pubmed.ncbi.nlm.nih.gov/27125836/`.

[65] Richard Baker. "Gait analysis methods in rehabilitation". In: *Journal of neuroengineering and rehabilitation* 3 (Mar. 2006). ISSN: 1743-0003. DOI: `10.1186/1743-0003-3-4`. URL: `https://pubmed.ncbi.nlm.nih.gov/16512912/`.

[66] Steffi L. Colyer et al. "A Review of the Evolution of Vision-Based Motion Analysis and the Integration of Advanced Computer Vision Methods Towards Developing a Markerless System". In: *Sports medicine - open* 4 (1 Dec. 2018). ISSN: 2199-1170. DOI: `10.1186/S40798-018-0139-Y`. URL: `https://pubmed.ncbi.nlm.nih.gov/29869300/`.

[67] Hausmann SB et al. "Measuring and modeling the motor system with machine learning". In: *Current opinion in neurobiology* 70 (Oct. 2021), pp. 11–23. ISSN: 1873-6882. DOI: `10.1016/J.CONB.2021.04.004`. URL: `https://pubmed.ncbi.nlm.nih.gov/34116423/`.

[68] Thiago Antonio da Costa Souto et al. "Artificial Intelligence in the Combination of Technology with Ergonomics for Estimation of Correct Posture Based on Python". In: *International Journal of Advanced Research* 11 (2023), pp. 183–190. ISSN: 2320-5407. URL: `https://www.journalijar.com`.

[69] Xuqi Zhu et al. "A Kalman Filter based Approach for Markerless Pose Tracking and Assessment". In: *2022 27th International Conference on Automation and Computing: Smart Systems and Manufacturing, ICAC 2022* (2022). DOI: `10.1109/ICAC55051.2022.9911152`.

[70] Zhe Cao et al. "OpenPose: Realtime Multi-Person 2D Pose Estimation using Part Affinity Fields". In: *IEEE Transactions on Pattern Analysis and Machine Intelligence* 43 (1 Dec. 2018), pp. 172–186. ISSN: 19393539. DOI: `10.1109/TPAMI.2019.2929257`. URL: `https://arxiv.org/abs/1812.08008v2`.

[71] A Maksimovic et al. "Gait characteristics in older adults with diabetes and impaired fasting glucose: The Rotterdam Study". In: *Journal of Diabetes and its Complications* 30 (Apr. 2016), pp. 61–66.

[72] *Gait - Physiopedia*. URL: `https://www.physio-pedia.com/Gait`.

[73] *Gait Parameters*. URL: `https://help.plantiga.com/spatiotemporal-gait-parameters`.

[74] M Bertoli et al. "Estimation of spatio-temporal parameters of gait from magneto-inertial measurement units: multicenter validation among Parkinson, mildly cognitively impaired and healthy older adults". In: *BioMedical Engineering OnLine* 17 (Apr. 2018), p. 58.

[75] S S Kuys et al. "Gait speed in ambulant older people in long term care: A systematic review and meta-analysis". In: *Journal of the American Medical Directors Association* 15 (Apr. 2014), pp. 194–200.

[76] J Xu et al. "Configurable, wearable sensing and vibrotactile feedback system for real-time postural balance and gait training: proof-of-concept". In: *Journal of NeuroEngineering and Rehabilitation* 14 (Apr. 2017), p. 102.

[77] R Cham et al. "Striatal dopaminergic denervation and gait in healthy adults". In: *Experimental Brain Research* 185 (Apr. 2008), pp. 391–398.

[78] T V Barreira et al. "Cadence patterns and peak cadence in US children and adolescents". In: *Medicine Science in Sports Exercise* 44 (Apr. 2012), pp. 1721–1727.

[79] N M Peel, S S Kuys, and K Klein. "Gait speed as a measure in geriatric assessment in clinical settings: A systematic review". In: *The Journals of Gerontology Series A* 68 (Apr. 2013), pp. 39–46.

[80] J Looper and L S Chandler. "How do toddlers increase their gait velocity?" In: *Gait Posture* 37 (Apr. 2013), pp. 631–633.

[81] R L Cromwell et al. "Tae kwon do: An effective exercise for improving balance and walking ability in older adults". In: *The Journals of Gerontology Series A: Biological Sciences and Medical Sciences* 62 (Apr. 2007), pp. 641–646.

[82] Schwenk M et al. "Frailty and technology: a systematic review of gait analysis in those with frailty". In: *Gerontology* 60 (1 Dec. 2014), pp. 79–89. ISSN: 1423-0003. DOI: 10.1159/000354211. URL: https://pubmed.ncbi.nlm.nih.gov/23949441/.

[83] Dolatabadi E, Taati B, and Mihailidis A. "An Automated Classification of Pathological Gait Using Unobtrusive Sensing Technology". In: *IEEE transactions on neural systems and rehabilitation engineering : a publication of the IEEE Engineering in Medicine and Biology Society* 25 (12 Dec. 2017), pp. 2336–2346. ISSN: 1558-0210. DOI: 10.1109/TNSRE.2017.2736939. URL: https://pubmed.ncbi.nlm.nih.gov/28792901/.

[84] Valery L Feigin et al. "The global burden of neurological disorders: translating evidence into policy". In: *The Lancet Neurology* 19 (3 Mar. 2020), pp. 255–265. ISSN: 1474-4422. DOI: 10.1016/s1474-4422(19)30411-9. URL: http://dx.doi.org/10.1016/s1474-4422(19)30411-9.

[85] Elizabeth C Wonsetler and Mark G Bowden. "A systematic review of mechanisms of gait speed change post-stroke. Part 1: spatiotemporal parameters and asymmetry ratios". In: *Topics in Stroke Rehabilitation* 24 (6 Feb. 2017), pp. 435–446. ISSN: 1945-5119. DOI: 10.1080/10749357.2017.1285746. URL: http://dx.doi.org/10.1080/10749357.2017.1285746.

[86] Elizabeth C. Wonsetler and Mark G. Bowden. "A systematic review of mechanisms of gait speed change post-stroke. Part 2: exercise capacity, muscle activation, kinetics, and kinematics". In: *Topics in stroke rehabilitation* 24 (5 2017), pp. 394–403. ISSN: 1945-5119. DOI: 10.1080/10749357.2017.1282413. URL: https://pubmed.ncbi.nlm.nih.gov/28218021/.

[87] An-Lun Hsu, Pei-Fang Tang, and Mei-Hwa Jan. "Analysis of impairments influencing gait velocity and asymmetry of hemiplegic patients after mild to moderate stroke". In: *Archives of Physical Medicine and Rehabilitation* 84 (8 Aug. 2003), pp. 1185–1193. ISSN: 0003-9993. DOI: 10.1016/s0003-9993(03)00030-3. URL: http://dx.doi.org/10.1016/s0003-9993(03)00030-3.

[88] Susan L Mitchell et al. "Patterns of Outcome Measurement in Parkinson's Disease Clinical Trials". In: *Neuroepidemiology* 19 (2 2000), pp. 100–108. ISSN: 1423-0208. DOI: 10.1159/000026244. URL: http://dx.doi.org/10.1159/000026244.

[89] Claudia Ramaker et al. "Systematic evaluation of rating scales for impairment and disability in Parkinson's disease". In: *Movement Disorders* 17 (5 May 2002), pp. 867–876. ISSN: 1531-8257. DOI: 10.1002/mds.10248. URL: http://dx.doi.org/10.1002/mds.10248.

[90] P Martínez-Martín et al. "Unified Parkinson's disease rating scale characteristics and structure". In: *Movement Disorders* 9 (1 Jan. 1994), pp. 76–83. ISSN: 1531-8257. DOI: 10.1002/mds.870090112. URL: http://dx.doi.org/10.1002/mds.870090112.

[91] Cathy K Cui and Simon J G Lewis. "Future Therapeutic Strategies for Freezing of Gait in Parkinson's Disease". In: *Frontiers in Human Neuroscience* 15 (Nov. 2021). ISSN: 1662-5161. DOI: 10.3389/fnhum.2021.741918. URL: http://dx.doi.org/10.3389/fnhum.2021.741918.

[92] Nick Gebruers et al. "Monitoring of Physical Activity After Stroke: A Systematic Review of Accelerometry-Based Measures". In: *Archives of Physical Medicine and Rehabilitation* 91 (2 Feb. 2010), pp. 288–297. ISSN: 0003-9993. DOI: 10.1016/j.apmr.2009.10.025. URL: http://dx.doi.org/10.1016/j.apmr.2009.10.025.

[93] Stacey E Aaron, Chris M Gregory, and Annie N Simpson. "Lower Odds of Poststroke Symptoms of Depression When Physical Activity Guidelines Met: National Health and Nutrition Examination Survey 2011–2012". In: *Journal of Physical Activity and Health* 13 (8 Aug. 2016), pp. 903–909. ISSN: 1543-5474. DOI: 10.1123/jpah.2015-0446. URL: http://dx.doi.org/10.1123/jpah.2015-0446.

[94] Adebimpe O Obembe and Janice J Eng. "Rehabilitation Interventions for Improving Social Participation After Stroke: A Systematic Review and Meta-analysis". In: *Neurorehabilitation and Neural Repair* 30 (4 July 2015), pp. 384–392. ISSN: 1552-6844. DOI: 10.1177/1545968315597072. URL: http://dx.doi.org/10.1177/1545968315597072.

[95] Debbie Rand et al. "Daily physical activity and its contribution to the health-related quality of life of ambulatory individuals with chronic stroke". In: *Health and quality of life outcomes* 8 (Aug. 2010). ISSN: 1477-7525. DOI: 10.1186/1477-7525-8-80. URL: https://pubmed.ncbi.nlm.nih.gov/20682071/.

[96] Natalie A Fini et al. "How to Address Physical Activity Participation After Stroke in Research and Clinical Practice". In: *Stroke* 52 (6 June 2021). ISSN: 1524-4628. DOI: 10.1161/strokeaha.121.034557. URL: http://dx.doi.org/10.1161/strokeaha.121.034557.

[97] Natalie A Fini et al. "How Physically Active Are People Following Stroke? Systematic Review and Quantitative Synthesis". In: *Physical Therapy* 97 (7 Apr. 2017), pp. 707–717. ISSN: 1538-6724. DOI: 10.1093/ptj/pzx038. URL: http://dx.doi.org/10.1093/ptj/pzx038.

[98] Sujata Pradhan and Valerie E Kelly. "Quantifying physical activity in early Parkinson disease using a commercial activity monitor". In: *Parkinsonism amp; Related Disorders* 66 (Sept. 2019), pp. 171–175. ISSN: 1353-8020. DOI: 10.1016/j.parkreldis.2019.08.001. URL: http://dx.doi.org/10.1016/j.parkreldis.2019.08.001.

[99] Carlotta Caramia et al. "IMU-Based Classification of Parkinson's Disease from Gait: A Sensitivity Analysis on Sensor Location and Feature Selection". In: *IEEE Journal of Biomedical and Health Informatics* 22 (6 Nov. 2018), pp. 1765–1774. DOI: 10.1109/JBHI.2018.2865218.

[100] Lai DT, Begg RK, and Palaniswami M. "Computational intelligence in gait research: a perspective on current applications and future challenges". In: *IEEE transactions on information technology in biomedicine : a publication of the IEEE Engineering in Medicine and Biology Society* 13 (5 2009), pp. 687–702. ISSN: 1558-0032. DOI: 10.1109/TITB.2009.2022913. URL: https://pubmed.ncbi.nlm.nih.gov/19447724/.

[101] König N et al. "Can Gait Signatures Provide Quantitative Measures for Aiding Clinical Decision-Making? A Systematic Meta-Analysis of Gait Variability Behavior in Patients with Parkinson's Disease". In: *Frontiers in human neuroscience* 10 (June 2016). ISSN: 1662-5161. DOI: 10.3389/FNHUM.2016.00319. URL: https://pubmed.ncbi.nlm.nih.gov/27445759/.

[102] HaoYuan Hsiao et al. "Contribution of Paretic and Nonparetic Limb Peak Propulsive Forces to Changes in Walking Speed in Individuals Poststroke". In: *Neurorehabilitation and Neural Repair* 30 (8 July 2016), pp. 743–752. ISSN: 1552-6844. DOI: 10.1177/1545968315624780. URL: http://dx.doi.org/10.1177/1545968315624780.

[103] Louis N Awad et al. "These legs were made for propulsion: advancing the diagnosis and treatment of post-stroke propulsion deficits". In: *Journal of NeuroEngineering and Rehabilitation* 17 (1 Oct. 2020). ISSN: 1743-0003. DOI: 10.1186/s12984-020-00747-6. URL: http://dx.doi.org/10.1186/s12984-020-00747-6.

[104] Dominic James Farris et al. "Revisiting the mechanics and energetics of walking in individuals with chronic hemiparesis following stroke: from individual limbs to lower limb joints". In: *Journal of NeuroEngineering and Rehabilitation* 12 (1 Feb. 2015). ISSN: 1743-0003. DOI: 10.1186/s12984-015-0012-x. URL: http://dx.doi.org/10.1186/s12984-015-0012-x.

[105] Lydia G Brough, Steven A Kautz, and Richard R Neptune. "Muscle contributions to pre-swing biomechanical tasks influence swing leg mechanics in individuals post-stroke during walking". In: *Journal of NeuroEngineering and Rehabilitation* 19 (1 June 2022). ISSN: 1743-0003. DOI: 10.1186/s12984-022-01029-z. URL: http://dx.doi.org/10.1186/s12984-022-01029-z.

[106] A L Hall et al. "Relationships between muscle contributions to walking subtasks and functional walking status in persons with post-stroke hemiparesis". In: *Clinical Biomechanics* 26 (5 June 2011), pp. 509–515. ISSN: 0268-0033. DOI: 10.1016/j.clinbiomech.2010.12.010. URL: http://dx.doi.org/10.1016/j.clinbiomech.2010.12.010.

[107] R R Neptune, F E Zajac, and S A Kautz. "Muscle force redistributes segmental power for body progression during walking". In: *Gait amp; Posture* 19 (2 Apr. 2004), pp. 194–205. ISSN: 0966-6362. DOI: 10.1016/s0966-6362(03)00062-6. URL: http://dx.doi.org/10.1016/s0966-6362(03)00062-6.

[108] Ahmed A Moustafa et al. "Motor symptoms in Parkinson's disease: A unified framework". In: *Neuroscience amp; Biobehavioral Reviews* 68 (Sept. 2016), pp. 727–740. ISSN: 0149-7634. DOI: 10.1016/j.neubiorev.2016.07.010. URL: http://dx.doi.org/10.1016/j.neubiorev.2016.07.010.

[109] Jan Slemenšek et al. "Human Gait Activity Recognition Machine Learning Methods". In: *Sensors* 23 (2 Jan. 2023), p. 745. ISSN: 14248220. DOI: 10.3390/S23020745/S1. URL: https://www.mdpi.com/1424-8220/23/2/745.

[110] Preeti Khera and Neelesh Kumar. "Role of machine learning in gait analysis: a review". In: *Journal of medical engineering technology* 44 (8 Nov. 2020), pp. 441–467. ISSN: 1464-522X. DOI: 10.1080/03091902.2020.1822940. URL: https://pubmed.ncbi.nlm.nih.gov/33078988/.

[111] Batta Mahesh. "Machine Learning Algorithms-A Review". In: *International Journal of Science and Research* (2018). ISSN: 2319-7064. DOI: 10.21275/ART20203995. URL: www.ijsr.net.

[112] Zhi Hua Zhou. "Machine Learning". In: *Machine Learning* (Jan. 2021), pp. 1–458. DOI: 10.1007/978-981-15-1967-3/COVER.

[113] Chandra Prakash, Rajesh Kumar, and Namita Mittal. "Recent developments in human gait research: parameters, approaches, applications, machine learning techniques, datasets and challenges". In: *Artificial Intelligence Review* 49 (1 Jan. 2018), pp. 1–40. ISSN: 15737462. DOI: 10.1007/S10462-016-9514-6/METRICS. URL: https://link.springer.com/article/10.1007/s10462-016-9514-6.

[114] Stephanie Studenski et al. "Gait Speed and Survival in Older Adults". In: *JAMA* 305 (1 Jan. 2011), pp. 50–58. ISSN: 0098-7484. DOI: 10.1001/JAMA.2010.1923. URL: https://jamanetwork.com/journals/jama/fullarticle/644554.

[115] Roman Schniepp et al. "Clinical and neurophysiological risk factors for falls in patients with bilateral vestibulopathy". In: *Journal of Neurology* 264 (2 Feb. 2017), pp. 277–283. DOI: 10.1007/S00415-016-8342-6.

[116] Philippe Terrier. "Gait Recognition via Deep Learning of the Center-of-Pressure Trajectory". In: *Applied Sciences 2020, Vol. 10, Page 774* 10 (3 Jan. 2020), p. 774. DOI: 10.3390/APP10030774. URL: https://www.mdpi.com/2076-3417/10/3/774.

[117] Metin Bicer et al. "Generative deep learning applied to biomechanics: A new augmentation technique for motion capture datasets". In: *Journal of Biomechanics* 144 (Nov. 2022), p. 111301. ISSN: 0021-9290. DOI: 10.1016/J.JBIOMECH.2022.111301.

[118] Eva Dorschky et al. "CNN-Based Estimation of Sagittal Plane Walking and Running Biomechanics From Measured and Simulated Inertial Sensor Data". In: *Frontiers in Bioengineering and Biotechnology* 8 (June 2020), p. 528071. ISSN: 22964185. DOI: 10.3389/FBIOE.2020.00604/BIBTEX.

[119] Tilman Rauker et al. "Toward Transparent AI: A Survey on Interpreting the Inner Structures of Deep Neural Networks". In: *Proceedings - 2023 IEEE Conference on Secure and Trustworthy Machine Learning, SaTML 2023* (July 2022), pp. 464–483. DOI: 10.1109/SaTML54575.2023.00039. URL: https://arxiv.org/abs/2207.13243v6.

[120] Oliver Bringmann et al. "Automated HW/SW co-design for edge AI: State, challenges and steps ahead". In: *Proceedings - 2021 International Conference on Hardware/Software Codesign and System Synthesis, CODES+ISSS 2021* (Sept. 2021), pp. 11–20. DOI: 10.1145/3478684.3479261. URL: https://dl.acm.org/doi/10.1145/3478684.3479261.

[121] Xiaofei Wang et al. "Convergence of Edge Computing and Deep Learning: A Comprehensive Survey". In: *IEEE Communications Surveys and Tutorials* 22 (2 Apr. 2020), pp. 869–904. ISSN: 1553877X. DOI: 10.1109/COMST.2020.2970550.

[122] Thomas Elsken, Jan Hendrik Metzen, and Frank Hutter. "Neural Architecture Search: A Survey". In: *Journal of Machine Learning Research* 20 (Aug. 2018). ISSN: 15337928. URL: https://arxiv.org/abs/1808.05377v3.

[123] K. M. Rashid and J. Louis. "Window-warping: A time series data augmentation of IMU data for construction equipment activity identification". In: *Proceedings of the 36th International Symposium on Automation and Robotics in Construction, ISARC 2019* (2019), pp. 651–657. DOI: 10.22260/ISARC2019/0087.

[124] Amandine Schmutz et al. "A Method to Estimate Horse Speed per Stride from One IMU with a Machine Learning Method". In: *Sensors 2020, Vol. 20, Page 518* 20 (2 Jan. 2020), p. 518. DOI: 10.3390/S20020518. URL: https://www.mdpi.com/1424-8220/20/2/518/.

[125] Andreas Holzinger et al. "Explainable AI Methods - A Brief Overview". In: *Lecture Notes in Computer Science (including subseries Lecture Notes in Artificial Intelligence and Lecture Notes in Bioinformatics)* 13200 LNAI (2022), pp. 13–38. ISSN: 16113349. DOI: 10.1007/978-3-031-04083-2_2/FIGURES/3. URL: https://link.springer.com/chapter/10.1007/978-3-031-04083-2_2.

[126] Christoph Molnar et al. "Model-agnostic feature importance and effects with dependent features: a conditional subgroup approach". In: *Data Mining and Knowledge Discovery* 38 (5 Sept. 2024), pp. 2903–2941. ISSN: 1573756X. DOI: 10.1007/S10618-022-00901-9/TABLES/8. URL: https://link.springer.com/article/10.1007/s10618-022-00901-9.

[127] David Rügamer, Chris Kolb, and Nadja Klein. "Semi-Structured Distributional Regression". In: *The American Statistician* 78 (1 2024), pp. 88–99. ISSN: 15372731. DOI: 10.1080/00031305.2022.2164054. URL: https://www.tandfonline.com/doi/abs/10.1080/00031305.2022.2164054.

[128]   Christine S. Autenrieth et al. "Decline in Gait Performance Detected by an Electronic Walkway System in 907 Older Adults of the Population-Based KORA-Age Study". In: *Gerontology* 59 (2 2013), pp. 165–173. ISSN: 0304-324X. DOI: 10.1159/000342206. URL: https://www.karger.com/Article/FullText/342206.

[129]   Paolo Bonato. "Wearable Sensors/Systems and Their Impact on Biomedical Engineering". In: *IEEE Engineering in Medicine and Biology Magazine* 22 (3 May 2003), pp. 18–20. ISSN: 07395175. DOI: 10.1109/MEMB.2003.1213622.

[130]   Mehmet Engin et al. "Recent developments and trends in biomedical sensors". In: *Measurement: Journal of the International Measurement Confederation* 37 (2 Mar. 2005), pp. 173–188. ISSN: 02632241. DOI: 10.1016/J.MEASUREMENT.2004.11.002.

[131]   Shu Nishiguchi et al. "Reliability and validity of gait analysis by android-based smartphone". In: *Telemedicine journal and e-health : the official journal of the American Telemedicine Association* 18 (4 May 2012), pp. 292–296. ISSN: 1556-3669. DOI: 10.1089/TMJ.2011.0132. URL: https://pubmed.ncbi.nlm.nih.gov/22400972/.

[132]   H. J. Luinge, P. H. Veltink, and C. T.M. Baten. "Ambulatory measurement of arm orientation". In: *Journal of biomechanics* 40 (1 2007), pp. 78–85. ISSN: 0021-9290. DOI: 10.1016/J.JBIOMECH.2005.11.011. URL: https://pubmed.ncbi.nlm.nih.gov/16455089/.

[133]   Luca Palmerini et al. "Quantification of motor impairment in Parkinson's disease using an instrumented timed up and go test". In: *IEEE Transactions on Neural Systems and Rehabilitation Engineering* 21 (4 2013), pp. 664–673. ISSN: 15344320. DOI: 10.1109/TNSRE.2012.2236577.

[134]   Zoltan Mari and Dietrich Haubenberger. "Remote measurement and home monitoring of tremor". In: *Journal of the Neurological Sciences* 435 (Apr. 2022). ISSN: 18785883. DOI: 10.1016/j.jns.2022.120201. URL: http://www.jns-journal.com/article/S0022510X22000636/fulltext.

[135]   Murtadha D. Hssayeni et al. "Wearable Sensors for Estimation of Parkinsonian Tremor Severity during Free Body Movements". In: *Sensors 2019, Vol. 19, Page 4215* 19 (19 Sept. 2019), p. 4215. ISSN: 1424-8220. DOI: 10.3390/S19194215. URL: https://www.mdpi.com/1424-8220/19/19/4215.

[136]   Issam Boukhennoufa et al. "Wearable sensors and machine learning in post-stroke rehabilitation assessment: A systematic review". In: *Biomedical Signal Processing and Control* 71 (Jan. 2022), p. 103197. ISSN: 1746-8094. DOI: 10.1016/J.BSPC.2021.103197.

[137]   Q. Li et al. "Walking speed and slope estimation using shank-mounted inertial measurement units". In: *2009 IEEE International Conference on Rehabilitation Robotics, ICORR 2009* (2009), pp. 839–844. DOI: 10.1109/ICORR.2009.5209598.

[138]   Shigeru Tadano, Ryo Takeda, and Hiroaki Miyagawa. "Three Dimensional Gait Analysis Using Wearable Acceleration and Gyro Sensors Based on Quaternion Calculations". In: *Sensors 2013, Vol. 13, Pages 9321-9343* 13 (7 July 2013), pp. 9321–9343. ISSN: 1424-8220. DOI: 10.3390/S130709321. URL: https://www.mdpi.com/1424-8220/13/7/9321.

[139]   K. Aminian et al. "Spatio-temporal parameters of gait measured by an ambulatory system using miniature gyroscopes". In: *Journal of biomechanics* 35 (5 2002), pp. 689–699. ISSN: 0021-9290. DOI: 10.1016/S0021-9290(02)00008-8. URL: https://pubmed.ncbi.nlm.nih.gov/11955509/.

[140]   Ion P.I. Pappas et al. "A Reliable Gyroscope-Based Gait-Phase Detection Sensor Embedded in a Shoe Insole". In: *IEEE Sensors Journal* 4 (2 Apr. 2004), pp. 268–274. ISSN: 1530437X. DOI: 10.1109/JSEN.2004.823671.

[141]   Zhaojun Xue et al. "Infrared gait recognition based on wavelet transform and support vector machine". In: *Pattern Recognition* 43 (8 Aug. 2010), pp. 2904–2910. ISSN: 0031-3203. DOI: 10.1016/J.PATCOG.2010.03.011.

[142] Zhen Peng Bian et al. "Fall detection based on body part tracking using a depth camera". In: *IEEE journal of biomedical and health informatics* 19 (2 Mar. 2015), pp. 430–439. ISSN: 2168-2208. DOI: 10.1109/JBHI.2014.2319372. URL: https://pubmed.ncbi.nlm.nih.gov/24771601/.

[143] Thiago Teixeira et al. "PEM-ID: Identifying people by gait-matching using cameras and wearable accelerometers". In: (Oct. 2009), pp. 1–8. DOI: 10.1109/ICDSC.2009.5289412. URL: https://www.researchgate.net/publication/224605186_PEM-ID_Identifying_people_by_gait-matching_using_cameras_and_wearable_accelerometers.

[144] Wei Wang, Alex X. Liu, and Muhammad Shahzad. "Gait recognition using WiFi signals". In: *UbiComp 2016 - Proceedings of the 2016 ACM International Joint Conference on Pervasive and Ubiquitous Computing* (Sept. 2016), pp. 363–373. DOI: 10.1145/2971648.2971670. URL: https://dl.acm.org/doi/10.1145/2971648.2971670.

[145] Robert M. Kanko et al. "Assessment of spatiotemporal gait parameters using a deep learning algorithm-based markerless motion capture system". In: *Journal of Biomechanics* 122 (June 2021), p. 110414. ISSN: 0021-9290. DOI: 10.1016/J.JBIOMECH.2021.110414.

[146] Hao Shu Fang et al. "RMPE: Regional Multi-person Pose Estimation". In: *Proceedings of the IEEE International Conference on Computer Vision* 2017-October (Dec. 2017), pp. 2353–2362. ISSN: 15505499. DOI: 10.1109/ICCV.2017.256.

[147] Laurie Needham et al. "The accuracy of several pose estimation methods for 3D joint centre localisation". In: *Scientific Reports* 11 (1 Dec. 2021), p. 20673. ISSN: 20452322. DOI: 10.1038/S41598-021-00212-X. URL: https://www.ncbi.nlm.nih.gov/pmc/articles/PMC8526586.

[148] Colyer SL et al. "A Review of the Evolution of Vision-Based Motion Analysis and the Integration of Advanced Computer Vision Methods Towards Developing a Markerless System". In: *Sports medicine - open* 4 (1 Dec. 2018). ISSN: 2199-1170. DOI: 10.1186/S40798-018-0139-Y. URL: https://pubmed.ncbi.nlm.nih.gov/29869300/.

[149] Martin Sandau et al. "Markerless motion capture can provide reliable 3D gait kinematics in the sagittal and frontal plane". In: *Medical engineering physics* 36 (9 2014), pp. 1168–1175. ISSN: 1873-4030. DOI: 10.1016/J.MEDENGPHY.2014.07.007. URL: https://pubmed.ncbi.nlm.nih.gov/25085672/.

[150] Dushyant Mehta et al. "VNect: Real-time 3D Human Pose Estimation with a Single RGB Camera". In: *ACM Transactions on Graphics* 36 (4 2017). ISSN: 15577368. DOI: 10.1145/3072959.3073596. URL: http://dx.doi.org/10.1145/3072959.3073596.

[151] Shmuel Springer and Galit Yogev Seligmann. "Validity of the Kinect for Gait Assessment: A Focused Review". In: *Sensors (Basel, Switzerland)* 16 (2 Feb. 2016). ISSN: 14248220. DOI: 10.3390/S16020194. URL: https://www.ncbi.nlm.nih.gov/pmc/articles/PMC4801571.

[152] Alexander Mathis et al. "DeepLabCut: markerless pose estimation of user-defined body parts with deep learning". In: *Nature Neuroscience 2018 21:9* 21 (9 Aug. 2018), pp. 1281–1289. ISSN: 1546-1726. DOI: 10.1038/s41593-018-0209-y. URL: https://www.nature.com/articles/s41593-018-0209-y.

[153] Matteo Moro et al. "Markerless gait analysis in stroke survivors based on computer vision and deep learning: A pilot study". In: *Proceedings of the ACM Symposium on Applied Computing* (Mar. 2020), pp. 2097–2104. DOI: 10.1145/3341105.3373963. URL: https://www.researchgate.net/publication/340436850_Markerless_gait_analysis_in_stroke_survivors_based_on_computer_vision_and_deep_learning_a_pilot_study.

[154] Nobuyasu Nakano et al. "Evaluation of 3D Markerless Motion Capture Accuracy Using OpenPose With Multiple Video Cameras". In: *Frontiers in Sports and Active Living* 2 (May 2020), p. 538330. ISSN: 2624-9367. DOI: 10.3389/FSPOR.2020.00050.

[155] Nidhi Seethapathi et al. "Movement science needs different pose tracking algorithms". In: (July 2019). URL: https://arxiv.org/abs/1907.10226v1.

[156] Sherveen Riazati et al. "Absolute Reliability of Gait Parameters Acquired With Markerless Motion Capture in Living Domains". In: *Frontiers in Human Neuroscience* 16 (June 2022), p. 867474. ISSN: 16625161. DOI: 10.3389/FNHUM.2022.867474/BIBTEX.

[157] Ross A. Clark et al. "Three-dimensional cameras and skeleton pose tracking for physical function assessment: A review of uses, validity, current developments and Kinect alternatives". In: *Gait posture* 68 (Feb. 2019), pp. 193–200. ISSN: 1879-2219. DOI: 10.1016/J.GAITPOST.2018.11.029. URL: https://pubmed.ncbi.nlm.nih.gov/30500731/.

[158] Anne Schmitz et al. "The measurement of in vivo joint angles during a squat using a single camera markerless motion capture system as compared to a marker based system". In: *Gait Posture* 41 (2 Feb. 2015), pp. 694–698. ISSN: 0966-6362. DOI: 10.1016/J.GAITPOST.2015.01.028.

[159] Hamed Sarbolandi, Damien Lefloch, and Andreas Kolb. "Kinect range sensing: Structured-light versus Time-of-Flight Kinect". In: *Computer Vision and Image Understanding* 139 (Oct. 2015), pp. 1–20. ISSN: 1077-3142. DOI: 10.1016/J.CVIU.2015.05.006.

[160] MotionMetrix. *Technology – MotionMetrix*. Accessed: 2024-12-05. n.d. URL: https://www.motionmetrix.se/4-technology/.

[161] Jung Hwan Shin et al. "Quantitative Gait Analysis Using a Pose-Estimation Algorithm with a Single 2D-Video of Parkinson's Disease Patients". In: *Journal of Parkinson's Disease* 11 (3 Apr. 2021), pp. 1271–1283. ISSN: 1877718X. DOI: 10.3233/JPD-212544/ASSET/IMAGES/10.3233_JPD-212544-FIG5.JPG. URL: https://journals.sagepub.com/doi/full/10.3233/JPD-212544.

[162] Ratan Das et al. "Recent Trends and Practices Toward Assessment and Rehabilitation of Neurodegenerative Disorders: Insights From Human Gait". In: *Frontiers in Neuroscience* 16 (Apr. 2022), p. 859298. ISSN: 1662453X. DOI: 10.3389/FNINS.2022.859298/BIBTEX.

[163] Nadav Eichler et al. "3D motion capture system for assessing patient motion during Fugl-Meyer stroke rehabilitation testing". In: *IET Computer Vision* 12 (7 Oct. 2018), pp. 963–975. ISSN: 1751-9640. DOI: 10.1049/IET-CVI.2018.5274. URL: https://onlinelibrary.wiley.com/doi/full/10.1049/iet-cvi.2018.5274.

[164] Hector R. Martinez et al. "Accuracy of Markerless 3D Motion Capture Evaluation to Differentiate between On/Off Status in Parkinson's Disease after Deep Brain Stimulation". In: *Parkinson's Disease* 2018 (1 Jan. 2018), p. 5830364. ISSN: 2042-0080. DOI: 10.1155/2018/5830364. URL: https://onlinelibrary.wiley.com/doi/full/10.1155/2018/5830364.

[165] iPi Soft. *iPi Motion Capture*. Accessed: 2024-11-26. URL: https://www.ipisoft.com/.

[166] The Captury. *The Captury: Markerless Motion Capture*. Accessed: 2024-11-26. URL: https://captury.com/.

[167] Theia Markerless. *Theia Markerless Motion Capture*. Accessed: 2024-11-26. URL: https://www.theiamarkerless.ca/.

[168] Argyro Kotsifaki, Rodney Whiteley, and Clint Hansen. "Dual Kinect v2 system can capture lower limb kinematics reasonably well in a clinical setting: concurrent validity of a dual camera markerless motion capture system in professional football players". In: *BMJ Open Sport Exercise Medicine* 4 (1 Dec. 2018). ISSN: 2055-7647. DOI: 10.1136/BMJSEM-2018-000441. URL: https://bmjopensem.bmj.com/content/4/1/e000441.

[169] Steen Harsted et al. "Concurrent validity of lower extremity kinematics and jump characteristics captured in pre-school children by a markerless 3D motion capture system". In: *Chiropractic & Manual Therapies* 27.1 (2019), p. 39. ISSN: 2045-709X. DOI: 10.1186/s12998-019-0261-z. URL: https://doi.org/10.1186/s12998-019-0261-z.

[170] L. Becker. *Evaluation of joint angle accuracy using markerless silhouette-based tracking and hybrid tracking against traditional marker tracking.* Accessed: 2024-11-26. Feb. 2016. URL: http://www.simi.com/fileadmin/user_upload/Dokumente/Downloads/Poster_1_evaluation_specific_joint_movements.pdf.

[171] Shuai Tao, Mineichi Kudo, and Hidetoshi Nonaka. "Privacy-Preserved Behavior Analysis and Fall Detection by an Infrared Ceiling Sensor Network". In: *Sensors 2012, Vol. 12, Pages 16920-16936* 12 (12 Dec. 2012), pp. 16920–16936. ISSN: 1424-8220. DOI: 10.3390/S121216920. URL: https://www.mdpi.com/1424-8220/12/12/16920.

[172] Alex Kendall, Matthew Grimes, and Roberto Cipolla. "PoseNet: A Convolutional Network for Real-Time 6-DOF Camera Relocalization". In: *in Proc. IEEE Int. Conf. Comput. Vis. (ICCV)* (May 2015), pp. 2938–2946. URL: http://arxiv.org/abs/1505.07427.

[173] Erika D'Antonio et al. "Validation of a 3D Markerless System for Gait Analysis Based on OpenPose and Two RGB Webcams". In: *IEEE Sensors Journal* 21 (15 Aug. 2021), pp. 17064–17075. ISSN: 15581748. DOI: 10.1109/JSEN.2021.3081188.

[174] Aditya Viswakumar et al. "Human Gait Analysis Using OpenPose". In: *Proceedings of the IEEE International Conference Image Information Processing* 2019-November (Nov. 2019), pp. 310–314. ISSN: 2640074X. DOI: 10.1109/ICIIP47207.2019.8985781. URL: https://www.researchgate.net/publication/339175256_Human_Gait_Analysis_Using_OpenPose.

[175] Weijun Tao et al. "Gait analysis using wearable sensors". In: *Sensors (Basel, Switzerland)* 12 (2 Feb. 2012), pp. 2255–2283. ISSN: 1424-8220. DOI: 10.3390/S120202255. URL: https://pubmed.ncbi.nlm.nih.gov/22438763/.

[176] John H. Hollman, Eric M. McDade, and Ronald C. Petersen. "Normative spatiotemporal gait parameters in older adults". In: *Gait posture* 34 (1 May 2011), pp. 111–118. ISSN: 1879-2219. DOI: 10.1016/J.GAITPOST.2011.03.024. URL: https://pubmed.ncbi.nlm.nih.gov/21531139/.

[177] V. Macellari, C. Giacomozzi, and R. Saggini. "Spatial-temporal parameters of gait: reference data and a statistical method for normality assessment". In: *Gait posture* 10 (2 Oct. 1999), pp. 171–181. ISSN: 0966-6362. DOI: 10.1016/S0966-6362(99)00021-1. URL: https://pubmed.ncbi.nlm.nih.gov/10502651/.

[178] Andreas Katsiaras et al. "Skeletal muscle fatigue, strength, and quality in the elderly: the Health ABC Study". In: *Journal of applied physiology (Bethesda, Md. : 1985)* 99 (1 July 2005), pp. 210–216. ISSN: 8750-7587. DOI: 10.1152/JAPPLPHYSIOL.01276.2004. URL: https://pubmed.ncbi.nlm.nih.gov/15718402/.

[179] Ciara M. O'Connor et al. "Automatic detection of gait events using kinematic data". In: *Gait posture* 25 (3 Mar. 2007), pp. 469–474. ISSN: 0966-6362. DOI: 10.1016/J.GAITPOST.2006.05.016. URL: https://pubmed.ncbi.nlm.nih.gov/16876414/.

[180] Adrian Bauman et al. "Progress and Pitfalls in the Use of the International Physical Activity Questionnaire (IPAQ) for Adult Physical Activity Surveillance". In: *Journal of Physical Activity and Health* 6 (s1 Jan. 2009), S5–S8. ISSN: 1543-5474. DOI: 10.1123/JPAH.6.S1.S5. URL: https://journals.humankinetics.com/view/journals/jpah/6/s1/article-pS5.xml.

[181] Maria Hagströmer, Pekka Oja, and Michael Sjöström. "The International Physical Activity Questionnaire (IPAQ): a study of concurrent and construct validity". In: *Public Health Nutrition* 9 (6 Sept. 2006), pp. 755–762. ISSN: 1475-2727. DOI: 10.1079/PHN2005898. URL: https://www.cambridge.org/core/journals/public-health-nutrition/article/international-physical-activity-questionnaire-ipaq-a-study-of-concurrent-and-construct-validity/A78914A4CFE41987A40C122FDF8BE229.

[182] Bernard Auvinet et al. "Reference data for normal subjects obtained with an accelerometric device". In: *Gait posture* 16 (2 Oct. 2002), pp. 124–134. ISSN: 0966-6362. DOI: 10.1016/S0966-6362(01)00203-X. URL: https://pubmed.ncbi.nlm.nih.gov/12297254/.

[183] Mohammad Mostafa Namar, Omid Jahanian, and Hasan Koten. "The Start of Combustion Prediction for Methane-Fueled HCCI Engines: Traditional vs. Machine Learning Methods". In: *Mathematical Problems in Engineering* 2022 (2022). ISSN: 15635147. DOI: 10.1155/2022/4589160.

[184] Arunabha M. Roy. "Adaptive transfer learning-based multiscale feature fused deep convolutional neural network for EEG MI multiclassification in brain–computer interface". In: *Engineering Applications of Artificial Intelligence* 116 (Nov. 2022), p. 105347. ISSN: 0952-1976. DOI: 10.1016/J.ENGAPPAI.2022.105347.

[185] Richard Williamson and Brian J. Andrews. "Gait event detection for FES using accelerometers and supervised machine learning". In: *IEEE transactions on rehabilitation engineering : a publication of the IEEE Engineering in Medicine and Biology Society* 8 (3 2000), pp. 312–319. ISSN: 1063-6528. DOI: 10.1109/86.867873. URL: https://pubmed.ncbi.nlm.nih.gov/11001511/.

[186] Heikki J. Ailisto et al. "Identifying people from gait pattern with accelerometers". In: *Biometric Technology for Human Identification II* 5779 (Mar. 2005), p. 7. ISSN: 0277786X. DOI: 10.1117/12.603331. URL: https://www.researchgate.net/publication/241529587_Identifying_people_from_gait_pattern_with_accelerometers.

[187] Rezaul K. Begg, Marimuthu Palaniswami, and Brendan Owen. "Support vector machines for automated gait classification". In: *IEEE Transactions on Biomedical Engineering* 52 (5 May 2005), pp. 828–838. ISSN: 00189294. DOI: 10.1109/TBME.2005.845241. URL: https://www.researchgate.net/publication/7852808_Support_Vector_Machines_for_Automated_Gait_Classification.

[188] Bogdan Pogorelc and Matjaž Gams. "Detecting gait-related health problems of the elderly using multidimensional dynamic time warping approach with semantic attributes". In: *Multimedia Tools and Applications* 66 (1 Sept. 2013), pp. 95–114. ISSN: 13807501. DOI: 10.1007/S11042-013-1473-1/METRICS. URL: https://link.springer.com/article/10.1007/s11042-013-1473-1.

[189] Andrea Mannini, Vincenzo Genovese, and Angelo Maria Sabatini. "Online decoding of hidden Markov models for gait event detection using foot-mounted gyroscopes". In: *IEEE journal of biomedical and health informatics* 18 (4 2014), pp. 1122–1130. ISSN: 2168-2208. DOI: 10.1109/JBHI.2013.2293887. URL: https://pubmed.ncbi.nlm.nih.gov/25014927/.

[190] Kamiar Aminian and Bijan Najafi. "Capturing human motion using body-fixed sensors: outdoor measurement and clinical applications". In: *Computer Animation and Virtual Worlds* 15 (2 May 2004), pp. 79–94. ISSN: 1546-427X. DOI: 10.1002/CAV.2. URL: https://onlinelibrary.wiley.com/doi/full/10.1002/cav.2https://onlinelibrary.wiley.com/doi/abs/10.1002/cav.2https://onlinelibrary.wiley.com/doi/10.1002/cav.2.

[191] Fouaz S. Ayachi et al. "Wavelet-based algorithm for auto-detection of daily living activities of older adults captured by multiple inertial measurement units (IMUs)". In: *Physiological measurement* 37 (3 Feb. 2016), pp. 442–461. ISSN: 1361-6579. DOI: 10.1088/0967-3334/37/3/442. URL: https://pubmed.ncbi.nlm.nih.gov/26914432/.

[192] Catrine E. Tudor-Locke and Anita M. Myers. "Methodological considerations for researchers and practitioners using pedometers to measure physical (ambulatory) activity". In: *Research quarterly for exercise and sport* 72 (1 2001), pp. 1–12. ISSN: 0270-1367. DOI: 10.1080/02701367.2001.10608926. URL: https://pubmed.ncbi.nlm.nih.gov/11253314/.

[193] Yunhoon Cho, Hyuntae Cho, and Chong Min Kyung. "Design and Implementation of Practical Step Detection Algorithm for Wrist-Worn Devices". In: *IEEE Sensors Journal* 16 (21 Nov. 2016), pp. 7720–7730. ISSN: 1530437X. DOI: 10.1109/JSEN.2016.2603163.

[194] S. Jayalath, N. Abhayasinghe, and I Murray. "A gyroscope based accurate pedometer algorithm". In: *International Conference on Indoor 178 Positioning and Indoor Navigation.* Vol. 28. 2013. ISBN: 978-1-4799-4043-1.

[195] V. Macellari and C. Giacomozzi. "Multistep pressure platform as a stand-alone system for gait assessment." In: *Medical Biological Engineering Computing* 34 (4 July 1996), pp. 299–304. ISSN: 0140-0118. DOI: 10.1007/BF02511242. URL: https://europepmc.org/article/MED/8935497.

[196] Joseph M. Mahoney and Matthew B. Rhudy. "Methodology and validation for identifying gait type using machine learning on IMU data". In: *https://doi.org/10.1080/03091902.2019.1599073* 43 (1 Jan. 2019), pp. 25–32. DOI: 10.1080/03091902.2019.1599073. URL: https://www.tandfonline.com/doi/abs/10.1080/03091902.2019.1599073.

[197] Matthew B. Rhudy and Joseph M. Mahoney. "A comprehensive comparison of simple step counting techniques using wrist- and ankle-mounted accelerometer and gyroscope signals". In: *Journal of Medical Engineering and Technology* 42 (3 Apr. 2018), pp. 236–243. ISSN: 1464522X. DOI: 10.1080/03091902.2018.1470692. URL: https://pubmed.ncbi.nlm.nih.gov/29846134/.

[198] Mahya Shahbazi et al. "Multimodal Sensorimotor Integration for Expert-in-The-Loop Telerobotic Surgical Training". In: *IEEE Transactions on Robotics* 34 (6 Dec. 2018), pp. 1549–1564. ISSN: 1552-3098. DOI: 10.1109/TRO.2018.2861916. URL: https://nyuscholars.nyu.edu/en/publications/multimodal-sensorimotor-integration-for-expert-in-the-loop-telero.

[199] Jacob Goldberger et al. "Neighbourhood Components Analysis". In: *Advances in Neural Information Processing Systems.* Ed. by L. Saul, Y. Weiss, and L. Bottou. Vol. 17. MIT Press, 2004. URL: https://proceedings.neurips.cc/paper_files/paper/2004/file/42fe880812925e520249e808937738d2-Paper.pdf.

[200] Wei Yang, Kuanquan Wang, and Wangmeng Zuo. "Neighborhood component feature selection for high-dimensional data". In: *Journal of Computers* 7 (1 2012), pp. 162–168. ISSN: 1796203X. DOI: 10.4304/JCP.7.1.161-168.

[201] Ran Gilad-Bachrach, Amir Navot, and Naftali Tishby. "Margin based feature selection - theory and algorithms". In: *Proceedings of the Twenty-First International Conference on Machine Learning.* ICML '04. Banff, Alberta, Canada: Association for Computing Machinery, 2004, p. 43. ISBN: 1581138385. DOI: 10.1145/1015330.1015352. URL: https://doi.org/10.1145/1015330.1015352.

[202] Bo Chen et al. "Large margin feature weighting method via linear programming". In: *IEEE Transactions on Knowledge and Data Engineering* 21 (10 Oct. 2009), pp. 1475–1488. ISSN: 10414347. DOI: 10.1109/TKDE.2008.238.

[203] Yijun Sun, Sinisa Todorovic, and Steve Goodison. "Local-learning-based feature selection for high-dimensional data analysis". In: *IEEE transactions on pattern analysis and machine intelligence* 32 (9 2010), pp. 1610–1626. ISSN: 1939-3539. DOI: 10.1109/TPAMI.2009.190. URL: https://pubmed.ncbi.nlm.nih.gov/20634556/.

[204] Ian H. Witten et al. "Data Mining: Practical Machine Learning Tools and Techniques". In: *Data Mining: Practical Machine Learning Tools and Techniques* (Nov. 2016), pp. 1–621. DOI: 10.1016/C2009-0-19715-5.

[205] Marina Sokolova and Guy Lapalme. "A systematic analysis of performance measures for classification tasks". In: *Information Processing Management* 45 (4 July 2009), pp. 427–437. ISSN: 0306-4573. DOI: 10.1016/J.IPM.2009.03.002.

[206] Tom Fawcett. "An introduction to ROC analysis". In: *Pattern Recognition Letters* 27 (8 June 2006), pp. 861–874. ISSN: 0167-8655. DOI: 10.1016/J.PATREC.2005.10.010.

[207] David Jiménez-Grande et al. "Kinematic biomarkers of chronic neck pain measured during gait: A data-driven classification approach". In: *Journal of Biomechanics* 118 (2021), pp. 5162–5166. ISSN: 18732380. DOI: 10.1016/j.jbiomech.2020.110190.

[208] F. Alton et al. "A kinematic comparison of overground and treadmill walking". In: *Clinical Biomechanics* 13 (6 Sept. 1998), pp. 434–440. ISSN: 0268-0033. DOI: `10.1016/S0268-0033(98)00012-6`.

[209] Nachiappan Chockalingam et al. "Comparison of Pelvic Complex Kinematics During Treadmill and Overground Walking". In: *Archives of Physical Medicine and Rehabilitation* 93 (12 Dec. 2012), pp. 2302–2308. ISSN: 0003-9993. DOI: `10.1016/J.APMR.2011.10.022`.

[210] Marie B. Semaan et al. "Is treadmill walking biomechanically comparable to overground walking? A systematic review". In: *Gait Posture* 92 (Feb. 2022), pp. 249–257. ISSN: 0966-6362. DOI: `10.1016/J.GAITPOST.2021.11.009`.

[211] Joseph McGrath et al. "Upper body activity classification using an inertial measurement unit in court and field-based sports: A systematic review". In: *Proceedings of the Institution of Mechanical Engineers, Part P: Journal of Sports Engineering and Technology* 235 (2 June 2021), pp. 83–95. ISSN: 1754338X. DOI: `10.1177/1754337120959754/ASSET/IMAGES/LARGE/10.1177_1754337120959754-FIG1.JPEG`. URL: `https://journals.sagepub.com/doi/full/10.1177/1754337120959754?casa_token=xIM8ynSaDyAAAAAA%3ABHeyNmkgrHsKoQobXnevK4PxehK773zsPybKndVVVzQv3c3fzTW71Zn8RloDSEtD`

[212] Andrew Hua et al. "Evaluation of Machine Learning Models for Classifying Upper Extremity Exercises Using Inertial Measurement Unit-Based Kinematic Data". In: *IEEE Journal of Biomedical and Health Informatics* 24 (9 Sept. 2020), pp. 2452–2460. ISSN: 21682208. DOI: `10.1109/JBHI.2020.2999902`.

[213] Siavash Khaksar et al. "Application of inertial measurement units and machine learning classification in cerebral palsy: Randomized controlled trial". In: *JMIR Rehabilitation and Assistive Technologies* 8 (4 2021), pp. 1–18. ISSN: 23692529. DOI: `10.2196/29769`.

[214] Fu-Cheng Wang et al. "Detection and Classification of Stroke Gaits by Deep Neural Networks Employing Inertial Measurement Units". In: *Sensors 2021, Vol. 21, Page 1864* 21 (5 Mar. 2021), p. 1864. ISSN: 1424-8220. DOI: `10.3390/S21051864`. URL: `https://www.mdpi.com/1424-8220/21/5/1864`.

[215] Christopher G. Goetz et al. "Movement Disorder Society-sponsored revision of the Unified Parkinson's Disease Rating Scale (MDS-UPDRS): scale presentation and clinimetric testing results". In: *Movement disorders : official journal of the Movement Disorder Society* 23 (15 Nov. 2008), pp. 2129–2170. ISSN: 1531-8257. DOI: `10.1002/MDS.22340`. URL: `https://pubmed.ncbi.nlm.nih.gov/19025984/`.

[216] Bernard X.W. Liew et al. "Classifying individuals with and without patellofemoral pain syndrome using ground force profiles – Development of a method using functional data boosting". In: *Gait and Posture* 80 (March 2020), pp. 90–95. ISSN: 18792219. DOI: `10.1016/j.gaitpost.2020.05.034`. URL: `https://doi.org/10.1016/j.gaitpost.2020.05.034`.

[217] Bernard X.W. Liew et al. "Classifying neck pain status using scalar and functional biomechanical variables – development of a method using functional data boosting". In: *Gait and Posture* 76 (2020), pp. 146–150. ISSN: 18792219. DOI: `10.1016/j.gaitpost.2019.12.008`. URL: `https://doi.org/10.1016/j.gaitpost.2019.12.008`.

[218] Sarah Brockhaus, David Rügamer, and Sonja Greven. "Boosting Functional Regression Models with FDboost". In: *Journal of Statistical Software* 94 (May 2017), pp. 1–50. ISSN: 15487660. DOI: `10.48550/arxiv.1705.10662`. URL: `https://arxiv.org/abs/1705.10662v3`.

[219] Sunwook Kim and Maury A. Nussbaum. "Performance evaluation of a wearable inertial motion capture system for capturing physical exposures during manual material handling tasks". In: *Ergonomics* 56 (2 Feb. 2013), pp. 314–326. ISSN: 1366-5847. DOI: `10.1080/00140139.2012.742932`. URL: `https://pubmed.ncbi.nlm.nih.gov/23231730/`.

[220] Xavier Robert-Lachaine et al. "Validation of inertial measurement units with an optoelectronic system for whole-body motion analysis". In: *Medical and Biological Engineering and Computing* 55 (4 Apr. 2016), pp. 609–619. ISSN: 17410444. DOI: `10.1007/S11517-016-1537-2`.

[221] Christoph Schiefer et al. "Optimization of inertial sensor-based motion capturing for magnetically distorted field applications". In: *Journal of biomechanical engineering* 136 (12 Dec. 2014). ISSN: 1528-8951. DOI: `10.1115/1.4028822`. URL: `https://pubmed.ncbi.nlm.nih.gov/25321344/`.

[222] Aurelio Cappozzo et al. "Human movement analysis using stereophotogrammetry. Part 1: Theoretical background". In: *Gait and Posture* 21 (2 2005), pp. 186–196. ISSN: 09666362. DOI: `10.1016/j.gaitpost.2004.01.010`. URL: `https://pubmed.ncbi.nlm.nih.gov/15639398/`.

[223] Pietro Picerno, Andrea Cereatti, and Aurelio Cappozzo. "Joint kinematics estimate using wearable inertial and magnetic sensing modules". In: *Gait posture* 28 (4 Nov. 2008), pp. 588–595. ISSN: 0966-6362. DOI: `10.1016/J.GAITPOST.2008.04.003`. URL: `https://pubmed.ncbi.nlm.nih.gov/18502130/`.

[224] Q. Li et al. "Walking speed estimation using a shank-mounted inertial measurement unit". In: *Journal of biomechanics* 43 (8 May 2010), pp. 1640–1643. ISSN: 1873-2380. DOI: `10.1016/J.JBIOMECH.2010.01.031`. URL: `https://pubmed.ncbi.nlm.nih.gov/20185136/`.

[225] Antonio I. Cuesta-Vargas, Alejandro Galán-Mercant, and Jonathan M. Williams. "The use of inertial sensors system for human motion analysis". In: *Physical Therapy Reviews* 15 (6 Dec. 2010), p. 462. ISSN: 1743288X. DOI: `10.1179/1743288X11Y.0000000006`. URL: `/pmc/articles/PMC3566464//pmc/articles/PMC3566464/?report=abstracthttps://www.ncbi.nlm.nih.gov/pmc/articles/PMC3566464/`.

[226] Stefano Corazza et al. "Markerless motion capture through visual hull, articulated ICP and subject specific model generation". In: *International Journal of Computer Vision* 87 (1-2 Mar. 2010), pp. 156–169. ISSN: 09205691. DOI: `10.1007/S11263-009-0284-3/METRICS`. URL: `https://link.springer.com/article/10.1007/s11263-009-0284-3`.

[227] Els Knippenberg et al. "Markerless motion capture systems as training device in neurological rehabilitation: a systematic review of their use, application, target population and efficacy". In: *Journal of neuroengineering and rehabilitation* 14 (1 June 2017). ISSN: 1743-0003. DOI: `10.1186/S12984-017-0270-X`. URL: `https://pubmed.ncbi.nlm.nih.gov/28646914/`.

[228] Andrea Castelli et al. "A 2D Markerless Gait Analysis Methodology: Validation on Healthy Subjects". In: (2015). DOI: `10.1155/2015/186780`. URL: `http://dx.doi.org/10.1155/2015/186780`.

[229] Zhe Cao et al. "Realtime Multi-Person 2D Pose Estimation using Part Affinity Fields". In: *Proceedings - 30th IEEE Conference on Computer Vision and Pattern Recognition, CVPR 2017* 2017-January (Nov. 2016), pp. 1302–1310. DOI: `10.1109/CVPR.2017.143`. URL: `https://arxiv.org/abs/1611.08050v2`.

[230] Tsung Yi Lin et al. "Microsoft COCO: Common Objects in Context". In: *Lecture Notes in Computer Science (including subseries Lecture Notes in Artificial Intelligence and Lecture Notes in Bioinformatics)* 8693 LNCS (PART 5 May 2014), pp. 740–755. ISSN: 16113349. DOI: `10.1007/978-3-319-10602-1_48`. URL: `https://arxiv.org/abs/1405.0312v3`.

[231] BIPM. *Measurement Compatibility*. URL: `https://jcgm.bipm.org/vim/en/2.47.html`. (accessed: 2024-05-10).

[232] Neil J. Cronin et al. "Markerless 2D kinematic analysis of underwater running: A deep learning approach". In: *Journal of Biomechanics* 87 (Apr. 2019), pp. 75–82. ISSN: 0021-9290. DOI: `10.1016/J.JBIOMECH.2019.02.021`.

[233] Daniel L. Miranda et al. "Kinematic differences between optical motion capture and biplanar videoradiography during a jump–cut maneuver". In: *Journal of Biomechanics* 46 (3 Feb. 2013), pp. 567–573. ISSN: 0021-9290. DOI: 10.1016/J.JBIOMECH.2012.09.023.

[234] Matteo Moro et al. "Markerless vs. Marker-Based Gait Analysis: A Proof of Concept Study". In: *Sensors* 22 (5 Mar. 2022). ISSN: 14248220. DOI: 10.3390/s22052011.

[235] S. Corazza et al. "A markerless motion capture system to study musculoskeletal biomechanics: visual hull and simulated annealing approach". In: *Annals of biomedical engineering* 34 (6 June 2006), pp. 1019–1029. ISSN: 0090-6964. DOI: 10.1007/S10439-006-9122-8. URL: https://pubmed.ncbi.nlm.nih.gov/16783657/.

[236] Alex Ong, Ian Sujae Harris, and Joseph Hamill. "The efficacy of a video-based marker-less tracking system for gait analysis". In: *Computer methods in biomechanics and biomedical engineering* 20 (10 July 2017), pp. 1089–1095. ISSN: 1476-8259. DOI: 10.1080/10255842.2017.1334768. URL: https://pubmed.ncbi.nlm.nih.gov/28569549/.